CENTRO DE INVESTIGACIÓN Y DE ESTUDIOS AVANZADOS DEL INSTITUTO POLITÉCNICO NACIONAL

UNIDAD ZACATENCO

DEPARTAMENTO DE INGENIERÍA ELÉCTRICA

SECCIÓN DE ELECTRÓNICA DEL ESTADO SÓLIDO

TESIS

FABRICATION AND CHARACTERIZATION OF UNDOPED AND CO-DOPED ZnO THIN FILMS

PRESENTA:

VINOTH KUMAR JAYARAMAN

Para obtener el grado de:

DOCTORADO EN CIENCIAS

En la especialidad de

INGENIERÍA ELÉCTRICA

Directores de tesis:

Dra. María de la Luz Olvera Amador

Dr. Arturo Maldonado Álvarez

MÉXICO D.F, NOVIEMBRE 2016

ACKNOWLEDGMENTS

I am grateful to my supervisors, Dra. María de la Luz Olvera & Dr. Arturo Maldonado Álvarez for their generous guidance and support made it possible for me to work on a topic that was of great interest to me. It was a great pleasure to work them.

I would like to express my special thanks to Dr. Yasuhiro Matsumoto Kuwabara for giving an opportunity to learn sputtering technique and to carry out the experiments. In addition I thank him for his valuable comments during thesis revisions.

I am thankful to Dr. Miguel Meléndez Lira for his suggestions and comments for my experimental work and thesis.

I am grateful to my thesis committee members Dr. Gabriel Romero Paredes Rubio, and Dr. Ramón Peña Sierra for their expert comments related to my thesis.

I specially thank Dr. Yuri for his help in obtaining SIMS results.

I would like to thank Miguel Angel Luna for his assistance in cleaning the substrates and measuring thickness of the films.

I thank Adolfo Tavira for his help in XRD characterization. In addition, I thank Araceli Palafox, and Dr. Jaime Vega Perez for their help during film fabrication in the laboratory.

I am grateful to Dr. Jorge Roque (LANE-Cinvestav) for his work in obtaining the scanning electron microscopy images.

I am thankful to my parents, family, and friends for their continuous love, encouragement and support.

Finally, I would like to thank Consejo Nacional de Ciencia y Tecnología (CONACYT), for supporting me financially.

PREFACE

This thesis features with the fabrication of undoped and co-doped zinc oxide thin films prepared by ultrasonic spray pyrolysis and sputtering. The quality of the thin films was analyzed using structural, morphological, optical, electrical characterization and figure of merit estimation. The description of the chapters of this thesis is given below.

Chapter 1 includes a brief description of transparent conductive oxides (TCOs) as well as the characteristics of some semiconducting materials which fulfill the characteristics required for reliable manufacturing.

Chapter 2 describes the theory, properties, and applications of ZnO. The electrical, optical, piezoelectric, magnetic and pyroelectric were discussed in details. The deposition methods of ZnO like sputtering, thermal evaporation, ultrasonic spray pyrolysis, sol-gel, and chemical bath depositions were included. The various applications were also added.

Chapter 3 includes all the experimental details. The various solution conditions such as water content, co-doping concentration, acetic acid content, equal variations of acetic acid and water, different precursors, and ball milling effects were discussed here for ultrasonic spray pyrolysis. In addition, the experimental conditions for obtaining undoped and co-doped ZnO thin films by sputtering also included.

Chapter 4 explains the physical properties of all undoped and aluminium and indium co-doped ZnO thin films obtained by ultrasonic spray pyrolysis. The detailed analysis of structural, morphological, optical and electrical properties was included.

Chapter 5 includes the physical properties of all the films obtained by sputtering. The detailed analysis of structural, morphological, optical and electrical properties was included with respect to changes in sputtering parameters. It covers undoped ZnO, and indium and gallium co-doped ZnO characteristics.

Chapter 6 deals with the conclusions of this work. This section includes the major achievements of this work.

Chapter 7 describes the future work.

ABSTRACT

This work features with the fabrication of undoped and co-doped zinc oxide (ZnO) thin films prepared by ultrasonic spray pyrolysis and sputtering.

By ultrasonic spray, undoped ZnO thin films were deposited on sodalime glass substrates using zinc acetylacetonate as precursor. The physical characteristics of ZnO films were studied with respect to changes in the water content in the starting solution. This showed us how the water influences in changing the properties. Since the undoped ZnO thin films were highly resistive, we found a novel chemical approach to fabricate aluminium and indium co-doped ZnO thin films by ultrasonic spray pyrolysis. In this method, we modified the co-dopants concentrations equally, and obtained a thin film with a minimum sheet resistance (22-25 Ω/□) with transmittance (85%), which in turn resulted in the highest figure of merit ($8.3\pm0.55 \times 10^{-3}/\Omega$). We have utilized zinc acetate dihydrate, aluminium acetyl acetonate, and indium acetate, as zinc, aluminium, and indium precursors, respectively. Various experimental variables, such as co-dopants concentration, acetic acid:water volume content, and type of Al-dopant precursor, were studied.

Additionally, for the first time, the ball milling of the precursor prior to film fabrication, was tested and reported for the deposition of transparent and conductive thin films deposited by ultrasonic spray pyrolysis technique. The results show that ball milling treatment of zinc precursor enhances the characteristics of ZnO thin films, opening the way to the manufacturing of high quality materials.

In the case of sputtering, undoped homogeneous ZnO thin films were obtained by optimizing several sputtering conditions such as target-substrate distance, power, and substrate rotation speed. We found that the rotation speed of the substrate influences in fabricating highly homogeneous films.

Further, In and Ga co-doped ZnO thin films were fabricated on glass substrates by co-sputtering, by utilizing two targets ZnO/Ga_2O_3 and In. We have obtained thin films showing the minimum sheet resistance values (270-340Ω/□) with a transmittance 91%. All the films deposited by ultrasonic spray pyrolysis and sputtering were characterized using X-ray diffractometry, Scanning electron microscopy, UV-vis spectrophotometry, and sheet

resistance measurements. These characterizations were followed to determine the structural, morphological, optical and electrical (sheet resistance) properties. Further, in order to check the suitability of co-doped ZnO thin films for TCO (Transparent Conductive Oxide) applications, figure of merit was estimated thereby the quality of the films was examined.

RESUMEN

Este trabajo presenta resultados obtenidos sobre la fabricación de películas delgadas de óxido de zinc (ZnO), sin dopar y co-dopadas, depositadas mediante rocío pirolítico ultrasónico y pulverización catódica, "sputtering".

Mediante depósito por spray, películas delgadas de ZnO sin dopar fueron depositadas en sustratos de vidrio usando acetyl acetonato de zinc como precursor. Las características físicas de las películas fueron estudiadas en función de los cambios del contenido de agua en la solución de partida. Esto nos mostró cómo el agua influye en el cambio de sus propiedades. Ya que las películas de ZnO sin dopar son altamente resistivas, nosotros hemos encontrado un procedimiento novedoso para la fabricación de películas delgadas de ZnO puras y dopadas mediante rocío pirolítico ultrasónico. En este trabajo hemos modificado las concentraciones de co-dopantes por igual, y se obtuvieron películas delgadas con una resistencia de hoja mínima del orden de (22-25 Ω/□) y una transmitancia óptica mayor a 85%, valores que condujeron a la mayor figura de mérito. En este trabajo utilizamos acetato de zinc di-hidratado, acetil-acetonato de aluminio, y acetato de indio, como precursores de zinc, aluminio, e indio, respectivamente. Los diferentes parámetros experimentales, tales como la concentración de co-dopantes, contenido de ácido acético, volumen de agua y el tipo de precursor de aluminio se variaron para realizar los depósitos.

También, por primera vez, el molido del precursor previo al depósito de las películas, se puso a prueba para el depósito de películas delgadas transparentes y conductoras depositadas por la técnica de rocío pirolítico ultrasónico. Los resultados muestran que el tratamiento mediante molienda mecánica del precursor a base de bolas mejora las características de películas delgadas de ZnO, abriendo la posibilidad de la fabricación de materiales de alta calidad.

En el caso de la técnica de sputtering, películas delgadas homogéneas de ZnO sin dopar se obtuvieron mediante la optimización de diferentes condiciones de depósito, tales como la distancia muestra-sustrato, potencia, así como la velocidad de rotación del sustrato. Se encontró que la velocidad de rotación del sustrato influye significativamente en la fabricación de películas altamente homogéneas.

Por otro lado, el co-dopado de las películas de ZnO con In y Ga se fabricaron sobre sustratos de vidrio por co-sputtering mediante la utilización de dos fuentes, ZnO/Ga_2O_3 e In. De esta manera se

obtuvieron películas con valores mínimos de resistencia de hoja del orden de (270-340Ω/□) con una transmitancia mayor al 90%.

Todas las películas depositadas mediante rocío pirolítico ultrasónico y sputtering se caracterizaron mediante difractometría de rayos X, microscopia electrónica de barrido, espectrofotometría UV-visible y mediciones de resistencia de hoja. Estas caracterizaciones permitieron determinar las propiedades estructurales, morfológicas, ópticas y eléctricas de las películas. Adicionalmente, con el fin de comprobar la calidad de las películas de ZnO co-dopadas para su aplicación en la fabricación de electrodos conductores transparentes fue evaluado con el factor o figura de mérito mediante una expresión matemática bien conocida.

MAIN OBJECTIVE

To obtain the thin films of zinc oxide (ZnO) with high figure of merit (in the order of $10^{-2}/\Omega$) by ultrasonic spray pyrolysis, and sputtering.

SPECIFIC OBJECTIVES

1) To optimize the experimental conditions for undoped ZnO thin films by ultrasonic spray and sputtering.
2) To optimize the experimental conditions for achieving aluminium and indium co-doped ZnO thin films by ultrasonic spray pyrolysis.
3) To fabricate aluminium and indium co-doped ZnO thin films by ultrasonic spray pyrolysis using ball milled zinc precursor.
4) To optimize the experimental conditions for achieving indium and gallium co-doped ZnO thin films by co-sputtering.
5) To study the structural, morphological, optical, and electrical properties of the deposited thin films.
6) To calculate the figure of merit (Haacke´s method) in order to estimate the quality of the co-doped ZnO thin films.
7) To compare the quality of thin films obtained by ultrasonic spray and sputtering.

NOMENCLATURE OF THE SAMPLES

Sample ID	Description
S0	Undoped zinc oxide thin fim prepared with 0 ml water content in the starting solution
S5	Undoped zinc oxide thin fim prepared with 5 ml water content in the starting solution
S10	Undoped zinc oxide thin fim prepared with 10 ml water content in the starting solution
S0.5	Aluminium and Indium co-doped ZnO thin film prepared with 0.5 at.% of Al and 0.5at.% of In
S1	Aluminium and Indium co-doped ZnO thin film prepared with 1 at.% of Al and 1 at.% of In
S1.5	Aluminium and Indium co-doped ZnO thin film prepared with 1.5 at.% of Al and 1.5at.% of In
S2	Aluminium and Indium co-doped ZnO thin film prepared with 2 at.% of Al and 2 at.% of In
S3	Aluminium and Indium co-doped ZnO thin film prepared with 3 at.% of Al and 3 at.% of In
A-0	Aluminium and Indium co-doped ZnO thin film prepared with 0 ml of acetic acid content in the zinc precursor solution
A-25	Aluminium and Indium co-doped ZnO thin film prepared with 25 ml of acetic acid content in the zinc precursor solution
A-50	Aluminium and Indium co-doped ZnO thin film prepared with 50 ml of acetic acid content in the zinc precursor solution
A-75	Aluminium and Indium co-doped ZnO thin film prepared with 75 ml of acetic acid content in the zinc precursor solution
A-100	Aluminium and Indium co-doped ZnO thin film prepared with 100 ml of acetic acid content in the zinc precursor solution
S25	Aluminium and Indium co-doped ZnO thin film prepared with 25 ml of acetic acid and 25 ml of water content in the zinc precursor solution

S50	Aluminium and Indium co-doped ZnO thin film prepared with 50 ml of acetic acid and 50 ml of water content in the zinc precursor solution
S100	Aluminium and Indium co-doped ZnO thin film prepared with 100 ml of acetic acid and 100 ml of water content in the zinc precursor solution
S150	Aluminium and Indium co-doped ZnO thin film prepared with 150 ml of acetic acid and 150 ml of water content in the zinc precursor solution
ALCL1	Aluminium and Indium co-doped ZnO thin film prepared using aluminium chloride (1 at.%) as a Al-precursor
ALCL1.5	Aluminium and Indium co-doped ZnO thin film prepared using aluminium chloride (1.5 at.%) as a Al-precursor
ALCL2	Aluminium and Indium co-doped ZnO thin film prepared using aluminium chloride (2 at.%) as a Al-precursor
ALCL3	Aluminium and Indium co-doped ZnO thin film prepared using aluminium chloride (3 at.%) as a Al-precursor
ALS1	Aluminium and Indium co-doped ZnO thin film prepared using aluminium sulphate (1 at.%) as a Al-precursor
ALS1.5	Aluminium and Indium co-doped ZnO thin film prepared using aluminium sulphate (1.5 at.%) as a Al-precursor
ALS2	Aluminium and Indium co-doped ZnO thin film prepared using aluminium sulphate (2 at.%) as a Al-precursor
ALS3	Aluminium and Indium co-doped ZnO thin film prepared using aluminium sulphate (3 at.%) as a Al-precursor
ALAC	Aluminium and Indium co-doped ZnO thin film prepared using aluminium acetyl acetonate as a Al-precursor
ALCL	Aluminium and Indium co-doped ZnO thin film prepared using aluminium chloride as a Al-precursor
ALSP	Aluminium and Indium co-doped ZnO thin film prepared using aluminium sulphate as a Al-precursor
U10	Aluminium and Indium co-doped ZnO thin film prepared using unmilled zinc precursor
M10	Aluminium and Indium co-doped ZnO thin film prepared using milled zinc

	precursor
LD50	Undoped ZnO thin film deposited at a target-substrate distance of 14cm using 50W power
LD75	Undoped ZnO thin film deposited at a target-substrate distance of 14cm using 75W power
LD100	Undoped ZnO thin film deposited at a target-substrate distance of 14cm using 100W power
LD125	Undoped ZnO thin film deposited at a target-substrate distance of 14cm using 125W power
SD50	Undoped ZnO thin film deposited at a target-substrate distance of 7cm using 50W power
SD75	Undoped ZnO thin film deposited at a target-substrate distance of 7cm using 75W power
SD100	Undoped ZnO thin film deposited at a target-substrate distance of 7cm using 100W power
SD125	Undoped ZnO thin film deposited at a target-substrate distance of 7cm using 125W power
R0	Undoped ZnO thin deposited at 100W without substrate rotation (0 rpm)
R20	Undoped ZnO thin deposited at 100W with substrate rotation (20 rpm)
R40	Undoped ZnO thin deposited at 100W with substrate rotation (40 rpm)
R60	Undoped ZnO thin deposited at 100W with substrate rotation (60 rpm)
R80	Undoped ZnO thin deposited at 100W with substrate rotation (80 rpm)
I3	In and Ga co-doped ZnO thin film fabricated using 3W of indium power and 40W of Ga_2O_3 power.
I5	In and Ga co-doped ZnO thin film fabricated using 5W of indium power and 40W of Ga_2O_3 power.
I10	In and Ga co-doped ZnO thin film fabricated using 10W of indium power and 40W of Ga_2O_3 power.
I15	In and Ga co-doped ZnO thin film fabricated using 15W of indium power and 40W of Ga_2O_3 power.

LIST OF FIGURES

(a)50KX, and (b)20KX

4.11.4 Surface morphology of AIZO thin films(A-75) deposited with a zinc precursor solution contains 75ml acetic acid and 25ml of water, with (Al:In = 1.5:1.5at.%) doping concentration, at 425°C, at different magnifications (a)50KX, and (b)20KX

4.11.5 Surface morphology of AIZO thin films(A-100) deposited with a zinc precursor solution contains 100ml acetic acid and 0ml of water, with (Al:In = 1.5:1.5at.%) doping concentration, at 425°C, at different magnifications (a)50KX, and (b)20KX

4.12 Optical transmittance spectra of AIZO thin films deposited with different solvent proportions using (Al:In =1.5:1.5at.%) at 425°C (A-0 deposited with 0 ml of acetic acid and 100 ml of water, A-25 deposited with 25 ml of acetic acid and 75 ml of water, A-50 deposited with 50 ml of acetic acid and 50 ml of water, A-75 deposited with 75 ml of acetic acid and 25 ml of water, A-100 deposited with 100 ml of acetic acid and 0 ml of water)

4.13 Figure of merit of AIZO thin films (A-0 deposited with 0 ml of acetic acid and 100 ml of water, A-25 deposited with 25 ml of acetic acid and 75 ml of water, A-50 deposited with 50 ml of acetic acid and 50 ml of water, A-75 deposited with 75 ml of acetic acid and 25 ml of water, A-100 deposited with 100 ml of acetic acid and 0 ml of water)

4.14 X-ray diffraction patterns of AIZO thin films deposited with equal variations of acetic acid and water (S25 deposited from a zinc precursor solution containing 25ml of acetic acid and 25ml of water, S50 deposited from a zinc precursor solution containing 50ml of acetic acid and 50ml of water, S100 deposited from a zinc precursor solution containing 100ml of acetic acid and 100ml of water, S150 deposited from a zinc precursor solution containing 150ml of acetic acid and 150ml of water)

4.15.1 Surface morphology (at different magnifications) of AIZO thin film (S25) deposited using 25ml of acetic acid and 25ml of water in the zinc precursor solution (a)100KX, (b)50KX, and (c)10KX

4.15.2 Surface morphology (at different magnifications) of AIZO thin film (S50)

LIST OF TABLES

LIST OF ABBREVIATIONS

at.%	Atomic percentage
Al	Aluminium
In	Indium
Ga	Gallium
ZnO	Zinc oxide
AIZO	aluminium and indium co-doped zinc oxide
IGZO	Indium and gallium co-doped zinc oxide
XRD	X-ray diffraction
TC	Texture co-efficient
R_s	Sheet resistance
T_{550nm}	Optical transmittance at 500nm
HRSEM	High resolution scanning electron microscopy
UV-vis	Ultra violet – visible
ITO	Indium tin oxide
SnO_2	Tin oxide
E_g	Energy bandgap
USP	Ultrasonic spray pyrolysis
RF	Radio frequency
DC	Direct current
TCO	Transparent conductive oxide
FOM	Figure of Merit
rpm	Revolution per minute
AFM	Atomic force microscopy
TM	Transition metals
SIMS	Secondary ion mass spectroscopy

TABLE OF CONTENTS

CHAPTER 1: INTRODUCTION

CHAPTER 2: THEORY

CHAPTER 3: EXPERIMENTAL

CHAPTER 1

INTRODUCTION

In this chapter a brief description of transparent conductive oxides (TCOs) as well as the characteristics of some semiconducting materials which fulfill the characteristics required for reliable manufacturing is presented. Evaluation of TCOs by a reasonable Figure of Merit that evaluates conductivity and transmittance, is also mentioned. Finally, the development of the thesis on the basis of the state of the art, experimental work, characterization and discussion, is described.

1. 1. TCOs

Transparent conducting oxides (TCOs) are electrical conductive materials with a comparably low absorption of light. They are usually prepared with thin film technologies and used in opto-electronic devices [1]. Their conductivity can be tuned from insulating via semiconducting to conducting as well as their transparency adjusted. As they can be produced as n-type and p-type, they open a wide range of power saving opto-electrical circuitries and technological applications.

The impurity-doped semiconductors usually reported for the manufacturing of reliable TCO are ZnO, In_2O_3, SnO_2 and CdO, as well as the ternary compounds Zn_2SnO_4, $ZnSnO_3$, $Zn_2In_2O_5$, $Zn_3In_2O_6$, In_2SnO_4, $CdSnO_3$, and multi-component oxides consisting of combinations of ZnO, In_2O_3 and SnO_2. Sn doped In_2O_3 (ITO) and F doped SnO_2 TCO thin films are the preferable materials for most present applications [2]. The expanding use of TCO materials, especially for the production of transparent electrodes for optoelectronic device applications, is endangered by the scarcity and high price of In. This situation drives the search for alternative TCO materials to replace ITO [3].

The actual and potential applications of TCO thin films include: (a) transparent electrodes for flat panel displays, (b) transparent electrodes for photovoltaic cells, (c) transparent thin films transistors, (d) light emitting diodes, and (e) semiconductor lasers [4-8]. In addition, the availability of raw materials and the economics of the deposition method are also significant factors in choosing the most appropriate TCO material. The selection decision is generally made by maximizing the functioning of the TCO thin film by considering all relevant parameters, and minimizing the expenses.

1. 2. Materials for TCOs

1. 2. 1. ITO

Indium tin oxide (ITO) is the most widely used transparent conducting oxide because of its two key properties, its low electrical resistivity ($x10^{-4}$ ohm-cm), figure of merit in the order of $10^{-2}/\Omega$ and optical transparency (>90% with Eg~4eV). ITO thin films are still deposited with ion assisted plasma evaporation [9], (low temperature) electron beam evaporation [10], direct current (DC) [11], radio frequency (RF) magnetron sputtering [12], pulsed DC (PDC) [13], thermal evaporation [14] or pulsed laser deposition (PLD) [15]. The biggest problems about indium tin oxide is the high cost and the solid state reaction that occurs in the junction TCO/Si during the deposition of Si under a strongly reducing environment. A similar phenomena has reported in Dye Sensitized Organic Solar Cells. Moreover, ITO is expensive because of the shortage of indium. As we know, indium is a rare mineral, researchers are looking for other materials in order to replace ITO in their research activities [16]. Solar Cell manufacturing is then moving toward either tin oxide or zinc oxide for reliable TCOs.

1. 2. 2. SnO_2

Tin Oxide (SnO_2) thin films with stability in atmospheric conditions, chemical inertness, mechanical hardness and high temperatures resistance, is the most popular among the available transparent conducting oxides. SnO_2 has a wide bandgap (2.5-3eV), transparency to visible light and resistivity ($x10^{-3}$ Ωcm). The oxygen deficiency in SnO_2 makes it a conductive material. Thin films of SnO_2 have been widely used as front electrodes in solar cells and flat-panel displays, smart windows, phototransistors as well as IR heat mirrors, low emissive windows, etc. However, it has two weaknesses. First, SnO_2 is chemically reduced by H or SiH_4 plasma which leaves a thin layer of Sn which reduces its transmission. Second, SnO_2 has only about 93–95% internal transmission over the visible spectrum. In comparison, ZnO has been shown to be plasma resistant and to have 96–97% transmission over the visible spectrum [17].

1. 2. 3. Impurity doped ZnO

At present, single element doped ZnO semiconductors are promising alternatives to ITO for thin-film transparent electrode applications. The best candidates is AZO (Aluminium doped ZnO), which can have a low resistivity, e.g. on the order of 10^{-3} ohm-cm, and its source materials are inexpensive and non-toxic. However, the development of large area, high rate deposition techniques is needed. Transparent conducting, aluminum doped zinc oxide thin films (ZnO:Al) contain about 2 or 3 at.% aluminum and can be produced with spray pyrolysis [18], sol gel technology [19], electro deposition [20], DC sputtering [21], RF sputtering [22], chemical vapor deposition (CVD) [23], electron beam evaporation [24], and pulsed laser deposition [25]. Commonly, pure zinc oxides are n-doped with aluminum. Alternatively, n-doping can be done with metals such as gallium, magnesium, indium, tin, and scandium, [26-32]. p-doping of ZnO is technologically difficult, but nitrogen, and phosphorus, seem to be an adequate dopant [33,34].

1. 2. 4. Delafossite type transparent conducting oxides

Commonly, ITO- and ZnO-based TCO thin films are n-doped, as p-doping has been shown to be technologically more difficult. Fortunately, for delafossite compound semiconductors this is reverse. They typically show TCO properties with semiconducting p-type characteristics. Delafossites, CuAO, are commonly ternary material combinations of copper, one further metal (A), and oxygen, O [35]. Copper may be replaced by silver [36], palladium [37] or platinum [38]. Further metal, A, could be iron [39], cobalt [40] or chrome [41]. Delafossites have been grown from a melt by a slow cooling-method in air [42]. They were deposited using low temperature hydro/solvothermal processes [43], the sol-gel technology [44], and the spray pyrolysis technique [45]. Moreover, advanced methods such as magnetron sputtering of prefabricated targets [46], pulsed laser deposition [47], thermal evaporation [48], and e-beam evaporation technique [49] can be employed.

1. 3. Evaluation of electrical and optical properties

1. 3. 1 Electrical resistivity

The resistivity ρ is defined as the inverse of the conductivity σ. The conductivity σ is a product of the number of charge carriers n in a material, and the mobility μ of these charge carriers, times the elementary electron charge, e. For thin films of uniform thickness d, the

electrical resistance is sometimes expressed as the sheet resistance ($R_s=\rho/d$) [50]. In order to promote conductivity, the number of charge carriers can be increased by doping [51]. Dependant on the material this can be done by substitutional doping, creation of vacancies or implantation of interstitials. Dependant on the valence of dopants or, acceptor or donor states will induce p- or n-type.

1. 3. 2 Optical properties

An important feature of TCOs is the existence of a transmission window covering most part of the visible spectrum. In literature, the optical transmission is defined as the ratio between incoming light intensity and transmitted intensity averaged over all values in between 400 nm and 700 nm. The typical spectral dependence of TCOs [52] is schematically shown in figure (Fig.1.1).

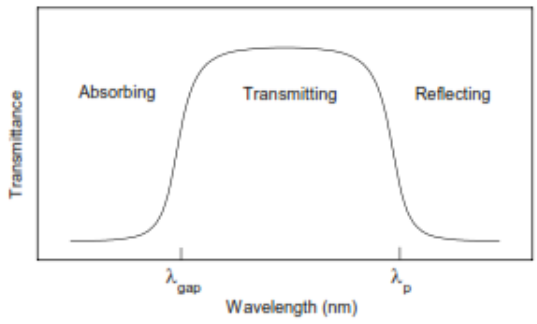

Fig. 1. 1. Spectral dependence of semiconducting transparent materials: λ_{gap} and λ_p are the wavelengths at which the bandgap absorption and reflection takes place respectively.

1. 3. 3 Correlation of electrical and optical properties

The method of preparation is of great importance for growing high quality TCO films. The physical properties of TCO thin films are strongly dependant on the structure, morphology and composition of the thin films, and the nature of the impurities. These factors are influenced by the deposition parameters of the different growth techniques. For TCO thin film preparation, a wide variety of growth techniques has been reported and examined extensively. Effective TCOs should possess both high electrical conductivity and high transmittance. Thus the ratio between the transmittance (T) and sheet resistance (R) of transparent conducting films is a figure of merit (FOM) for rating these materials. Haacke

defined a more suitable FOM to estimate the quality [53]. This figure of merit is defined as: Figure of Merit (FOM) $\Phi_{TC}=T^{10}/R_S$, where, T is the optical transmittance at 550nm, and R_S is the sheet resistance by which the quality of the films can be examined. Among the various TCO materials mentioned above, we preferred ZnO in this work for the several advantages such as abundant, non-toxic, biosafe, low-cost, large-scale production does not present environmental and health hazards, excellent optical and electrical properties.

1. 4. Presentation of this thesis

This work features with the fabrication of undoped and co-doped zinc oxide thin films on glass substrates by ultrasonic spray pyrolysis and sputtering. The quality of the thin films were analyzed using structural, morphological, optical, electrical characterization and figure of merit estimation. The four important part of the thesis is given below.

1. 4. 1. Undoped ZnO thin films fabrication by ultrasonic spray pyrolysis

Undoped ZnO thin films were prepared using zinc acetylacetonate as zinc precursor. Zn precursor was dissolved in a mixture of deionized water, methanol, and a constant acetic acid volume. The deposition was carried out at a substrate temperature of 450°C for 12 min for different water content in the starting solutions. Structural, morphological, optical and electrical properties were studied in with respect to changes in the water content in the starting solution.

1. 4. 2. Al and In co-doped ZnO thin films (AIZO) fabrication by ultrasonic spray pyrolysis

AIZO thin films were fabricated using appropriate zinc precursor solution (zinc acetate dihydrate), and dopants solutions (aluminium and indium precursor) depositions were executed. With these depositions, several parameters were optimized such as co-dopants concentration, acetic acid:water content, types of dopants precursors, and precursor ball milling to achieve figure of merit in the order of $10^{-2}/\Omega$. Physical properties such as structural, morphological, optical and electrical properties were studied with respect to the parameters mentioned above.

1. 4. 3. Undoped ZnO thin films fabrication by sputtering

Undoped zinc oxide (ZnO) thin films were deposited on soda-lime glass substrates by radio frequency (rf) sputtering at room temperature. The physical properties such as structural, morphological, optical, and electrical properties were studied by varying the sputtering power (50, 75, 100 and 125W), target-substrate distance (7-14cm) and substrate rotation speeds (0, 20, 40, 60, and 80 rpm).

1. 4. 4. In and Ga co-doped ZnO (IGZO) thin films fabrication by sputtering

IGZO thin films were grown on soda lime glass substrates by dc sputtering at room temperature. Depositions were carried out using different sputtering powers. We have examined the morphological, optical, and electrical properties with respect to change in sputtering power.

The reasons why did we prefer some important experimental conditions for the fabrication of undoped and co-doped zinc oxide thin films on glass substrates by ultrasonic spray pyrolysis and sputtering are given in the state of the art.

1. 5. State of the art

In the scientific literature, we found that there are reports based on the parameters such as temperature, solution flow rate, and solution volume for the fabrication of undoped ZnO thin films by ultrasonic spray pyrolysis [54-61]. However, no investigation has been carried out to analyze the physical properties with respect to changes in the water content in the starting solution. In this respect, we have modified the water content and studied the effect on structural, morphological, and optical properties.

In addition, we have proposed a new and simple way to fabricate co-doped ZnO thin films by ultrasonic spray pyrolysis. Additionally, we have optimized several experimental conditions, in order to achieve high figure of merit. The various parameters that we have verified were co-dopants concentration, acetic acid and water content, equal variations in solvents content, and different dopant precursor.

Mechanochemistry is a branch of chemistry which is concerned with chemical and physico-chemical transformations of substances in all states of aggregation produced by the effect of mechanical energy. It has been proposed that processes under the influence of mechanical activation can be subdivided into primary and secondary ones. The primary process (e.g. increase of internal and surface energy, and increase of surface area) generally increases the reactivity of the substance. The secondary processes (e.g. aggregation, and recrystallization) take place spontaneously in activated systems and may appear even during or after milling [62,63].

We thought this could be a key step in the deposition of films by the USP technique. In this work, it is expected that during the pretreatment (ball milling) of precursor, zinc acetate, the external energy added by the activation can also lead to bond breakage and even chemical reaction, which could significantly improve the dissolution and properties of the mist formed affecting the growth process of ZnO.

The reason for the selection of milling the precursor previous to dissolution lies in the fact that a previous work reported by Thrinath et al. [64] showed that electrical and optical properties of chemically sprayed Al doped ZnO thin films enhanced as compared with films deposited with untreated precursor. The role of the milling process of the precursors on the physical characteristics of ZnO:Al thin films deposited on sodocalcic glass substrates by an ultrasonic spray technique was presented. The main registered effect was the decrease in electrical resistivity compared to those samples deposited from unmilled precursors, since a variation of around one order of magnitude was obtained. Thus, the milling of the precursors was considered as a prior process that enhances the transport properties of chemically sprayed films. Additionally a change of the morphology with the milling time of the precursors was observed.

The hypothesis for milling the precursor previous to starting solution preparation is that new chemical species are formed under moderate energy milling. These species will change the synthesis process for ZnO as well as the properties of fabricated thin films.

In this respect, we have the studied AIZO thin film properties using ball milling of a precursor. This study showed that milling a precursor prior to thin film fabrication results

in enhancement of structural, morphological, optical, and electrical properties. This work has been appreciated by a reviewer of Materials Letters as follows: *The authors report extremely important topics, and this work deserves immediate publication.*

It is worthy to mention that our work is the first to report in the scientific community regarding co-doping of ZnO by ultrasonic spray pyrolysis.

The second part of my work includes the deposition of undoped ZnO, and IGZO (In and Ga co-doped ZnO) on glass substrates by sputtering.

The essential sputtering parameters are deposition power, pressure, substrate temperature, and distance between the target and the substrate [65-72]. In the scientific literature, substrate rotation is reported as a parameter to obtain homogeneous films [73], however, no systematic investigation has been found in optimizing the speed of substrate rotation for obtaining highly homogenous films. In this respect, we have deposited ZnO thin films by reactive sputtering at various substrate rotation speeds. We found that substrate rotation speed is influencing structural, optical, and morphological properties.

Further, we have fabricated IGZO thin films by co-sputtering. In this method, we have used two targets simultaneously and sputtered. We have placed Zinc Oxide/Gallium Oxide target in direct current magnetron and Indium target in radio frequency magnetron. Depositions were performed with respect to changes in the deposition power of indium. In addition, it is worth to mention that no work has been reported regarding IGZO thin films by co-sputtering.

1. 6. REFERENCES

[1] T.H. Kao, J.Y. Chen, C.H. Chiu, C.W. Huang, W.W. Wu, Opto-electrical properties of Sb-doped p-type ZnO nanowires, Appl. Phys. Lett. 104 (2014) 1–6. doi:10.1063/1.4869355.

[2] Ziad Y. Banyamin, Peter J. Kelly, Glen West, Jeffery Boardman, Electrical and Optical Properties of Fluorine Doped Tin Oxide Thin Films Prepared by Magnetron Sputtering, coatings, 2014, 4, 732-746 .

[3] S. Chen, S. Wang, ZnO:H indium-free transparent conductive electrodes for active-matrix display applications, Appl. Phys. Lett. 105 (2014). doi:10.1063/1.4903499.

[4] F. Html, Y. Liu, Y. Li, H. Zeng, ZnO-Based Transparent Conductive Th in Films : Doping , Performance , and Processing, 2013 (2013) 2–9.

[5] M. Zhang, X. Gao, A. Barra, P. Chang, L. Huang, R. Hellwarth, et al., Core-shell structured Si/ZnO photovoltaics, Mater. Lett. 140 (2015) 59–63. doi:10.1016/j.matlet.2014.10.083.

[6] A.M. Ma, M. Gupta, F.R. Chowdhury, M. Shen, K. Bothe, K. Shankar, et al., Zinc oxide thin film transistors with Schottky source barriers, Solid. State. Electron. 76 (2012) 104–108. doi:10.1016/j.sse.2012.05.005.

[7] S.J. Pearton, F. Ren, Advances in ZnO-based materials for light emitting diodes, Curr. Opin. Chem. Eng. 3 (2014) 51–55. doi:10.1016/j.coche.2013.11.002.

[8] D. Vanmaekelbergh, L.K. van Vugt, ZnO nanowire lasers., Nanoscale. 3 (2011) 2783–2800. doi:10.1039/c1nr00013f.

[9] S. Laux, N. Kaiser, a. Zöller, R. Götzelmann, H. Lauth, H. Bernitzki, Room-temperature deposition of indium tin oxide thin films with plasma ion-assisted evaporation, Thin Solid Films. 335 (1998) 1–5. doi:10.1016/S0040-6090(98)00861-X.

[10] J. George, C.. Menon, Electrical and optical properties of electron beam evaporated ITO thin films, Surf. Coatings Technol. 132 (2000) 45–48. doi:10.1016/S0257-8972(00)00726-X.

[11] O. Tuna, Y. Selamet, G. Aygun, L. Ozyuzer, High quality ITO thin films grown by dc and RF sputtering without oxygen, J. Phys. D. Appl. Phys. 43 (2010) 055402. doi:10.1088/0022-3727/43/5/055402.

[12] F. Kurdesau, G. Khripunov, a. F. da Cunha, M. Kaelin, a. N. Tiwari, Comparative study of ITO layers deposited by DC and RF magnetron sputtering at room temperature, J. Non. Cryst. Solids. 352 (2006) 1466–1470. doi:10.1016/j.jnoncrysol.2005.11.088.

[13] W.J. Lee, Y.K. Fang, J.-J. Ho, C.-Y. Chen, S.-F. Chen, R.-Y. Tsai, et al., Optimizing indium tin oxide thin films with bipolar d.c.-pulsed magnetron sputtering for electrochromic device applications, J. Mater. Sci. Mater. Electron. 13 (2002) 751–756. doi:10.1023/A:1021504414559.

[14] M.K.M. Ali, K. Ibrahim, M.Z. Pakhuruddin, M.G. Faraj, Optical and Electrical Properties of Indium Tin Oxide (ITO) Thin Films Prepared by Thermal Evaporation Method on Polyethylene Terephthalate (PET) Substrate, Adv. Mater. Res. 545 (2012) 393–398. doi:10.4028/www.scientific.net/AMR.545.393.

[15] V. Craciun, D. Craciun, X. Wang, T.J. Anderson, R.K. Singh, Highly conducting indium tin oxide films grown by ultraviolet-assisted pulsed laser deposition at low temperatures, Thin Solid Films. 453-454 (2004) 256–261. doi:10.1016/j.tsf.2003.11.132.

[16] http://www.sciencedirect.com/science/article/pii/0379678783900716

[17] A. Alkaya, R. Kaplan, H. Canbolat, S.S. Hegedus, A comparison of fill factor and recombination losses in amorphous silicon solar cells on ZnO and SnO_2, Renewable Energy 34 (2009) 1595–1599.

[18] S. Rahmane, M.S. Aïda, A. Chala, H. Ben Temam, A. Djouadi, Elaboration of transparent undoped ZnO and Al-doped ZnO thin films by spray pyrolysis and their properties, Plasma Process. Polym. 4 (2007) 356–358. doi:10.1002/ppap.200730908.

[19] M.J. Alam, D.C. Cameron, Preparation and properties of transparent conductive aluminum-doped zinc oxide thin films by sol–gel process, J. Vac. Sci. Technol. A Vacuum, Surfaces, Film. 19 (2001) 1642. doi:10.1116/1.1340659.

[20] O. Baka, a. Azizi, S. Velumani, G. Schmerber, a. Dinia, Effect of Al concentrations on the electrodeposition and properties of transparent Al-doped ZnO thin films, J. Mater. Sci. Mater. Electron. 25 (2014) 1761–1769. doi:10.1007/s10854-014-1796-3.

[21] T. Minami, Y. Ohtani, T. Miyata, T. Kuboi, Transparent conducting Al-doped ZnO thin films prepared by magnetron sputtering with dc and rf powers applied in combination, J. Vac. Sci. Technol. A Vacuum, Surfaces, Film. 25 (2007) 1172. doi:10.1116/1.2748809.

[22] H.-W. Wu, R.-Y. Yang, C.-M. Hsiung, C.-H. Chu, Characterization of aluminum-doped zinc oxide thin films by RF magnetron sputtering at different substrate temperature and sputtering power, J. Mater. Sci. Mater. Electron. (2012) 166–171. doi:10.1007/s10854-012-0769-7.

[23] W.-H. Kim, W.J. Maeng, M.-K. Kim, H. Kim, Low Pressure Chemical Vapor Deposition of Aluminum-Doped Zinc Oxide for Transparent Conducting Electrodes, J. Electrochem. Soc. 158 (2011) D495–D499. doi:10.1149/1.3599055.

[24] S.J. Kang, Y.H. Joung, Optical and hall properties of Al-doped ZnO thin films fabricated by pulsed laser deposition with various substrate temperatures, J. Mater. Sci. Mater. Electron. 24 (2013) 1863–1868. doi:10.1007/s10854-012-1024-y.

[25] H. Agura, H. Okinaka, S. Hoki, T. Aoki, A. Suzuki, T. Matsushita, et al., Low-resistive and transparent AZO films prepared by PLD in magnetic field, Electr. Eng. Japan (English Transl. Denki Gakkai Ronbunshi). 151 (2005) 40–45. doi:10.1002/eej.20026.

[26] L. Chow, O. Lupan, G. Chai, H. Khallaf, L.K. Ono, B. Roldan Cuenya, et al., Synthesis and characterization of Cu-doped ZnO one-dimensional structures for miniaturized sensor applications with faster response, Sensors Actuators, A Phys. 189 (2013) 399–408. doi:10.1016/j.sna.2012.09.006.

[27] R. Chauhan, A. Kumar, R.P. Chaudhary, Photocatalytic studies of silver doped ZnO nanoparticles synthesized by chemical precipitation method, J. Sol-Gel Sci. Technol. 63 (2012) 546–553. doi:10.1007/s10971-012-2818-3.

[28] R. Wang, A. W. Sleight, D. Cleary, High conductivity in gallium-doped zinc oxide powders, Chem. Mater. 8 (1996) 433–439. doi:10.1021/cm950372k.

[29] J. Singh, P. Kumar, K.S. Hui, K.N. Hui, K. Ramam, R.S. Tiwari, et al., Synthesis, band-gap tuning, structural and optical investigations of Mg doped ZnO nanowires, CrystEngComm. 14 (2012) 5898. doi:10.1039/c2ce06650e.

[30] J. Su, H. Li, Y. Huang, X. Xing, J. Zhao, Y. Zhang, Electronic transport properties of In-doped ZnO nanobelts with different concentration., Nanoscale. 3 (2011) 2182–7. doi:10.1039/c1nr10018a.

[31] V. Shelke, B.K. Sonawane, M.P. Bhole, D.S. Patil, Electrical and optical properties of transparent conducting tin doped ZnO thin films, J. Mater. Sci. Mater. Electron. 23 (2012) 451–456. doi:10.1007/s10854-011-0462-2.

[32] M. Lorenz, C. Schmidt, G. Benndorf, T. Böntgen, H. Hochmuth, R. Böttcher, et al., Degenerate interface layers in epitaxial scandium-doped ZnO thin films, J. Phys. D. Appl. Phys. 46 (2013) 065311. doi:10.1088/0022-3727/46/6/065311.

[33] M.-L. Tu, Y.-K. Su, C.-Y. Ma, Nitrogen-doped p-type ZnO films prepared from nitrogen gas radio-frequency magnetron sputtering, J. Appl. Phys. 100 (2006) 053705. doi:10.1063/1.2337766.

[34] J.C. Fan, K.M. Sreekanth, Z. Xie, S.L. Chang, K. V. Rao, P-Type ZnO materials: Theory, growth, properties and devices, Prog. Mater. Sci. 58 (2013) 874–985. doi:10.1016/j.pmatsci.2013.03.002.

[35] A. Stadler, Transparent Conducting Oxides—An Up-To-Date Overview, Materials (Basel). 5 (2012) 661–683. doi:10.3390/ma5040661.

[36] W.C. Sheets, E.S. Stampler, M.I. Bertoni, M. Sasaki, T.J. Marks, T.O. Mason, et al., Silver delafossite oxides, Inorg. Chem. 47 (2008) 2696–2705. doi:10.1021/ic702197h.

[37] http://www.sciencedirect.com/science/article/pii/0025540886901558

[38] M. A. Marquardt, N. A. Ashmore, D.P. Cann, Crystal chemistry and electrical properties of the delafossite structure, Thin Solid Films. 496 (2006) 146–156. doi:10.1016/j.tsf.2005.08.316.

[39] E. Mugnier, A. Barnab, L. Presmanes, P. Tailhades, Thin films preparation by rf-sputtering of copper/iron ceramic targets with Cu/Fe = 1: From nanocomposites to delafossite compounds, Thin Solid Films. 516 (2008) 1453–1456. doi:10.1016/j.tsf.2007.05.030.

[40] J. Tate, M.K. Jayaraj, A. D. Draeseke, T. Ulbrich, A. W. Sleight, K. A. Vanaja, et al., p-Type oxides for use in transparent diodes, Thin Solid Films. 411 (2002) 119–124. doi:10.1016/S0040-6090(02)00199-2.

[41] S.H. Lim, S. Desu, A. C. Rastogi, Chemical spray pyrolysis deposition and characterization of p-type CuCr1-xMgxO2 transparent oxide semiconductor thin films, J. Phys. Chem. Solids. 69 (2008) 2047–2056. doi:10.1016/j.jpcs.2008.03.007.

[42] J. Pellicer-Porres, A. Segura, D. Kim, Refractive index of the CuAlO 2 delafossite, Semicond. Sci. Technol. 24 (2009) 015002. doi:10.1088/0268-1242/24/1/015002.

[43] T. Sato, K. Sue, H. Tsumatori, M. Suzuki, S. Tanaka, A. Kawai-Nakamura, et al., Hydrothermal synthesis of CuAlO2 with the delafossite structure in supercritical water, J. Supercrit. Fluids. 46 (2008) 173–177. doi:10.1016/j.supflu.2008.04.002.

[44] J. Wang, P. Zheng, D. Li, Z. Deng, W. Dong, R. Tao, et al., Preparation of delafossite-type CuCrO2 films by sol-gel method, J. Alloys Compd. 509 (2011) 5715–5719. doi:10.1016/j.jallcom.2011.02.149.

[45] A.H.O. Alkhayatt, S.M. Thahab, I.A. Zgair, Nanocrystalline CuFeO 2 Delafossite Thin Films Prepared on, (n.d.) 165–168.

[46] H. Sun, M. Arab Pour Yazdi, P. Briois, J.F. Pierson, F. Sanchette, A. Billard, Towards delafossite structure of Cu-Cr-O thin films deposited by reactive magnetron sputtering: Influence of substrate temperature on optoelectronics properties, Vacuum. 114 (2015) 101–107. doi:10.1016/j.vacuum.2015.01.009.

[47] F. Mao, T. Nyberg, T. Thersleff, A.M. Andersson, U. Jansson, Combinatorial magnetron sputtering of AgFeO2 thin films with the delafossite structure, Mater. Des. 91 (2016) 132–142. doi:10.1016/j.matdes.2015.11.092.

[48] N. Wongcharoen, T. Gaewdang, T. Wongcharoen, Structural and Thermoelectric Properties of Zn-Doped Cuprous Aluminate Delafossite, Adv. Mater. Res. 747 (2013) 333–336. doi:10.4028/www.scientific.net/AMR.747.333.

[49] A. Stadler, Transparent Conducting Oxides—An Up-To-Date Overview, Materials (Basel). 5 (2012) 661–683. doi:10.3390/ma5040661

[50] http://hyperphysics.phy-astr.gsu.edu/hbase/electric/resis.html

[51] V.K. Jayaraman, A.M. Álvarez, Y.M. Kuwabara, Y. Koudriavstev, M.D.L.L. Olvera Amador, Effect of co-doping concentration on structural, morphological, optical and electrical properties of aluminium and indium co-doped ZnO thin films deposited by ultrasonic spray pyrolysis, Mater. Sci. Semicond. Process. 47 (2016) 32–36. doi:10.1016/j.mssp.2016.02.011.

[52] F. Simons, Physics of doped tin dioxide films for spectral-selective surfaces, Solar Energy materials, 1, 3(4), 221-231.

[53] G. Haacke, New figure of merit for transparent conductors, J. Appl. Phys. 47 (1976) 4086–4089. doi:10.1063/1.323240.

[54] C. Huang, M. Wang, Substrate Temperature Dependence of ZnO Films Prepared by Ultrasonic Spray Pyrolysis, Jpn. J. Appl. Phys. 35 6208. (n.d.).

[55] A.K. Prasad, S. Dhara, Effect of substrate temperature on microstructural , vibrational and electrical properties of ZnO nanostructured thin films, Nanosystems, 7 (2016) 506–508. doi:10.17586/2220-8054-2016-7-3-506-508.

[56] Y. Benkhetta, A. Attaf, H. Saidi, A. Bouhdjar, H. Benjdidi, I.B. Kherchachi, et al., Optik Influence of the solution flow rate on the properties of zinc oxide (ZnO) nano-crystalline films synthesized by ultrasonic spray process, Opt. - Int. J. Light Electron Opt. 127 (2016) 3005–3008. doi:10.1016/j.ijleo.2015.11.236.

[57] R.S. Gaikwad, G.R. Patil, M.B. Shelar, B.N. Pawar, R.S. Mane, S.H. Han, et al., Nanocrystalline ZnO Films Deposited by Spray Pyrolysis :, International Journal of Self_Propagating High_Temperature Synthesis, 2012, Vol. 21, No. 3, pp. 178–182. doi:10.3103/S106138621203003X.

[58] A. Attaf, Y. Benkhetta, H. Saidi, A. Bouhdjar, H. Bendjedidi, M. Nouadji, et al., The effect of the solution flow rate on the properties of zinc oxide (ZnO) thin films deposited by ultrasonic spray The Effect of The Solution Flow Rate on The Properties of Zinc Oxide (ZnO) Thin Films Deposited by Ultrasonic Spray, AIP Conference Proceedings 1653, 020015 (2016). doi:10.1063/1.4914206.

[59] Y. Aoun, B. Benhaoua, B. Gasmi, S. Benramache, Structural , optical and electrical properties of zinc oxide thin films deposited by a spray pyrolysis technique, Journal of Semiconductors, 36 (2015) 1–5. doi:10.1088/1674-4926/36/1/013002.

[60] A. R. Bari, L. A. Patil, Characterizations of Ultrasonically Prepared Nanostructured ZnO powder and NH 3 Sensing Performance of its Thick Film Sensor, P.M. Science (2016) 1–5. doi:10.1016/j.mspro.2014.07.210Get.

[61] S. Benramache, A. Rahal, B. Benhaoua, The effects of solvent nature on spray-deposited ZnO thin film prepared from Zn ($CH_3COO)_2$, $2H_2O$, Optik 125 (2014) 2013–2015.

[62] P. Bala, M. Criado, F. Delogu, Z. Cherkezova-zheleva, E. Gaffet, F. Jose, et al., Chem Soc Rev, (2013) 7571–7637. doi:10.1039/c3cs35468g.

[63] Q. Tan, J. Li, Recycling Metals from Wastes : A Novel Application of Mechanochemistry, Environmental science and Engg. (2015) 49, 5849-5961. doi:10.1021/es506016w.

[64] T. Ramireddy, V. Venugopal, J. Bellam, A. Maldonado et al, Effect of the Milling Time of the Precursors on the Physical Properties of Sprayed Aluminum-Doped Zinc Oxide (ZnO:Al), Materials 2012, 5, 1404-1412.

[65] C. Tien, K. Yu, T. Tsai, M. Liu, Applied Surface Science Effect of RF power on the optical , electrical , mechanical and structural properties of sputtering Ga-doped ZnO thin films, Appl. Surf. Sci. 354 (2015) 79–84. doi:10.1016/j.apsusc.2015.02.154.

[66] D. Hwang, K. Bang, M. Jeong, J. Myoung, Effects of RF power variation on properties of ZnO thin films and electrical properties of p – n homojunction,Journal of crystal growth, 254 (2003) 449–455. doi:10.1016/S0022-0248(03)01205-3.

[67] W.L. Dang, Y.Q. Fu, J.K. Luo, A.J. Flewitt, W.I. Milne, Deposition and characterization of sputtered ZnO films, Superlattices and Microstructures, 42 (2007) 89–93. doi:10.1016/j.spmi.2007.04.081.

[68] N. Ameera, A. Shuhaimi, S. Najwa, K.M. Hakim, M. Mazwan, Effects of Pressure Dependence on Nanocolumnar Zinc Oxide Deposited by RF Magnetron Sputtering, Advanced Materials Research, 832 (2014) 787–791. doi:10.4028/www.scientific.net/AMR.832.787.

[69] S. Eisermann, J. Sann, A. Polity, B.K. Meyer, Sputter deposition of ZnO thin fi lms at high substrate temperatures, Thin Solid Films. 517 (2009) 5805–5807. doi:10.1016/j.tsf.2009.02.145.

[70] A.A. Ahmad, A.M. Alsaad, B.A. Albiss, M.A.- Akhras, H.M. El-nasser, I.A. Qattan, The effect of substrate temperature on structural and optical properties of D . C . sputtered ZnO thin fi lms, Phys. B Phys. Condens. Matter. 470-471 (2015) 21–32. doi:10.1016/j.physb.2015.05.005.

[71] P.Y. Dave, K.H. Patel, K. V Chauhan, A. Kumar, S.K. Rawal, " Examination of zinc oxide films prepared by magnetron sputtering ," Procedia Technology 23 (2016) 328–335. doi:10.1016/j.protcy.2016.03.034.

[72] R.O. Ndong, H.M. Omanda, P. Souloungangа, Effect of target to substrate distance on the properties of rf sputtered ZnO thin films, IJRRAS, 17 (2013) 122–126.

[73] J. B. Lee, H. J. Kim, S. G. Kim, C. S. Hwang, S. Hong, Y. H. Shin, N. H. Lee, Deposition of ZnO thin films by magnetron sputtering for a film bulk acoustic resonator, Thin Solid Films. 435 (2003) 179–185.

CHAPTER 2

THEORY

This chapter describes zinc oxide's (ZnO) history, properties such as structural, electrical, optical, piezoelectric, magnetic, and thermal. Further, the different techniques that can be employed to prepare ZnO thin films are given such as physical and chemical techniques. Finally, the various applications for which the fabricated films can be employed are discussed in detail.

2. 1. History of ZnO

The data collections in scopus give more than 85,779 (21st July 2016) publications for zinc oxide (ZnO) [1]. During the past few years, the rate of ZnO entries excedes 7000 per annum. This does not mean that ZnO is a new semiconductor; indeed it is an old semiconductor. ZnO is being investigated systematically since 1912 [2]. Perhaps the first use of ZnO for electronic applications was in build your own radio sets in the 1920's [3]. A Schottky barrier was created by contacting a ZnO crystal with a copper wire, providing the rectification needed to convert the AC radio waves to DC signals. The first wide spread use of ZnO in electronics was for varistors, allowing reliable surge protection. Without this advance, use of electronics in the home would not have been posible without constantly replacing components [4]. The renewed interested in ZnO as an optoelectronic material has been triggered by reports on p-type conductivity, diluted ferromagnetic properties, thin film oxide field effect transistors, and considerable progress in nanostructure fabrication [5].

A major driving force of research on zinc oxide as a semiconductor material is its prospective use as a wide band gap semiconductor for light emitting devices and for transparent or high temperature electronics [6].

ZnO has an exciton binding energy of 60 meV. This is higher than the effective thermal energy at 300 K (26 meV). Therefore, excitonic gain mechanisms could be expected at room temperature for ZnO-based light emitting devices. However, a prerequisite is to prepare p-type zinc oxide, which is normally an n-type semiconductor. In the last decade, a lot of efforts were undertaken, to prepare p-type ZnO by doping with nitrogen, phosphorous, and arsenic [7,8].

2. 2. Properties of ZnO

2. 2.1. Crystal structure and Chemical Binding

II group element Zn, and VI group element O make a compound semiconductor ZnO. The electronic configuration of Zn and O are $1s^2\ 2s^2\ 2p^6\ 3s^2\ 3p^6\ 3d^{10}\ 4s^2$, and $1s^2\ 2s^2\ 2p^4$. ZnO crystal structure is determined by tetrahedrally coordinated bonding geometry Each zinc ion has four oxygen neighbour ions in a tetrahedral configuration and viceversa. The bonding between Zn and O is covalent. The tetrahedrons has bi-layers, each one consisting of a zinc and an oxygen layer. This arrangement of tetrahedrons results in hexagonal wurtzite structure (Fig. 2.1) depending on the stacking sequence of bi-layers [2].

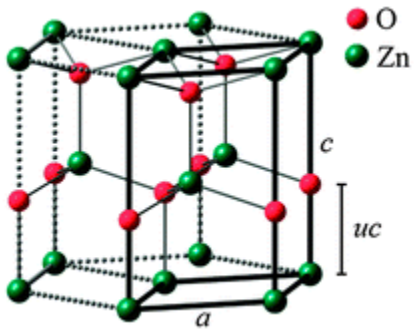

Fig. 2.1. ZnO wurtzite structure [9].

At ambient pressure and temperature, ZnO crystals are in wurtzite structure as shown in above Fig.2.1. This is a hexagonal lattice and is characterized by two interconnecting sublattices of Zn^{2+} and O^{2-}, such that each Zn ion is surrounded by a tetrahedra of O ions, and vice-versa. This tetrahedral coordination gives rise to polar symmetry along the hexagonal axis. This polarity is responsable for a number of the properties of ZnO, including piezoelectricity and spontaneous polarization, and is also a key factor in crystal growth, etching and defect generation.

The four most common face terminations of wurtzite ZnO are the polar Zn terminated (0001) and O terminated $(000\bar{1})$ faces (c-axis oriented), and the non-polar $(11\bar{2}0)$ (a-axis) and $(10\bar{1}0)$ faces which both contain an equal number of Zn and O atoms. The polar faces are known to posses different physical properties, and the O terminated face possess a slightly different electronic structure to the other three faces. Additionally, the polar

surfaces and the (1010) surface are found to be stable, however the $(11\bar{2}0)$ face is less stable and generally has a higher level of Surface roughness than its counterparts. The (0001) plane is also basal. The lattice parameters of the hexagonal unit cell are a=3.2495 Å, and c=5.2069 Å , and the density is 5.608 gcm^{-3}.

In an ideal wurtzite crystal, the axial ratio c/a and the u parameter (which is a measure of the amount by which each atom is displaced with respect to the next along the c-axis) are correlated by the relationship $uc/a=(3/8)^{1/2}$, where $c/a=(8/3)^{1/2}$ and u=3/8 for an ideal crystal. ZnO crystals deviate from this ideal arrangement by changing both of these values. This deviation occurs such that tetrahedral distances are kept roughly constant in the lattice. Experimentally, for wurtzite ZnO, the real values of u and c/a were determined in the range u=0.3817-0.3856 and c/a=1.593-1.6035 [10-12].

2. 2. 2. Electrical properties

There has been an intense study on the electrical properties of undoped ZnO material (films, single crystals, and 1D nanostructures), both experimentally and theoretically. The undoped ZnO is an intrinsic n-type semiconductor. In order to enhance the electrical properties it is mandatory to dope ZnO with a suitable material. Basically, good donors or acceptors should have an ionic radius close to that of the host ion in order to retain the lattice structure and must also have close electronegativity to energetically favor its incorporation into the lattice. Table 2.1 summarizes the valence and ionic radii of various candidate dopant atoms for ZnO [13].

Table 2.1. Valence and ionic radius of elements suitable for doping with ZnO

Atom	**Valence**	**Ionic radius (Å)**
Zn	2+	0.60
Al	3+	0.39
Ga	3+	0.47
In	3+	0.62
As	3+	0.58
P	3+	0.58
F	1-	1.31

Li	1+	0.59
Na	1+	1.13

It has been demonstrated that Al, Ga, and In are good shallow and efficient donors when they replace Zn according to the equation:

$$D^o \leftrightarrow D^+ + e^-$$

where D^o and D^+ are the neutral and ionized donors, respectively.

Similarly, for p type doping, the equation will be,

$$A^o \leftrightarrow A^- + \text{hole}$$

Where A^o and A^- are the neutral and ionized acceptors, respectively.

2. 2. 3. Optical properties

ZnO has a band gap of 3.37 eV, which corresponds to emission in the UV region. This band gap is very close to that of GaN (3.39eV), and GaN has been the subject of much research over the past years, even being incorporated into the recent Blu-Ray drives. However, ZnO has some significant advantages in its large free exciton binding energy (60 meV compared to 21-25 meV for GaN) that allows for efficient excitonic emission at room temperature.

The application of semiconductors in electro-optical devices relies on their ability to efficiently emit or detect light. If photons of energy greater than or equal to the bandgap are incident on a semiconductor, they may excite an electron from the valence band to the conduction band. In this process, the photon is absorbed and an electron–hole pair is created. In the reverse process, an electron in the conduction band may return to the valence band and recombine with a hole, the energy lost by the electron creating a photon. As the energies of the electron and the hole will generally be very close to the bottom of the conduction band and the top of the valence band, respectively, the emitted photon will have energy approximately equal to the bandgap of the semiconductor.

The optical properties of a semiconductor are connected with both intrinsic and extrinsic effects. They have been studied by several methods, such as photoluminescence (PL), cathodoluminescence (CL), and electroluminescence (EL). Among them, continuous-wave (CW) PL is a suitable tool to determine the crystalline quality and the presence of

impurities in the material as well as exciton fine structures. PL spectra of ZnO nanostructures measured at room temperature and low temperature have been intensively studied. In particular, 1D ZnO nanostructures have attracted a great attention with a possibility to develop nanoscale electronic and optoelectronic devices. The PL spectrum of ZnO nanostructures typically consists of a UV emission and possibly one or more visible bands due to defects and/or impurities [13]. Thus optical and electrical properties are important aspects in designing a device. Hence we have made a search with respect to optical and electrical and tabulated some of the results in Table 2.2.

Table 2.2. Compilation of electrial resistivity and optical transmittance from recent works

Sl. No	Technique	Dopant	Resistivity Ω cm	Transmittance (%)	Year	REF.
1	USP	B	2.40×10^{-3}	80	2015	[14]
2	USP	Al	$2x10^{-2}$	78	2014	[15]
3	USP	Al	$2.6x10^{-3}$	70	2015	[16]
4	SP	In	$6.86x10^{1}$	75	2015	[17]
5	USP	In	$3.42x10^{-3}$	52	2014	[18]
6	USP	Ga	$4.21x10^{-3}$	82	2012	[19]
7	USP	Al	$2x10^{-2}$	80	2014	[20]
8	Sputtering	Al	$5.23x10^{-4}$	80	2013	[21]
9	Sputtering	Al	$2.25x10^{-3}$	35	2013	[22]
10	Sputtering	Al	$3.3x10^{-4}$	83	2012	[23]
11	Sputtering	In	$3.61x10^{-4}$	74	2014	[24]
12	Sputtering	Ga	$3.4x10^{-3}$	75	2011	[25]
13	Sputtering	Ga	$4.4x10^{-4}$	85	2007	[26]
14	Sputtering	Al, Ga	$4x10^{-4}$	92	2013	[27]
15	PLD	Al, Ga	$2.2x10^{-4}$	95	2009	[28]
16	Sputtering	Al, Ga	$4.3x10^{-4}$	92	2014	[29]
17	Sputtering	Al, In	$2.6x10^{-4}$	81	2011	[30]
18	Sputtering	In, Ga	$5.91x10^{-4}$	83	2015	[31]

19	Sputtering	In, Ga	$8x10^{-3}$	82	2013	[32]
20	Spray pyrolysis	In, F	$6.1x10^{-2}$	75	2016	[33]
21	Spray pyrolysis	Al, In	$3.3x10^{-1}$	83	2016	[33]

2. 2. 4. Morphological properties

Using deposition techniques nanocombs, nanorings, nanohelixes/nanosprings, nanobows, nanobelts, nanowires, and nanocages of ZnO have been synthesized under specific growth conditions. These unique nanostructures unambiguously demonstrate that ZnO is probably the richest family of nanostructures among all materials, both in structures and properties. The nanostructures could have novel applications in optoelectronics, sensors, transducers, and biomedical science because it is bio-safe [34].

2. 2. 5. Piezoelectric properties

The materials with piezoelectricity can convert mechanical energy into electrical energy, and vice versa, which is very promising to solve the energy problems in the near future, so the investigations of materials with high piezoelectric coefficients have been appealing research topics for long time.

As an important semiconductor, ZnO has attracted extensive interest owing to its highest piezoelectric coefficient among the II-VI compounds. Comparing with similar II-VI compounds such as ZnS, CdS, and CdSe, which share the same wurtzite structure, the piezoelectric tensor of ZnO is at least two times of those materials. Therefore, the researches of the piezoelectricity in ZnO have been always a hot topic. It is very important for the future application, because fine tuning of the piezoelectric properties for specific device applications can be achieved by control of the ZnO lattice constant, for example by epitaxial growth on an appropriate substrate.

Because of its high piezoelectricity, semiconducting and some other excellent properties, ZnO has been used in plenty of practical nanodevices. The piezoresistive element could be used to detect the strain as well as provide the feedback signal for the ZnO actuator. Wang et al. utilized the piezoelectric properties of ZnO nanowires to invent direct-current nanogenerator [35]. They successfully converted nanoscale mechanical energy into electrical energy by means of piezoelectric ZnO nanowire (NW) arrays. The coupling of

piezoelectric and semiconducting properties in ZnO creates a strain field and charge separation across the NWs as a result of its bending. The rectifying characteristic of the schottky barrier formed between the metal tip and the NWs leads to electrical current generation. This approach has the potential of converting mechanical, or vibrational energy into electricity for powering nanodevices [36].

2. 2. 6. Magnetic properties

Diamagnetic oxides can, under certain conditions, become ferromagnetic at room temperature and therefore are promising candidates for future material in spintronic devices. Contrary to early predictions, doping ZnO with uniformly distributed magnetic ions is not essential to obtain ferromagnetic samples. Instead, the nanostructure seems to play the key role, as room temperature ferromagnetism was also found in nanograined, undoped ZnO. However, the origin of room temperature ferromagnetism in primarily non–magnetic oxides like ZnO is still unexplained and a controversial subject within the scientific community [37].

2. 2. 7. Thermal properties

As in all solids, the atoms in a semiconductor at nonzero temperature are in ceaseless motion, oscillating about their equilibrium states. The amplitude of the vibrations increases with temperature, and the thermal properties of the semiconductor determine the response of the material to temperature changes. Thermal expansion, specific heat, and pyroelectricity are among the standard material properties that define the linear relationships between mechanical, electrical, and thermal variables. These thermal properties and thermal conductivity depend on the ambient temperature, and the ultimate temperature limit to study these effects is the melting temperature, which is 1975 K for ZnO. It should also be noted that because ZnO is widely used in thin-film form deposited on foreign substrates, the properties of the ZnO films also depend on the inherent properties of the substrates, such as lattice constants and thermal expansion coefficients [38].

2. 2. 8. Amenability to wet chemical etching

Semiconductor device fabrication processes greatly benefit from the amenability to ‘low-temperature wet chemical etching’. It has been reported that ZnO thin films can be etched with acidic, alkaline as well as mixture solutions.

The possibility of low-temperature chemical etching adds great flexibility in the processing, designing and integration of electronic and optoelectronic devices [39].

2. 3. Fabrication of ZnO thin films

Growth technique played a significant role in controlling the properties of ZnO films, because the same material deposited using two different techniques, usually had different physical properties. This was due to the fact that the electrical and optical properties of the films strongly depended on the structure, morphology and the nature of impurities present. Moreover the films grown using any particular technique might have different properties due to the variation of various deposition parameters and hence the properties can be tailored by controlling the deposition parameters.

The specific technique that has been used to grow the ZnO thin films include chemical vapour deposition (CVD), Sol gel, Ultrasonic Spray Pyrolysis (USP), Pulsed Laser Deposition, Sputtering and evaporation of oxide materials. Each process has its own merits and demerits.

2. 3. 1. Thermal evaporation

A thermal evaporator uses an electric resistance heater to melt the material and raise its vapor pressure to a useful range. This is done in a high vacuum, both to allow the vapor to reach the substrate without reacting with or scattering against other gas phase atoms in the chamber, and reduce the incorporation of impurities from the residual gas in the vacuum chamber. Thermal evaporation is the simplest way of depositing material onto a substrate. One major disadvantage of this is that a lot of material is lost in the process [40].

2. 3. 2. Magnetron Sputtering

Magnetron sputtering has developed rapidly over the last decade to the point where it has become established as the process of choice for the deposition of a wide range of industrially important coatings [41]. In the basic sputtering process, a target is bombarded by energetic ions generated in a glow discharge plasma, situated in front of the target. The bombardment process causes the removal (sputtering) of target atoms, which may then deposit on a substrate as a thin film. Secondary electrons are also emitted from the target surface as a result of the ion bombardment, and these electrons play an important role in maintaining the plasma. The basic sputtering process has been known for many years and

many materials have been successfully deposited using this technique [42,43]. However, the process is limited by low deposition rates, low ionisation eciencies in the plasma, and high substrate heating e!ects. These limitations have been overcome by the development of magnetron sputtering.

Magnetrons make use of the fact that a magnetic field configured parallel to the target surface can constrain secondary electron motion to the vicinity of the target. The magnets are arranged in such a way that one pole is positioned at the central axis of the target and the second pole is formed by a ring of magnets around the outer edge of the target (Fig.2.2). Trapping the electrons in this way substantially increases the probability of an ionising electron-atom collision occurring. The increased ionisation efficiency of a magnetron results in a dense plasma in the target region. This, in turn, leads to increased ion bombardment of the target, giving higher sputtering rates and, therefore, higher deposition rates at the substrate. In addition, the increased ionisation efficiency achieved in the magnetron mode allows the discharge to be maintained at lower operating pressures (typically, 10^{-3} mbar) [44].

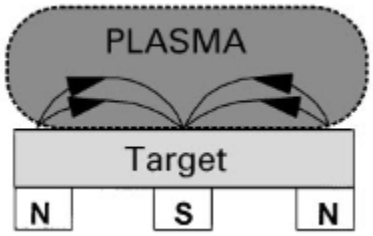

Fig. 2.2. Magnetic field and plasma formation [44].

All sputtered particles leaving the target can collide with the gas atoms present in the vacuum chamber during transit to the substrate. The same is true for ions which are neutralized and reflected at the target, and for negative ions formed at the target. Collisions will alter particle energy, direction, and momentum, and therefore also the morphology and microstructure of the growing film. The most important parameter influencing gas phase transport is pressure [45] .

There are various types of magnetron sputtering such as radio frequency (RF), direct current (DC), high power impulse magnetron sputtering (HPIMS), and reactive magnetron sputtering. These are explained below in detail.

In RF sputtering, when applying a high frequency (typically 13.56 MHz) power source between two electrodes, the light (low mass) electrons respond instantaneously to the rapidly varying field, while the heavier ions are inertially confined. That is, the ion transit time to either electrode is very much less than the rf period forcing both electrodes to charge negatively. In order to maintain charge neutrality per cycle, the entire rf waveform must then shift down in voltage such that each electrode is positive (attracting electrons) for less than 1% of an rf period and the ions, to first order, respond to an average applied voltage which is approximately one-half the rf peak-to-peak potential [46].

Fig. 2.3. Sputtering deposition unit

In the case of DC sputtering, when argon gas is introduced into a vacuum chamber at a pressure of 1 to 10 mTorr, dc voltage ionizes Argon atoms and creates a plasma, hot gas-like phase consisting of ions and electrons, in the chamber. This plasma is also known as a glow discharge due to the light emitted. These Argon ions are now charged and are accelerated to the target. Their collision with the target ejects target atoms, which travel to the substrate and eventually settle. Electrons released during argon ionization are accelerated to the anode substrate, subsequently colliding with additional argon atoms, creating more ions and free electrons in the process, continuing the cycle [47].

HPIMS uses a large energy impulse supplied to the cathode over a very short time period, typically ~ 100 µs. This requires a very different type of power supply, the heart of which is a large bank of capacitors. The HIPIMS process delivers a large low energy flux of ions to the substrate. Peak powers up to several MW/pulse with pulse widths between 100 and 150

μs must be generated by the power supply. Average powers are ~20 kW with frequencies up to 500 Hz. In addition to supplying pulsed power, arc suppression is also necessary. This process takes advantage of enhanced ionization resulting from the high energy pulse [48].

In the case of reactive sputtering, a reactive gas is use to form a compound along with argon. The reactive gas, e.g. oxygen. can react with the sputtered material to form a compound on the substrate. However, the addition of the reactive gas to the discharge influences the deposition process in several ways while increasing the complexity of the overall process. Some aspects of the reactive sputter deposition processes are discussed in this section [49]. Deposition of undoped ZnO, Al-doped ZnO, In-doped ZnO, and Ga-doped ZnO can be performed using DC/RF/reactive sputtering. The various parameters involved in sputtering are power, pressure, target-substrate distance and substrate temperature [50-114]. In the scientific literature, however, no systematic investigation has been found in optimizing the speed of substrate rotation for obtaining highly homogenous films. In this respect, we have deposited ZnO thin films by reactive sputtering at various substrate rotation speeds, using the system as shown in Fig. 2.3. We found that substrate rotation speed is influencing structural, optical, and morphological properties. Further, we have fabricated IGZO thin films by co-sputtering. In this method, we have used two targets simultaneously and sputtered.

2. 3. 3. Pulsed laser deposition

Pulsed laser deposition (PLD) is one of the sophisticated techniques for depositing transparent semiconducting oxides. Recently PLD technique attained importance among the different techniques employed to fabricate crystalline thin films with good crystallinity.

PLD technique involves evaporation of a solid target in a High Vacuum/Ultra High Vacuum chamber, by means of short and high-energy laser pulses. A pulsed laser beam vaporizes the surface of the target, and the vapour condenses on the substrate, producing a film with the same composition as the target. This is the result of the extremely high heating rate of the target surface (10^8 K/s) due to pulsed laser irradiation. It leads to the congruent evaporation of the target irrespective of the evaporating point of the constituent elements or compounds of the target. Because of the high heating rate of the ablated materials, laser deposition of crystalline film demands a much lower substrate temperature than other film growth techniques. For this reason, the semiconductor and the underlying

integrated circuit are not damaged from thermal degradation. Main components are a laser, optics, and a vacuum system. It not only involves the physical process of the laser-material interaction of the impact of high-power pulsed radiation on solid target, but also the formation of the plasma plume with high energetic species and even the transfer of the ablated material through the plasma plume onto the substrate surface. The targets used in PLD are small compared to the large size required for sputtering techniques. It is quite easy to produce multi-layered films of different materials by sequential ablation of assorted targets. Besides, by controlling the number of pulses, a fine control of film thickness down to even atomic monolayer can be achieved [115].

2. 3. 4. Ultrasonic spray pyrolysis

It consists mainly of the spraying unit, the starting solution feeding unit, and the temperature control unit. The starting solution is prepared by dissolving the desired precursors into solvent using a magnetic stirring. The solution is flowed to a ultrasonic humidifier, by which a mist formed. The mist is carried towards the heated substrate using nitrogen gas as a carrier gas. The temperature of the substrate is controlled by a temperature controller. This technique offers numerous advantages such as cost effectiveness, simple experimental setup and large area depositions [116-121]. In comparison with other thin film deposition methods, spray pyrolysis has many advantages including: open-atmosphere process, open reaction chamber, easy access to observe the deposition process and adjustment during the experiment. It has also the multi-layer fabrication capability which is very attractive for making functionally graded films. The composition of the film can be adjusted by changing the precursor solutions. Spray pyrolysis is of great practical interest in processing dense and porous films for SOFC electrolyte and electrodes, by optimizing the deposition variables such as: deposition temperature, substrate temperature, precursor composition and concentration, solvent composition, solution flow rate, carrier gas ratio and flow rate, etc [122-129]. Films can be also obtained on large surfaces at temperatures ~ 500 °C. One of the major advantages of spray pyrolysis over the vapor-phase routes is the possibility of producing multicomponent particles with exact desirable stoichiometry in the final product. In our work, we have deposited undoped ZnO by ultrasonic spray pyrolysis. In the scientific literature, we found that there are reports based on the parameters such as temperature, solution flow rate, and

solution volume [122-129]. However, no investigation has been carried out to analyze the physical properties with respect to changes in the water content in the starting solution. In this respect, we have modified the water content and deposited undoped ZnO thin films.

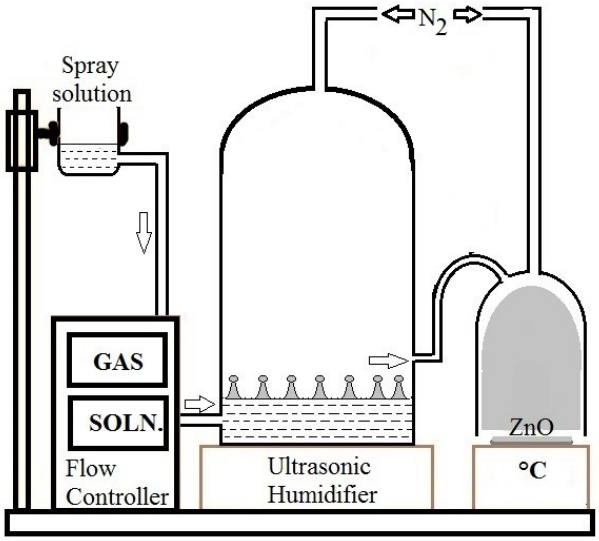

Fig. 2.4. Schematic of ultrasonic spray pyrolysis

In the literature there are several reports based on single element (Al/In/Ga/Mg) doped ZnO fabricated by ultrasonic spray pyrolysis [130-160]. However, no investigation has been carried out on co-doping by ultrasonic spray pyrolysis. In this respect, we have fabricated (using the system as shown in Fig. 2.4) AIZO thin films optimized several experimental conditions, in order to achieve high figure of merit. The various parameters that we have verified were co-dopants concentration, acetic acid and water content, equal variations in solvents content, and different dopant precursor.

2.3.5. Precursor ball milling and ultrasonic spray pyrolysis

Mechanochemistry is a branch of chemistry which is concerned with chemical and physico-chemical transformations of substances in all states of aggregation produced by the effect of mechanical energy. It has been proposed that processes under the influence of mechanical activation can be subdivided into primary and secondary ones. The primary process (e.g. increase in internal and surface energy, and increase in surface area) generally increases the reactivity of the substance. The secondary processes (e.g. aggregation, and recrystallization) take place spontaneously in activated systems and may appear even

during or after milling [161]. In addition, Mechanochemistry is a consolidated method in the manufacturing of materials and processes, and it has been applied in a wide range of fields, such as chemical engineering, materials engineering, mineral processing, the coal industry, the building industry, pharmacy, agriculture, and extractive metallurgy. The field of waste treatment has been also benefited from mechanochemistry, for instance, removing organic pollutants from the soil, waste rubber recycling, and fly ash modification. Future of mechanical milling is opening with everyday contribution in the professional literature [162].

Fig. 2.5. Pulverissette 7 (Fritsch) ball milling unit

We found in the literature that metal recycling is an essential component of the goal of closed-loop material systems and sustainability. Although the recycling rate for the "base metals" (iron, aluminum, zinc, copper etc.) is above 50%; it is less than 1% for the "rare" metals used for precise technological purposes in small quantities, such as indium, lithium, and rare earth elements. For example, It is reported that more than 80% (in fact, more than 90% in 2013) of the global indium production was used for ITO and is mainly used for liquid crystal display (LCD) and thin-layer photovoltaic manufacture. These metals are also more difficult to separate out by conventional processes [162].

Hydrometallurgy is one of the commonly used approaches for metal recycling, and mechanochemistry has demonstrated the ability to significantly modify and enhance those

process. Mechanochemical method can make the leaching process proceed easier for metals that could hardly be leached out from wastes. It also can improve the leaching efficiency and enhance the yield of the original process. It changes the technical route that the wastes have been treated through the introduction of new reactions to obtain a better recycling performance for metals. For instance, lead in waste CRT glass could hardly be leached out (<5%) when just conventional leaching process has been used, while with aid of mechanochemical method, the highest yield could reach more than 90% .

Studies conducted by researchers from Tohoku University, showed that broken In_2O_3 in ITO scrap into significantly finer particles using mechanochemical treatment, the effective surface area of In_2O_3 particles markedly increased. The yield for Indium recovering during the conventional acid leaching process (1 M H_2SO_4, ambient temperature, leaching time of 1 h) remarkably increased to 80% after 15 min of milling (35% more than the yield of 45% for unactivated ITO scrap). The yield reached 90−95% when the milling time was increased to 30 min [163,164].

The feasibility of using mechanical activation as a pretreatment method for recovering Rare Earth elements (REEs) from phosphors was first studied by Zhang and Saito.64 The samples were activated by planetary ball milling with a rotational speed of 700 rpm and subsequently subjected to acid leaching. The result showed that pretreatment by mechanical activation could significantly promote the leaching efficiency of REEs. It was shown that 70−80% of the yttrium (Y) and europium (Eu) in waste phosphor with 3 min of grinding could be leached out under room temperature (298 K) in 1h using dilute (1M) HCl, whereas the proportion of Y and Eu leached into acid solution came to less than 20% after 1 h leaching for unactivated phosphors, even with an HCl concentration of 1.2 M and reaction temperature of 313 K. Furthermore, after grinding for 2h, the proportion could reach more than 80% for all five of the REEs−Y, Eu, lanthanum (La), cerium (Ce), and terbium (Tb), in phosphor, in which the proportion of Y was approximately 100% [162].

Copper Recycling from Waste Printed Circuit Boards. Copper is a good conductor of electricity, second after silver in electrical conductivity, and it has been widely used in printed circuit boards (PCBs) for this unique feature. Its content in PCBs ranges from 5.80% to 26.8%.86 According to data released by National Bureau of Statistics (NBS) of

China and European Institute of Printed Circuits (EIPC), the production of PCBs in China is nearly 87.8 million m^2 in 2013, which accounts for about 42.6% of the global market share. Large amounts of waste PCBs are generated with the discard of EOL electronic products. Numerous studies have been conducted related to the recycling of copper from waste PCBs, which can be roughly classified into three categories: pyrometallurgy, hydrometallurgy, and physical route. However, mechanochemistry provides a novel approach for copper recycling from waste PCBs by transforming the copper into the corresponding compound of natural minerals. The formation of CuS by elemental copper and sulfur (with $\Delta G = -53.7$ kJ/mol) is thermodynamically favored, but the reaction cannot occur spontaneously without any external energy. In the recycling method proposed by Ou and Li, the sulfurization was introduced by the energy from the process of mechanical activation.

It should be noted that milling takes part of the conventional process only as a pretreatment of the materials, and that it does not substitute the process. In our case, the ball milling treatment (using the Pulverissette 7 (Fritsch) as in Fig. 2.5) of precursor prior to the USP deposition of thin films arose from the above mentioned discoveries [161-164]. In this work, it is expected that during the pretreatment (ball milling) of precursor, zinc acetate, the external energy added by the activation can also lead to bond breakage and even chemical reaction, which could significantly improve the dissolution and properties of the mist formed affecting the growth process of ZnO. The reduction in particle size and the increase in surface area of the precursor, after milling, could also enhance the formation of new chemical species that are incorporated in the early nucleation species, with the change in transport and optical properties of the materials.

2. 3. 6. Sol gel

The sol–gel process, allows elaborating a solid material from a solution by using a sol or a gel as an intermediate step, and at much lower temperatures than is possible by traditional methods of preparation. It enables the powderless processing of glasses and ceramics, and thin films or fibers directly from solution. The synthesis of solid materials via ‘chimie douce’ often involves wet chemistry reactions and sol–gel chemistry based on the transformation of molecular precursors into an oxide network by hydrolysis and

condensation reactions the main steps of preparation of thin films and powder by the sol–gel process. In this method the film preparation includes three parts: (i) preparation of the precursor solution; (ii) deposit of the prepared sol on the substrate; and (iii) heat treatment of the xerogel film. The xerogel is the dried gel at ambient pressure (the dried gel in supercritical conditions is called aerogel) [165].

2. 4. Applications of ZnO

Because of ZnO's diverse properties, both chemical and physical, zinc oxide is widely used in many areas. It plays an important role in a very wide range of applications, ranging from tyres to ceramics, from pharmaceuticals to agriculture, and from paints to chemicals [166]. The wide range of applications of ZnO is shown in Fig. 2.6. The various properties of ZnO which helps to design corresponding applications as shown in Table 2.3. In addition, detailed information of the important applications are described in the following subsections.

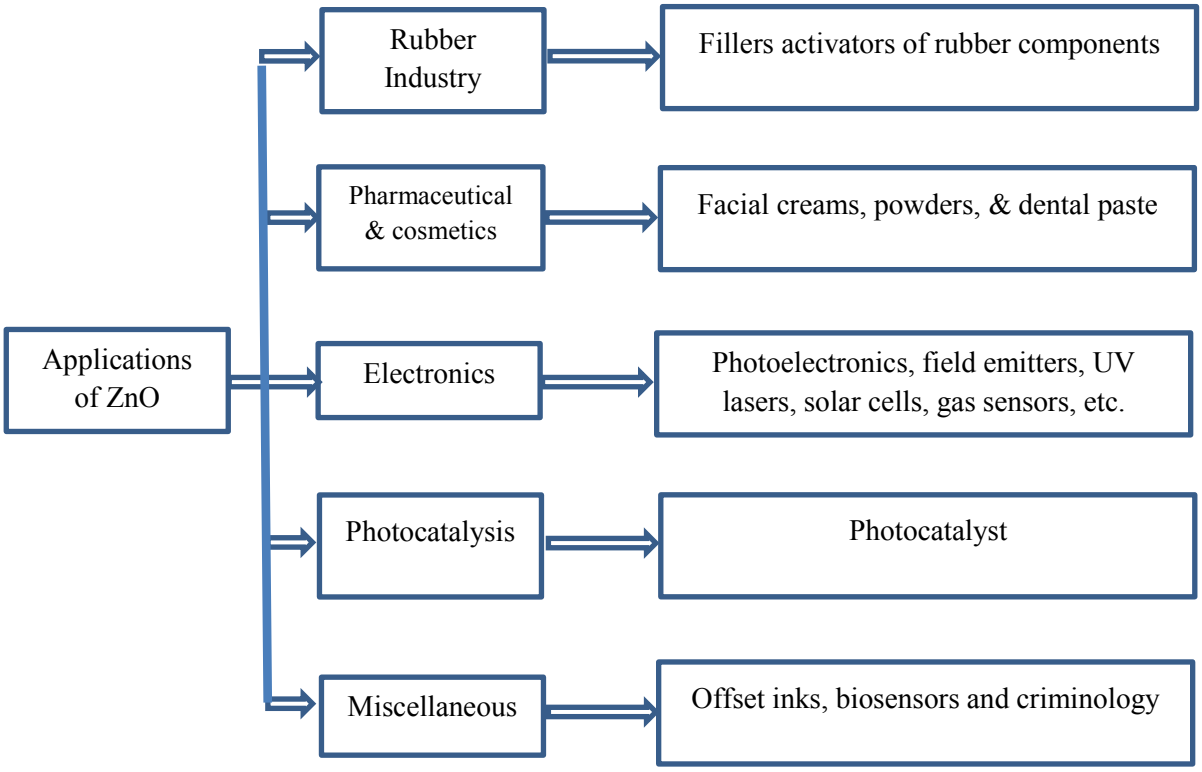

Fig.2.6. Schematic representation of general applications of ZnO

Table 2.3. Properties of ZnO and its respective applications

S. No.	***Property***	***Applications***
1	Electrical and Optical	Transparent Conductive Oxides
2	Electrical	Electronics
3	Photocatalytic degradation	Photocatalysis
4	Piezoelectricity	Actuators
5	Thermal and electrical	Gas sensors
6	Pyroelectricity	Pollution monitoring, Hot image detector
7	Magneticity	Spintronics
8	Electrochemical	Batteries

2. 4. 1. Solar cells

The rapidly increasing demand for energy together with more and more concerns about the environment force us to seek sustainable energy resources and clean energy technologies. As a result, photovoltaics have received increased interest in recent years. In order to further lower the cost of solar cells, organic solar cells based on fully organic semiconductors and hybrid solar cells based on a combination of organic and inorganic semiconductors have been intensively investigated as promising approaches to low-cost photovoltaics. Zinc oxide (ZnO) has received exceptional attention as a promising material for solar cell applications due to its nontoxicity, good stability, good electrical and optical properties, and low cost [167].

2. 4. 2. Transistors

A thin film transistor is a type of field-effect transistor that provides a common, inexpensive method of driving individual pixels in LCD and OLED displays. Increased drain currents resulting from high mobility are necessary for achieving high frame rates in high-resolution displays. Low deposition temperatures are essential for deposition on inexpensive, transparent substrates, such as glass and plastic. Zinc oxide is an ideal TFT semiconductor for these applications, having a higher mobility than amorphous silicon and lower deposition temperatures than polycrystalline silicon. Also, the high bandgap of ZnO (3.3eV) leads to a desirable level of transparency of the transistor itself. The use of high-κ

dielectrics in TFTs is becoming increasingly necessary, as smaller transistors lead to unacceptable levels of gate leakage current. A high-κ PZT (κ ~ 100) dielectric replacement for SiO_2 (κ = 3.9) would serve to lower transistor operating voltages and allow the insulator thickness to be maintained, thus reducing gate leakage without sacrificing capacitance [168].

2. 4. 3. Photocatalyst

Environmental pollution is one of the serious problem presently faced on a global scale. The increase in world population and the rampant unregulated industrial growth have all led to release of toxic agents and industrial waste into the waterways inturn causes serious effects such as pollution-related diseases, global warming, and abnormal climatic changes. The various pollutants that affect the environment are pheonols, fungicides (2-phenylphenol), herbicides (metamitron), insecticides (diazinon), pesticides (dimethoate), pharmaceuticals (amoxicillin, and tetracycline), dyes (acid red, methyl orange, acridine orange, methyl green, and methylene blue). Varieties of techniques have been employed to degrade those organic contaminants and advanced heterogeneous photocatalysis involving zinc oxide (ZnO) photocatalyst appears to be one of the most promising technology. In recent years, ZnO photocatalyst have attracted much attention due to their extraordinary characteristics. The high efficiency of ZnO photocatalyst in heterogeneous photocatalysis reaction requires a suitable architecture that minimizes electron loss during excitation state and maximizes photon absorption [169].

2. 4. 4. Actuators

Piezoelectric cantilevers can be used as actuators or sensors. As actuators, they utilize the converse piezoelectric effect to convert electrical energy into mechanical energy, i.e. displacement and force. As sensors, they operate in the opposite mode using the piezoelectric effect. Typical piezoelectric cantilever actuators include ultrasonic motors, atomic force microscopy (AFM) probes, microelectromechanical system (MEMS) switches, bandpass filters, and scanning MEMS mirrors, whereas piezoelectric cantilever sensors can be accelerometers, force sensors, or pressure sensors.

Among the broad range of piezoelectric materials, lead zirconate titanate (PZT) is most widely used due to its superior piezoelectricity. Piezoelectric devices can be made of bulk

or thin-film PZT. A wide variety of sensors and actuators based on bulk PZT are successfully manufactured using conventional technologies. Compared with its success in conventional transducers, applications of PZT in MEMS are rather limited due to integration issues of PZT thin films. Preparation of PZT usually involves high temperatures above 500°C. High-temperature processing can cause interfacial structural failures and changes in dopant profiles of electrical elements in integrated circuits. Apart from PZT, zinc oxide (ZnO) is another important piezoelectric material. Piezoelectricity of ZnO is generally one order smaller than that of PZT. The biggest advantage of ZnO over PZT is its greater flexibility in processing [170].

2. 4. 5. Gas sensors

Nowadays, the development of gas sensors to detect volatile and toxic gases (ethanol, propane, carbon monoxide etc) is imperative due to the concerns for environmental pollution and the safety requirements of industry and daily life. The sensing characters of a sensor depend on the shape and dimensionality of the sensing material a lot, so that multiplicate ZnO nanostructures have been synthesized and studied in the past decade. Researches have shown that one-dimensional (1D) ZnO nanostructures possess a large surface-to-volume ratio, which can absorb molecules on the surface. Upto now, 1D ZnO nanostructures, such as nanotubes, nanowires, nanorods and nano-tetrapods, have been synthesized by various physical and chemical methods and used to fabricate gas sensors [171].

2. 4. 6. Spintronics

Dilute Magnetic Semiconductors (DMS) are expected to be the main building blocks for the realization of semiconductor spin based electronics–spintronics. The giant magnetoresistance of these materials, i.e. large resistivity changes in response to an applied magnetic field, make them suitable for applications in magnetic sensors, magnetic random access memories and spintronic devices. In order to develop spintronics as a practical technology, it is necessary to explore materials whose magnetic property can be controlled by changing either the external field or the carrier concentration. From an industrial point of view, it is essential to fabricate ferromagnetic DMS with Curie temperature (Tc) above room temperature and a ferromagnetism that is intrinsic, rather than due to the presence of

dopant clusters. The synthesis of DMS as nanowires is particularly attractive for the fabrication of low dimensional, spin-based electronic and optoelectronic devices. Transition metals (TM) with partially filled d states (Sc, Ti, V, Cr, Mn, Fe, Co, Ni, and Cu) have been used as magnetic atoms in DMS. The electron spin of the partially filled d states are responsible for their magnetic behavior. In this regard, transition metal doped ZnO has emerged as an attractive candidate [172].

2. 4. 7. Batteries

Nanoscale materials are studied extensively for high performance batteries and fuel cells. Performance of electrochemical devices largely depends upon the surface area of the active materials. Decreasing particle size of the battery grade active materials results in a substantial increase in the surface area and porosity, which speeds up the reaction kinetics by providing high surface area and shorter distance for ionic species during charge/discharge process. Nano sized ZnO has a variety of applications in electrical, optical, magnetic and chemical fields. The reduction in particle size of ZnO modifies its physical and chemical properties due to surface area enhancement and quantum confinement. Portable power technology has not kept up with the demands of the modern portable electronic devices. Therefore, there is a need to develop an advanced battery system for portable devices like laptops and notebooks. Despite the development of advanced battery systems such as lithium ion and metal hydride, zinc silver oxide is still the best with respect to power density. Zn/AgO batteries have a long successful history of use for the military, space programs and underwater marine applications. The batteries with zinc anode are among the best choices for applications where volume and weight are critical and high power output is required, such as missiles, space and underwater applications [173].

2. 5. REFERENCES

[1] www.scopus.com

[2] ZnO From Fundamental Properties towards Novel Applications, Claus F. Klingshirn, Bruno K. Meyer, Andreas Waag, Axel Hoffmann, Jean Geurts, Springer, ISBN 978-3-642-10576-0.

[3] Zinc Oxide Bulk, Thin Films and Nanostructures: Processing, Properties, and Applications, C. Jagadish and S. Pearton (Eds.), Amsterdam, Elsevier, 2006.

[4] https://sites.google.com/site/zincoxidetco/project-definition

[5] Transparent conductive zinc oxide:Basics and applications in thin film solar cells, Klaus Ellmer, Andreas Klein, Bernd Rech, ISBN 978-3-540-73611-0.

[6] K. Nomura, H. Ohta, K. Ueda, T. Kamiya, M. Hirano, H. Hosono, Thin-film transistor fabricated in single-crystalline transparent oxide semiconductor., Science. 300 (2003) 1269–1272. doi:10.1126/science.1083212.

[7] D.C. Look, Electrical and optical properties of p-type ZnO, Semicond. Sci. Technol. 20 (2005) S55–S61. doi:10.1088/0268-1242/20/4/007.

[8] B. Meyer, J. Sann, A. Zeuner, Incorporation of acceptors in ZnO, Adv. Solid State Phys. 299 (2006) 289–299.

[9] M. Niskanen, M. Kuisma, O. Cramariuc, V. Golovanov, T.I. Hukka, N. Tkachenko, et al., Porphyrin adsorbed on the (10-10) surface of the wurtzite structure of ZnO--conformation induced effects on the electron transfer characteristics., Phys. Chem. Chem. Phys. 15 (2013) 17408–18. doi:10.1039/c3cp51685g.

[10] E. H. Kisi, M. M. Elcombe, Acta Cryst. C45 (1989) 1867. (http://scripts.iucr.org/cgi-bin/paper?s0108270189004269)

[11] J.E. Jaffe, a. C. Hess, Hartree-Fock study of phase changes in ZnO at high pressure, Phys. Rev. B. 48 (1993) 7903–7909. doi:10.1103/PhysRevB.48.7903.

[12] L. Gerward, J. S. Olsen, J. Synchrotron Radiat. 2 (1995) 233.(http://scripts.iucr.org/cgi-bin/paper?S0909049595009447)

[13] ZnO Nanostructures and Their Applications, Xiao Wei Sun and Yi Yang, 2012, Taylor & Francis Group, LLC.

[14] S. Karakaya, O. Ozbas, Boron doped nanostructure ZnO films deposited by ultrasonic spray pyrolysis, Appl. Surf. Sci. 328 (2015) 177–182. doi:10.1016/j.apsusc.2014.11.084.

[15] P. Arnou, J.W. Bowers, J.M. Walls, Aluminium-doped zinc oxide deposited by ultrasonic spray pyrolysis for thin film solar cell applications, (2014) 308–313.

[16] B.J. Babu, S. Velumani, J. Arenas-Alatorre, a. Kassiba, J. Chavez, H. Park, et al., Structural Properties of Ultrasonically Sprayed Al-Doped ZnO (AZO) Thin Films: Effect of

ZnO Buffer Layer on AZO, J. Electron. Mater. 44 (2015) 699–705. doi:10.1007/s11664-014-3541-3.

[17] C. Manoharan, G. Pavithra, S. Dhanapandian, P. Dhamodharan, Effect of In doping on the properties and antibacterial activity of ZnO films prepared by spray pyrolysis, Spectrochim. Acta Part A Mol. Biomol. Spectrosc. 149 (2015) 793–799. doi:10.1016/j.saa.2015.05.019.

[18] R. Biswal, A. Maldonado, J. Vega-Pérez, D.R. Acosta, M.D.L.L. Olvera, Indium doped zinc oxide thin films deposited by ultrasonic chemical spray technique, starting from zinc acetylacetonate and indium chloride, Materials (Basel). 7 (2014) 5038–5046. doi:10.3390/ma7075038.

[19] T. Prasada Rao, M. C. Santhosh Kumar, Resistivity Stability of Ga Doped ZnO Thin Films with Heat Treatment in Air and Oxygen Atmospheres, J. Cryst. Process Technol. 02 (2012) 72–79. doi:10.4236/jcpt.2012.22010.

[20] P. Arnou, J.W. Bowers, J.M. Walls, Aluminium-doped zinc oxide deposited by ultrasonic spray pyrolysis for thin film solar cell applications, (2014) 308–313.

[21] D.-S. Kim, J.-H. Park, S.-J. Lee, K.-J. Ahn, M.-S. Lee, M.-H. Ham, et al., Effects of oxygen concentration on the properties of Al-doped ZnO transparent conductive films deposited by pulsed DC magnetron sputtering, Mater. Sci. Semicond. Process. 16 (2013) 997–1001. doi:10.1016/j.mssp.2013.02.012.

[22] H.B. Zhou, H.Y. Zhang, L.W. Han, J.C. Han, Effects of sputtering power on the properties of Al-doped ZnO films deposited on amorphous silicon films substrate, Superlattices Microstruct. 64 (2013) 563–568. doi:10.1016/j.spmi.2013.10.024.

[23] H. Zhu, J. Hupkes, E. Bunte, S.M. Huang, Reactive sputtering of ZnO:Al thin films from rotatable dual metallic targets, Appl. Surf. Sci. 259 (2012) 582–589. doi:10.1016/j.apsusc.2012.07.080.

[24] N. Tsukamoto, S. Sensui, J. Jia, N. Oka, Y. Shigesato, Study on reactive sputtering to deposit transparent conductive amorphous In2O3-ZnO films using an In-Zn alloy target, Thin Solid Films. 559 (2014) 49–52. doi:10.1016/j.tsf.2013.10.109.

[25] S. Flickyngerová, M. Netrvalová, P. Šutta, I. Novotný, V. Tvarožek, P. Gašpierik, et al., Effects of sputtering power and pressure on properties of ZnO:Ga thin films prepared

by oblique-angle deposition, Thin Solid Films. 520 (2011) 1233–1237. doi:10.1016/j.tsf.2011.06.073.

[26] Q.-B. Ma, Z.Z. Ye, H.-P. He, L.-P. Zhu, B.-H. Zhao, Effects of deposition pressure on the properties of transparent conductive ZnO:Ga films prepared by DC reactive magnetron sputtering, Mater. Sci. Semicond. Process. 10 (2007) 167–172. doi:10.1016/j.mssp.2007.11.001.

[27] J. Liu, W. Zhang, D. Song, Q. Ma, L. Zhang, H. Zhang, et al., Investigation of aluminum-gallium co-doped zinc oxide targets for sputtering thin film and photovoltaic application, J. Alloys Compd. 575 (2013) 174–182. doi:10.1016/j.jallcom.2013.04.075.

[28] S. Jin-Hyun, S. Dong-Kyun, L. HeeYoung, L. Jai-Yeoul, C. Nam-In, L. Se-Jong, Characteristics of Gallium and Aluminum Co-doped ZnO (GAZO)\\Transparent Thin Films Deposited by Using the PLD Process, J. Korean Phys. Soc. 55 (2009) 947. doi:10.3938/jkps.55.947.

[29] S.-C. Chang, In-Line Sputtered Gallium and Aluminum Codoped Zinc Oxide Films for Organic Solar Cells, Int. J. Photoenergy. 2014 (2014) 1–6.

[30] T. Tohsophon, N. Wattanasupinyo, B. Silskulsuk, N. Sirikulrat, Effect of aluminum and indium co-doping on zinc oxide films prepared by dc magnetron sputtering, Thin Solid Films. 520 (2011) 726–729. doi:10.1016/j.tsf.2011.06.079.

[31] C.-M. Hsu, W.-C. Tzou, C.-F. Yang, Y.-J. Liou, Investigation of the High Mobility IGZO Thin Films by Using Co-Sputtering Method, Materials (Basel). 8 (2015) 2769–2781. doi:10.3390/ma8052769.

[32] J. Shi, C. Dong, W. Dai, J. Wu, Y. Chen, R. Zhan, The influence of RF power on the electrical properties of sputtered amorphous In—Ga—Zn—O thin films and devices, J. Semicond. 34 (2013) 084003. doi:10.1088/1674-4926/34/8/084003.

[33] A Hadri, M. Taibi, A El Hat, A Mzerd, Transparent and conductive Al/F and In co-doped ZnO thin films deposited by spray pyrolysis, J. Phys. Conf. Ser. 689 (2016) 012024. doi:10.1088/1742-6596/689/1/012024.

[34] Z.L. Wang, Nanostructures of zinc oxide, Mater. Today. 7 (2004) 26–33. doi:10.1016/S1369-7021(04)00286-X.

[35] Z.L. Wang, Piezoelectric Nanogenerators Based on Zinc Oxide Nanowire Arrays, Science (80-.). 312 (2006) 242–246. doi:10.1126/science.1124005.

[36] L.Z. Kou, W.L. Guo, C. Li, Piezoelectricity of ZNO and its nanostructures, 2008 Symp. Piezoelectricity, Acoust. Waves, Device Appl. SPAWDA 2008. (2008) 354–359. doi:10.1109/SPAWDA.2008.4775808.

[37] T. Tietze, P. Audehm, Y.-C. Chen, G. Schütz, B.B. Straumal, S.G. Protasova, et al., Interfacial dominated ferromagnetism in nanograined ZnO: a μSR and DFT study., Sci. Rep. 5 (2015) 8871. doi:10.1038/srep08871.

[38] www.wiley-vch.de/books/sample/3527408134_c01.pdf

[39] http://icorlab.ece.illinois.edu/07_CONFERENCE_02.pdf

[40]http://sindhu.ece.iisc.ernet.in/nanofab/twiki/pub/Main/ThermalEvaporation/thermal_evaporation_procedure.pdf

[41] Rossnagel SM. Sputter Deposition. In: Sproul WD, Legg KO, editors. Opportunities for Innovation: Advanced Surface Engineering. Switzerland: Technomic Publishing Co., 1995.

[42] Behrisch R, editor. Sputtering by particle bombardment. In: Applied Physics, vol. 47, Berlin: Springer, 1981.

[43] Townsend PD, Kelly JC, Hartley NEW. Ion Implantation, Sputtering and their Applications. London: Academic Press, 1976.

[44] P.J. Kelly, R.D. Arnell, Magnetron sputtering: a review of recent developments and applications Vacuum 56 (2000) 159-172.

[45] S. Mahieu, D. Depla, Applied Physics Letters 90 (2007) 121117/1-121117/2.

[46] S. Swann, Magnetron sputtering, Phys Techno 19(1988) 67-75.

[47] Deal, Griffin, Silicon VLSI Technology, Prentice hall publishers.

[48] https://biblio.ugent.be/publication/1095343/file/1095356

[49] L. Liljeholm, Reactive sputter deposition of functional thin films, Acta Universitatis Upsaliensis, ISSN:1651-6214.

[50] Y. Xu, M. Goto, R. Kato, Y. Tanaka, Y. Kagawa, Y. Xu, et al., Thermal conductivity of ZnO thin film produced by reactive sputtering Thermal conductivity of ZnO thin film produced by reactive sputtering, 084320 (2014). doi:10.1063/1.4706569.

[51] P. Xingping, W. Zhiguang, S. Yin, J.I. Tao, Z. Hang, Structural and photoluminescent properties of ZnO films deposited by radio frequency reactive sputtering, 50 (2007) 281–286. doi:10.1007/s11433-007-0007-0.

[52] R. Hong, H. Qi, J. Huang, H. He, Z. Fan, J. Shao, Influence of oxygen partial pressure on the structure and photoluminescence of direct current reactive magnetron sputtering ZnO thin films, Thin Solid Films. 473 (2005) 58–62. doi:10.1016/j.tsf.2004.06.159.

[53] D. Zhang, P. Fan, X. Cai, J. Huang, L. Ru, Z. Zheng, et al., Properties of ZnO thin films deposited by DC reactive magnetron sputtering under different plasma power, 2 (2009) 437–441. doi:10.1007/s00339-009-5234-y.

[54] Z. Li, W. Gao, ZnO thin films with DC and RF reactive sputtering, 58 (2004) 1363–1370. doi:10.1016/j.matlet.2003.09.028.

[55] T. Minami, T. Miyata, Y. Ohtani, P.-L.T. Minami, P-223 L : Late-News Poster : New Techniques for Producing AZO Thin Films Suitable for ITO Transparent Electrode Applications in LCDs, (2006) 470–473.

[56] C. Beneking, H. Wagner, A. Lo, Texture etched ZnO : Al coated glass substrates for silicon based thin film solar cells, 351 (1999) 247–253.

[57] C. Agashe, O. Kluth, G. Schope, H. Siekmann, Optimization of the electrical properties of magnetron sputtered aluminum-doped zinc oxide films for opto-electronic applications, 442 (2003) 167–172. doi:10.1016/S0040-6090(03)00966-0.

[58] J. Herrero, High conductivity and transparent ZnO : Al films prepared at low temperature by DC and MF magnetron sputtering, 515 (2006) 640–643. doi:10.1016/j.tsf.2005.12.227.

[59] H. Ko, W. Tai, K. Kim, S. Kim, S. Suh, Y. Kim, Growth of Al-doped ZnO thin films by pulsed DC magnetron sputtering, 277 (2005) 352–358. doi:10.1016/j.jcrysgro.2005.01.061.

[60] J.G. Lu, Z.Z. Ye, Y.J. Zeng, L.P. Zhu, L. Wang, J. Yuan, et al., Structural , optical , and electrical properties AZO films over a wide range of compositions, (2006) 1–11. doi:10.1063/1.2357638.

[61] O. Kluth, G. Scho, B. Rech, R. Menner, M. Oertel, K. Orgassa, et al., Comparative material study on RF and DC magnetron sputtered ZnO : Al films, 502 (2006) 311–316. doi:10.1016/j.tsf.2005.07.313.

[61] Z.H.U. Yun, W. Yue, W.A.N. Peng-fei, L.I. Hong-yu, W. Shou-yu, Optical and Mechanical Properties of Transparent Conductive Al-Doped ZnO Films Deposited by the Sputtering Method, 29 (2012) 1–4. doi:10.1088/0256-307X/29/3/038103.

[62] L. Zhifang, C. Guangyu, G. Shibin, D. Lingling, Development of aluminum-doped ZnO films for a-Si : H / c-Si : H solar cell applications, 34 (2013) 1–6. doi:10.1088/1674-4926/34/6/063004.

[63] A. Barhoumi, G. Leroy, B. Duponchel, J. Gest, L. Yang, N. Waldhoff, et al., Superlattices and Microstructures Aluminum doped ZnO thin films deposited by direct current sputtering : Structural and optical properties, SUPERLATTICES Microstruct. 82 (2015) 483–498. doi:10.1016/j.spmi.2015.03.007.

[64] F. Lu, Y. Sun, C. Xu, Properties of Al Doped ZnO Thin films by DC Reaction Magnetron Sputtering, (2011) 362–367. doi:10.4028/www.scientific.net/AMR.306-307.362.

[65] S. Sulyanov, Investigations of Synthesis Mechanisms of ZnO Thin Films in DC Magnetron Sputter Processes, 53 (2008) 59–62.

[66] P. Yao, S. Hang, M. Wu, Growth characteristics and properties of Al-doped ZnO thin films by DC magnetron sputtering from AZOY(R) target, 37 (2012).

[67] Z. Laghfour, T. Ajjammouri, S.A.S. Refki, D. V Nesterenko, Structural and opto-electrical properties of Al doped ZnO sputtered thin films, J. Mater. Sci. Mater. Electron. 26 (2015) 6730–6735. doi:10.1007/s10854-015-3277-8.

[68] M. Suchea, S. Christoulakis, N. Katsarakis, T. Kitsopoulos, G. Kiriakidis, Comparative study of zinc oxide and aluminum doped zinc oxide transparent thin films grown by direct current magnetron sputtering, 515 (2007) 6562–6566. doi:10.1016/j.tsf.2006.11.151.

[69] J. Lee, K.N. Hui, K.S. Hui, Y.R. Cho, H.H. Chun, Low resistivity of Ni-Al co-doped ZnO thin films deposited by DC magnetron sputtering at low sputtering power, Appl. Surf. Sci. 293 (2014) 55–61. doi:10.1016/j.apsusc.2013.12.071.

[70] H.B. Zhou, H.Y. Zhang, L.W. Han, J.C. Han, Effects of sputtering power on the properties of Al-doped ZnO films deposited on amorphous silicon films substrate, Superlattices Microstruct. 64 (2013) 563–568. doi:10.1016/j.spmi.2013.10.024.

[71] H. Zhu, J. H??pkes, E. Bunte, S.M. Huang, Reactive sputtering of ZnO:Al thin films from rotatable dual metallic targets, Appl. Surf. Sci. 259 (2012) 582–589. doi:10.1016/j.apsusc.2012.07.080.

[72] D.-S. Kim, J.-H. Park, S.-J. Lee, K.-J. Ahn, M.-S. Lee, M.-H. Ham, et al., Effects of oxygen concentration on the properties of Al-doped ZnO transparent conductive films deposited by pulsed DC magnetron sputtering, Mater. Sci. Semicond. Process. 16 (2013) 997–1001. doi:10.1016/j.mssp.2013.02.012.

[73] M. Gabás, P. Torelli, N.T. Barrett, M. Sacchi, J.R. Ramos Barrado, Electronic structure of Al- and Ga-doped ZnO films studied by hard X-ray photoelectron spectroscopy, APL Mater. 2 (2014). doi:10.1063/1.4863595.

[74] I. Miccoli, R. Spampinato, F. Marzo, P. Prete, N. Lovergine, Applied Surface Science DC-magnetron sputtering of ZnO : Al films on (00 . 1) Al 2 O 3 substrates from slip-casting sintered ceramic targets, Appl. Surf. Sci. 313 (2014) 418–423. doi:10.1016/j.apsusc.2014.05.225.

[75] H. Chen, J. Ding, W. Guo, Effect of sputtering parameters on photoluminescence properties of Al doped ZnO fi lms deposited on Si substrates, Ceram. Int. 40 (2014) 4847–4851. doi:10.1016/j.ceramint.2013.09.034.

[76] T. Guo, G. Dong, F. Gao, Y. Xiao, Q. Chen, X. Diao, Applied Surface Science High performance ZnO : Al films deposited on PET substrates using facing target sputtering, Appl. Surf. Sci. 282 (2013) 467–471. doi:10.1016/j.apsusc.2013.05.155.

[77] J.I. Owen, W. Zhang, Study on the in-line sputtering growth and structural properties of polycrystalline ZnO : Al on ZnO and glass a, 344 (2012) 12–18. doi:10.1016/j.jcrysgro.2012.01.043.

[78] Y.Y. Chen, J.R. Yang, S.L. Cheng, M. Shiojiri, Structural investigation of ZnO : Al fi lms deposited on the Si substrates by radio frequency magnetron sputtering, Thin Solid Films. 545 (2013) 183–187. doi:10.1016/j.tsf.2013.07.079.

[79] H. Zhu, E. Bunte, J. Hüpkes, S.M. Huang, Sputtering of ZnO : Al fi lms from dual tube targets with tilted magnetrons, Thin Solid Films. 519 (2011) 2366–2370. doi:10.1016/j.tsf.2010.10.072.

[80] S. Ruiliang, L. Wei, Z. Yi, C. Yongan, S. Yun, Finite element simulation and experimental research on ZnO : Al by magnetron sputtering, Thin Solid Films. 520 (2011) 887–890. doi:10.1016/j.tsf.2011.04.168.

[81] C. Li, M. Furuta, T. Matsuda, T. Hiramatsu, H. Furuta, T. Hirao, Effects of substrate on the structural , electrical and optical properties of Al-doped ZnO fi lms prepared by radio frequency magnetron sputtering, Thin Solid Films. 517 (2009) 3265–3268. doi:10.1016/j.tsf.2008.11.103.

[82] W. Yang, Z. Liu, D. Peng, F. Zhang, H. Huang, Applied Surface Science Room-temperature deposition of transparent conducting Al-doped ZnO films by RF magnetron sputtering method, 255 (2009) 5669–5673. doi:10.1016/j.apsusc.2008.12.021.

[83] Z. Zhang, C. Bao, S. Ma, L. Zhang, S. Hou, Effects of deposition power and pressure on the crystallinity of Al-doped ZnO thin films at glass substrates by low temperature RF magnetron sputtering, 48 (2012) 214–222.

[84] Y. Okuhara, H. Matsubara, C. Numako, M. Takata, Effective doping of Al in ZnO films by multi-target reactive sputtering for near-infrared reflection, 49 (2013) 15–20.

[85] J.H. Shin, D.K. Shin, H.Y. Lee, J.Y. Lee, Properties of multilayer gallium and aluminum doped ZnO(GZO/AZO) transparent thin films deposited by pulsed laser deposition process, Trans. Nonferrous Met. Soc. China (English Ed. 21 (2011) s96–s99. doi:10.1016/S1003-6326(11)61069-8.

[86] S. Flickyngerová, M. Netrvalová, P. Šutta, I. Novotný, V. Tvarožek, P. Gašpierik, et al., Effects of sputtering power and pressure on properties of ZnO:Ga thin films prepared by oblique-angle deposition, Thin Solid Films. 520 (2011) 1233–1237. doi:10.1016/j.tsf.2011.06.073.

[87] K.-W. Seo, H.-S. Shin, J.-H. Lee, K.-B. Chung, H.-K. Kim, The effects of thickness on the electrical, optical, structural and morphological properties of Al and Ga co-doped ZnO films grown by linear facing target sputtering, Vacuum. 101 (2014) 250–256. doi:10.1016/j.vacuum.2013.09.009.

[88] Q.-B. Ma, Z.Z. Ye, H.-P. He, L.-P. Zhu, B.-H. Zhao, Effects of deposition pressure on the properties of transparent conductive ZnO:Ga films prepared by DC reactive magnetron sputtering, Mater. Sci. Semicond. Process. 10 (2007) 167–172. doi:10.1016/j.mssp.2007.11.001.

[89] J. Liu, W. Zhang, D. Song, Q. Ma, L. Zhang, H. Zhang, et al., Investigation of aluminum-gallium co-doped zinc oxide targets for sputtering thin film and photovoltaic application, J. Alloys Compd. 575 (2013) 174–182. doi:10.1016/j.jallcom.2013.04.075.

[90] Q. Ma, Z. Ye, H. He, J. Wang, L. Zhu, B. Zhao, Preparation and characterization of transparent conductive ZnO : Ga films by DC reactive magnetron sputtering, 59 (2006) 1–5. doi:10.1016/j.matchar.2006.11.020.

[91] F. Wang, X.L. Chen, X.H. Geng, D.K. Zhang, C.C. Wei, Q. Huang, et al., Development of natively textured surface hydrogenated Ga-doped ZnO-TCO thin films for solar cells via magnetron sputtering, Appl. Surf. Sci. 258 (2012) 9005–9010. doi:10.1016/j.apsusc.2012.05.138.

[92] K. Shtereva, S. Flickyngerova, V. Tvarozek, I. Novotny, J. Kovac, A. Vincze, Characterization of gallium e nitrogen co-doped zinc oxide thin fi lms prepared by RF diode sputtering, Vaccum. 86 (2012) 652–656. doi:10.1016/j.vacuum.2011.07.006.

[93] W. Liu, S. Wu, C. Hung, C. Tseng, Y. Chang, Improving the optoelectronic properties of gallium ZnO transparent conductive thin films through titanium doping, J. Alloys Compd. 616 (2014) 268–274. doi:10.1016/j.jallcom.2014.06.175.

[94] M. Netrvalova, I. Novotny, L. Prusakova, V. Tvarozek, P. Sutta, In fl uence of deposition regime on physical properties of gallium doped zinc oxide fi lms, 86 (2012) 2–5. doi:10.1016/j.vacuum.2011.07.064.

[95] H. Lu, J. Jou, C. Chu, Surface & Coatings Technology In fl uence of RF magnetron sputtering conditions on the properties of transparent conductive gallium-doped magnesium zinc oxide thin films, Surf. Coat. Technol. 231 (2013) 539–542. doi:10.1016/j.surfcoat.2012.10.029.

[96] S. Shet, Y. Yan, N. Ravindra, J. Turner, M. Al-jassim, Applied Surface Science Photoelectrochemical behavior of mixed ZnO and GaN (ZnO : GaN) thin films prepared by sputtering technique, Appl. Surf. Sci. 270 (2013) 718–721. doi:10.1016/j.apsusc.2013.01.134.

[97] X. Yu, J. Ma, F. Ji, Y. Wang, X. Zhang, Preparation and properties of ZnO : Ga films prepared by r . f . magnetron sputtering at low temperature, 239 (2005) 222–226. doi:10.1016/j.apsusc.2004.05.266.

[98] X. Yu, J. Ma, F. Ji, Y. Wang, C. Cheng, H. Ma, Thickness dependence of properties of ZnO : Ga films deposited by rf magnetron sputtering, 245 (2005) 310–315. doi:10.1016/j.apsusc.2004.10.022.

[99] C. Yan, X. Chen, F. Wang, J. Sun, D. Zhang, C. Wei, et al., Textured surface ZnO : B /(hydrogenated gallium-doped ZnO) and (hydrogenated gallium-doped ZnO)/ ZnO : B transparent conductive oxide layers for Si-based thin fi lm solar cells, Thin Solid Films. 521 (2012) 249–252. doi:10.1016/j.tsf.2011.10.203.

[100] N.E. Duygulu, Effect of r . f . power variation on gallium doped zinc oxide thin fi lms, Vaccum. (2015) 1–9. doi:10.1016/j.vacuum.2015.05.036.

[101] S.Y. Lim, S. Brahma, C.P. Liu, R.C. Wang, J.L. Huang, Effect of indium concentration on luminescence and electrical properties of indium doped ZnO nanowires, Thin Solid Films. 549 (2013) 165–171. doi:10.1016/j.tsf.2013.09.001.

[102] A. Stadler, Transparent Conducting Oxides—An Up-To-Date Overview, Materials (Basel). 5 (2012) 661–683. doi:10.3390/ma5040661.

[103] S.-C. Chang, In-Line Sputtered Gallium and Aluminum Codoped Zinc Oxide Films for Organic Solar Cells, Int. J. Photoenergy. 2014 (2014) 1–6.

[104] K.H. Kim, H.W. Choi, K.H. Kim, Processing Research Effect of working pressure on the characteristics of Ga-Al doped ZnO thin films deposited by the facing targets sputtering method, 14 (2013) 194–197.

[105] S.H. Park, J.B. Park, P.K. Song, Characteristics of Al-doped, Ga-doped and In-doped zinc-oxide films as transparent conducting electrodes in organic light-emitting diodes, Curr. Appl. Phys. 10 (2010) S488–S490. doi:10.1016/j.cap.2010.02.036.

[106] N. Tsukamoto, S. Sensui, J. Jia, N. Oka, Y. Shigesato, Study on reactive sputtering to deposit transparent conductive amorphous In2O3-ZnO films using an In-Zn alloy target, Thin Solid Films. 559 (2014) 49–52. doi:10.1016/j.tsf.2013.10.109.

[107] S. Jin-Hyun, S. Dong-Kyun, L. HeeYoung, L. Jai-Yeoul, C. Nam-In, L. Se-Jong, Characteristics of Gallium and Aluminum Co-doped ZnO (GAZO)\\Transparent Thin Films Deposited by Using the PLD Process, J. Korean Phys. Soc. 55 (2009) 947. doi:10.3938/jkps.55.947.

[108] Y.C. Lin, T.Y. Chen, L.C. Wang, S.Y. Lien, Comparison of AZO , GZO , and AGZO Thin Films TCOs Applied for a-Si Solar Cells, 159 (2012) 599–604. doi:10.1149/2.108206jes.

[109] J.S. Hong, N. Matsushita, K.H. Kim, Investigation of the effect of oxygen gas on properties of GAZO thin films fabricated by facing targets sputtering system, 075007 (n.d.). doi:10.1088/0268-1242/29/7/075007.

[108] C. Huang, M. Wang, Q. Liu, Y. Cao, Z. Deng, Z. Huang, et al., Physical properties and growth kinetics of co-sputtered indium-zinc oxide films, 095019 (n.d.). doi:10.1088/0268-1242/24/9/095019.

[109] K. Djessas, I. Bouchama, J.L. Gauf, Z. Ben Ayadi, Effects of indium concentration on the properties of In-doped ZnO fi lms : Applications to silicon wafer solar cells, 555 (2014) 28–32. doi:10.1016/j.tsf.2013.08.109.

[110] M. Rezapour, N. Talebian, Synthesis and investigation of Indium doping and surfactant on the morphological , optical and UV / Vis photocatalytic properties of ZnO nanostructure, Ceram. Int. 40 (2014) 3453–3460. doi:10.1016/j.ceramint.2013.09.085.

[111] Y. Bin Xiao, S.M. Kong, E.H. Kim, C. Won, Solar Energy Materials & Solar Cells Characteristics of indium zinc oxide thin films prepared by direct current magnetron sputtering for flexible solar cells, Sol. Energy Mater. Sol. Cells. 95 (2011) 264–269. doi:10.1016/j.solmat.2010.02.016.

[112] K. Ung, S. Wook, A. V Moholkar, J. Ho, J. Ha, J. Hyeok, Effects of dopant (Al , Ga , and In) on the characteristics of ZnO thin films prepared by RF magnetron sputtering system, Curr. Appl. Phys. 10 (2010) S463–S467. doi:10.1016/j.cap.2010.02.028.

[113] F. Ye, X. Cai, F. Dai, D. Zhang, P. Fan, L. Liu, The field emission of indium-doped ZnO films fabricated by room temperature DC magnetron sputtering, Phys. B Phys. Condens. Matter. 407 (2012) 64–67. doi:10.1016/j.physb.2011.09.120.

[114] J.H. Hsieh, C. Li, S.J. Liu, W.S. Lin, Surface & Coatings Technology Sputtering process parameters to structural and electrical properties of indium zinc oxide thin fi lms, Surf. Coat. Technol. 228 (2013) S499–S504. doi:10.1016/j.surfcoat.2012.04.080.

[115] H. Krebs, M. Weisheit, S. Erik, T. Scharf, C. Fuhse, M. St, et al., Pulsed Laser Deposition (PLD) - a Versatile Thin Film Technique UHV-chamber, Adv. Solid State Phys. SE - 36. (2003) 505–518. doi:10.1007/978-3-540-44838-9_36.

[116] V.K. Jayaraman, A.M. Álvarez, Y.M. Kuwabara, Y. Koudriavstev, M.D.L.L. Olvera Amador, Effect of co-doping concentration on structural, morphological, optical and electrical properties of aluminium and indium co-doped ZnO thin films deposited by ultrasonic spray pyrolysis, Mater. Sci. Semicond. Process. 47 (2016) 32–36. doi:10.1016/j.mssp.2016.02.011.

[117] Alver U, Kilinc T, Bacaksiz E, Nezir S. Temperature dependence of ZnO rods produced by ultrasonic spray pyrolysis method. Mater Chem Phys,106 (2007)227–230.

[118] M. Gabás, N.T. Barrett, J.R. Ramos-Barrado, S. Gota, T.C. Rojas, M.C. López-Escalante,Chemical and electronic interface structure of spray pyrolysis de- posited undoped and Al-doped ZnO thin films on a commercial Cz-Si solar cell substrate, Sol. Energy Mater. Sol. Cells 93 (2009) 1356–1365, http://dx.doi.org/ 10.1016/j.solmat.2009.02.018.

[119] J.V. Kumar, A. Maldonado, M. Olvera, A simple and cost-effective zinc oxide thin film sensor for propane gas detection, Mater. Lett. 157 (2015) 169–171, http://dx.doi.org/10.1016/j.matlet.2015.05.065.

[120] I. Akyuz, S. Kose, F. Atay, V. Bilgin, The optical, structural and morphological properties of ultrasonically sprayed ZnO:Mn films, Semicond. Sci. Technol. 21 (2006) 1620–1626, http://dx.doi.org/10.1088/0268-1242/21/12/020.

[121] B.J. Babu, S. Velumani, A. Kassiba, J. Chavez, H. Park, S.Q. Hussain, et al., Structural properties of ultrasonically Sprayed Al-Doped ZnO (AZO), J. Electron. Mater. 44 (2015) 699–705, http://dx.doi.org/10.1007/s11664-014-3541-3.

[122] C. Huang, M. Wang, Substrate Temperature Dependence of ZnO Films Prepared by Ultrasonic Spray Pyrolysis, Jpn. J. Appl. Phys. 35 6208. (n.d.).

[123] A.K. Prasad, S. Dhara, Effect of substrate temperature on microstructural , vibrational and electrical properties of ZnO nanostructured thin films, Nanosystems, 7 (2016) 506–508. doi:10.17586/2220-8054-2016-7-3-506-508.

[124] Y. Benkhetta, A. Attaf, H. Saidi, A. Bouhdjar, H. Benjdidi, I.B. Kherchachi, et al., Optik Influence of the solution flow rate on the properties of zinc oxide (ZnO) nano-crystalline films synthesized by ultrasonic spray process, Opt. - Int. J. Light Electron Opt. 127 (2016) 3005–3008. doi:10.1016/j.ijleo.2015.11.236.

[125] R.S. Gaikwad, G.R. Patil, M.B. Shelar, B.N. Pawar, R.S. Mane, S.H. Han, et al., Nanocrystalline ZnO Films Deposited by Spray Pyrolysis :, International Journal of Self_Propagating High_Temperature Synthesis, 2012, Vol. 21, No. 3, pp. 178–182. doi:10.3103/S106138621203003X.

[126] A. Attaf, Y. Benkhetta, H. Saidi, A. Bouhdjar, H. Bendjedidi, M. Nouadji, et al., The effect of the solution flow rate on the properties of zinc oxide (ZnO) thin films deposited by ultrasonic spray The Effect of The Solution Flow Rate on The Properties of Zinc Oxide (ZnO) Thin Films Deposited by Ultrasonic Spray, AIP Conference Proceedings 1653, 020015 (2016). doi:10.1063/1.4914206.

[127] Y. Aoun, B. Benhaoua, B. Gasmi, S. Benramache, Structural , optical and electrical properties of zinc oxide thin films deposited by a spray pyrolysis technique, Journal of Semiconductors, 36 (2015) 1–5. doi:10.1088/1674-4926/36/1/013002.

[128] A. R. Bari, L. A. Patil, Characterizations of Ultrasonically Prepared Nanostructured ZnO powder and NH 3 Sensing Performance of its Thick Film Sensor, P.M. Science (2016) 1–5. doi:10.1016/j.mspro.2014.07.210Get.

[129] S. Benramache, A. Rahal, B. Benhaoua, The effects of solvent nature on spray-deposited ZnO thin film prepared from Zn ($CH_3COO)_2$, $2H_2O$, Optik 125 (2014) 2013–2015.

[130] S. Abed, M.S. Aida, K. Bouchouit, a. Arbaoui, K. Iliopoulos, B. Sahraoui, Non-linear optical and electrical properties of ZnO doped Ni Thin Films obtained using spray ultrasonic technique, Opt. Mater. (Amst). 33 (2011) 968–972. doi:10.1016/j.optmat.2011.01.018.

[131] U. Alver, T. Kılınç, E. Bacaksız, S. Nezir, Structure and optical properties of Zn1−xFexO thin films prepared by ultrasonic spray pyrolysis, Mater. Sci. Eng. B. 138 (2007) 74–77. doi:10.1016/j.mseb.2007.01.026.

[132] F.C.Y.B.M.S. Aida, Optical and electrical properties of Bi doped ZnO thin films deposited by ultrasonic spray pyrolysis, (2011) 499–505. doi:10.1007/s10854-010-0167-y.

[133] J. Xu, H. Wang, L. Yang, M. Jiang, S. Wei, T. Zhang, Low temperature growth of highly crystallized ZnO : Al films by ultrasonic spray pyrolysis from acetylacetone salt, Mater. Sci. Eng. B. 167 (2010) 182–186. doi:10.1016/j.mseb.2010.02.012.

[134] T.A.E.Y. Ma, S.O.O.C. Lee, Effects of aluminum content and substrate temperature on the structural and electrical properties of aluminum-doped ZnO ® lms prepared by ultrasonic spray pyrolysis, 1 (n.d.) 305–309.

[135] B. Ergin, E. Ketenci, F. Atay, Characterization of ZnO films obtained by ultrasonic spray pyrolysis technique, Int. J. Hydrogen Energy. 34 (2009) 5249–5254. doi:10.1016/j.ijhydene.2008.09.108.

[136] J. Wienke, A.S. Booij, ZnO : In deposition by spray pyrolysis — Influence of the growth conditions on the electrical and optical properties, 516 (2008) 4508–4512. doi:10.1016/j.tsf.2007.05.078.

[137] I. Akyuz, S. Kose, F. Atay, V. Bilgin, The optical, structural and morphological properties of ultrasonically sprayed ZnO:Mn films, Semicond. Sci. Technol. 21 (2006) 1620–1626. doi:10.1088/0268-1242/21/12/020.

[138] S. Korea, S. Science, B. Media, Influence of substrate temperature on ultraviolet emission of ZnO films prepared by ultrasonic spray pyrolysis, 1 (2006) 431–435. doi:10.1007/s10853-005-2280-5.

[139] Y.C. Kang, S.B. Park, Preparation of zinc oxide-dispersed silver particles by spray pyrolysis of colloidal solution, (1999) 129–133.

[140] M.. Tokumoto, a Smith, C.. Santilli, S.. Pulcinelli, a. . Craievich, E. Elkaim, et al., Structural electrical and optical properties of undoped and indium doped ZnO thin films prepared by the pyrosol process at different temperatures, Thin Solid Films. 416 (2002) 284–293. doi:10.1016/S0040-6090(02)00531-X.

[141] U. Alver, T. K, E. Bacaks, T. Küçükömero, S. Nezir, İ.H. Mutlu, et al., Synthesis and characterization of spray pyrolysis Zinc Oxide microrods, 515 (2007) 3448–3451. doi:10.1016/j.tsf.2006.10.016.

[142] J.H. Lee, B.O. Park, Characteristics of Al-doped ZnO thin films obtained by ultrasonic spray pyrolysis: Effects of Al doping and an annealing treatment, Mater. Sci. Eng. B Solid-State Mater. Adv. Technol. 106 (2004) 242–245. doi:10.1016/j.mseb.2003.09.040.

[143] U. Alver, T. Kılınc, E. Bacaksız, S. Nezir, Temperature dependence of ZnO rods produced by ultrasonic spray pyrolysis method, 106 (2007) 227–230. doi:10.1016/j.matchemphys.2007.05.031.

[144] L.N. Demyanets, V. V Kireev, L.E. Li, V. V Artemov, Thin Films of ZnO : M Synthesized by Ultrasonic Spray Pyrolysis, 56 (2011) 1587–1594. doi:10.1134/S0036023611100056.

[145] A. Djelloul, K. Bouzid, F. Guerrab, C.U.K. Erie, Role of Substrate Temperature on the Structural and Morphological Properties of ZnO Thin Films Deposited by Ultrasonic Spray Pyrolysis, 32 (2008) 49–58.

[146] J. Garnier, A. Bouteville, J. Hamilton, M.E. Pemble, I.M. Povey, A comparison of different spray chemical vapour deposition methods for the production of undoped ZnO thin fi lms, Thin Solid Films. 518 (2009) 1129–1135. doi:10.1016/j.tsf.2009.01.157.

[147] Y.K. Ã, H. Nishinaka, N. Kameyama, S. Fujita, Enhancement of electron mobility in ZnO layers with applying ultrasonic spray-assisted MOVPE and buffer layers, 310 (2008) 5016–5019. doi:10.1016/j.jcrysgro.2008.08.015.

[148] V. V Kireev, L.N. Dem, L.E. Li, V. V Artemov, Growth of Thin ZnO Films by Ultrasonic Spray Pyrolysis, 46 (2010) 154–162. doi:10.1134/S0020168510020123.

[149] J. Lee, S. Lee, B. Park, Fabrication and characteristics of transparent conducting In 2 O 3 – ZnO thin films by ultrasonic spray pyrolysis, 127 (2006) 267–271. doi:10.1016/j.mseb.2005.10.008.

[150] Y.L. Ee, H.K. Im, Y.R. Oh, Deposition of ZnO Thin Films by the Ultrasonic Spray Pyrolysis Technique, 40 (2001) 2423–2428.

[151] J. Lee, B. Yeo, B. Park, Effects of the annealing treatment on electrical and optical properties of ZnO transparent conduction films by ultrasonic spraying pyrolysis, 457 (2004) 333–337. doi:10.1016/j.tsf.2003.09.075.

[152] K. Liu, B.F. Yang, H. Yan, Z. Fu, M. Wen, Y. Chen, et al., Applied Surface Science Strong room-temperature ultraviolet emission from nanocrystalline ZnO and ZnO : Ag films grown by ultrasonic spray pyrolysis, 255 (2008) 2052–2056. doi:10.1016/j.apsusc.2008.06.203.

[153] M.G. Nolan, J.A. Hamilton, S.O. Brien, G. Bruno, L. Pereira, E. Fortunato, et al., Journal of Photochemistry and Photobiology A : Chemistry The characterisation of aerosol assisted CVD conducting , photocatalytic indium doped zinc oxide films, "Journal Photochem. Photobiol. A Chem. 219 (2011) 10–15. doi:10.1016/j.jphotochem.2011.01.010.

[154] L.A. Patil, A.R. Bari, M.D. Shinde, V. V Deo, D.P. Amalnerkar, Synthesis of ZnO Nanocrystalline Powder From Ultrasonic Atomization Technique , Characterization , and its Application in Gas Sensing, 11 (2011) 939–946.

[155] S. Sali, M. Boumaour, M. Kechouane, S. Kermadi, F. Aitamar, Nanocrystalline ZnO film deposited by ultrasonic spray on textured silicon substrate as an anti-reflection coating layer, Phys. B Phys. Condens. Matter. 407 (2012) 2626–2631. doi:10.1016/j.physb.2012.04.009.

[156] D. Shuang, X.X. Zhu, J.B. Wang, X.L. Zhong, G.J. Huang, C. He, Applied Surface Science The influence of Mn content on luminescence properties in Mn-doped ZnO films deposited by ultrasonic spray assisted chemical vapor deposition, 257 (2011) 6085–6088. doi:10.1016/j.apsusc.2011.02.001.

[157] P. Singh, A. Kumar, D.K. Ã, Growth and characterization of ZnO nanocrystalline thin films and nanopowder via low-cost ultrasonic spray pyrolysis, 306 (2007) 303–310. doi:10.1016/j.jcrysgro.2007.05.023.

[158] D. Walsh, L. Arcelli, V. Swinerd, J. Fletcher, S. Mann, B. Palazzo, et al., Aerosol-Mediated Fabrication of Porous Thin Films Using Ultrasonic Nebulization, (2007) 503–508.

[159] M. Wei, D. Zhi, J.L. Macmanus-driscoll, Structural characterisation of doped and undoped nanocrystalline zinc oxides deposited by ultrasonic spray assisted chemical vapour deposition, 26 (2006) 183–186. doi:10.1088/1742-6596/26/1/043.

[160] J. Zhao, X. Li, J. Bian, W. Yu, C. Zhang, Comparison of structural and photoluminescence properties of ZnO thin films grown by pulsed laser deposition and ultrasonic spray pyrolysis, 515 (2006) 1763–1766. doi:10.1016/j.tsf.2006.06.032.

[161] P. Bala, M. Criado, F. Delogu, Z. Cherkezova-zheleva, E. Gaffet, F. Jose, et al., Chem Soc Rev, (2013) 7571–7637. doi:10.1039/c3cs35468g.

[162] Q. Tan, J. Li, Recycling Metals from Wastes : A Novel Application of Mechanochemistry, Environmental science and Engg. (2015) 49, 5849-5961. doi:10.1021/es506016w.

[163] Q. Zhang, T. Aoyagi, C. Nagata, C, Room temperature extraction of indium from ITO scrap by a mechanochemical treatment. Shigen to Sozai 1999, 115 (3), 185-188.

[164] Y. Murakami, D. Shindo, Q. Zhang, Microstructural investigation on the mechanism to extract indium from wasted materials. Mater. Sci. Eng., A 2002, 332 (1-2), 64-69.
[165] L. Znaidi, Sol-gel-deposited ZnO thin films: A review, Mater. Sci. Eng. B Solid-State Mater. Adv. Technol. 174 (2010) 18–30. doi:10.1016/j.mseb.2010.07.001.
[166] A. Kołodziejczak-Radzimska, T. Jesionowski, Zinc Oxide—From Synthesis to Application: A Review, Materials (Basel). 7 (2014) 2833–2881. doi:10.3390/ma7042833.
[167] J. Huang, Q. Zheng, Applications of ZnO in organic and hybrid solar cells, Energy and environment science. (2011) 3861–3877. doi:10.1039/c1ee01873f.
[168] G. Cramer, Fabrication and Comparison of ZnO Thin Film Transistors with Various Gate Insulators, Electronics. (2006) 34–35.
[169] K. Mun, C. Wei, K. Sing, J. Ching, Recent developments of zinc oxide based photocatalyst in water treatment technology : A review, Water Res. 88 (2016) 428–448. doi:10.1016/j.watres.2015.09.045.
[170] Y. Yuan, K.S. Chow, H. Du, P. Wang, S. Yu, B. Liu, A ZnO thin-film driven microcantilever for nanoscale actuation and sensing, International journal of Smart and nano materials. 5411 (2013). doi:10.1080/19475411.2012.749959.
[171] L. Wang, Y. Kang, X. Liu, S. Zhang, W. Huang, S. Wang, ZnO nanorod gas sensor for ethanol detection, Sensors Actuators, B Chem. 162 (2012) 237–243. doi:10.1016/j.snb.2011.12.073.
[172] U. Philipose, G. Sapkota, Ferromagnetic ZnO Nanowires for Spintronic Ferromagnetic ZnO Nanowires for Spintronic Applications Applications, Intech open science. Chapter 3, 45-62. http://dx.doi.org/10.5772/52825.
[173] Shafiq Ullah, Fiaz Ahmed, Amin Badshah, Ataf Ali Altaf et al. Solvothermal Preparation of ZnO Nanorods as Anode Material for Improved Cycle Life Zn/AgO Batteries, Plos one, 8 (2013) 1-7.

CHAPTER 3

EXPERIMENTAL

In this chapter, the experimental details for the deposition of undoped ZnO and co-doped ZnO deposition on soda lime glass substrates by ultrasonic spray pyrolysis (USP) and sputtering are explained.

3. 1. Undoped ZnO thin film deposition by USP

The film deposition was carried out for three different 0.2 M precursor solutions, with the variation in water content (Table 3.1). Zinc acetylacetonate ($C_{10}H_{14}O_4Zn.xH_2O$, 98%, Sigma Aldrich) was dissolved in a mixture of deionized water, methanol (CH_3OH, J.T.Baker), and a constant acetic acid (CH_3COOH, J.T.Baker) volume, 1.5 ml. The solution flow rate was 1 ml/min. Nitrogen (from Infra) was used as carrier gas (90 psig). Soda lime glass was used as substrates for the deposition of ZnO thin films. The samples were named based on their water content in the starting solution, namely S0, S5, and S10 as indicated in Table 3.1. The deposition was carried out at a substrate temperature of 450°C for 12 min. The distance between the nozzle and the substrate was 15 cm. We have preferred 450°C as substrate temperature, since this temperature results in highly textured films as reported earlier [1].

Table 3.1. Experimental conditions for the preparation of undoped ZnO thin films

Sample ID	Deionized Water (ml)	Methanol (ml)	Acetic acid (ml)
S0	0	98.5	1.5
S5	5	93.5	1.5
S10	10	88.5	1.5

3. 2. Al and In co-doped ZnO thin film deposition by USP

Thin film preparations of AIZO (Al and In co-doped ZnO) thin films consists of two important steps: 1) solutions preparation 2) thin film deposition. The various solution preparation conditions are given in section 3.2.1. All the thin film deposition conditions are given in section 3.2.2 along with Table 3.2.

3. 2. 1. Solution preparation

Fabrication of AIZO (Al and In co-doped ZnO) thin films were carried out by using zinc, aluminium, and indium precursor solutions. Preparation of these solutions were presented in the following.

Zinc precursor solution of concentration 0.2M was prepared by dissolving zinc acetate dihydrate ($Zn(OOCCH_3)_2.2H_2O$, Alfa Aesar, 98-101%) in a mixture of acetic acid, deionized water, and methanol at different volume proportions as given in Table 3.2.

Table 3.2. Solvents proportions in the Zn precursor solution

Solution ID	Acetic acid (ml)	Deionized water (ml)	Methanol (ml)
S25	25	25	950
S50	50	50	900
S100	100	100	800
S150	150	150	700
A0	0	100	900
A25	25	75	900
A50	50	50	900
A75	75	25	900
A100	100	0	900

In order to study of the effect of aluminium precursor on the characteristics of co-doped ZnO thin films, by selecting aluminium acetylacetonate ($C_{15}H_{21}AlO_6$, Alfa Aesar, 99%), aluminium chloride ($AlCl_3.6H_2O$, Alfa Aesar, Reagent grade), and aluminium sulphate ($Al_2(SO_4)_3 \bullet xH_2O$ (x≈14-18), Alfa Aesar, 97%), separately depositions were performed. The respective aluminum precursor was prepared by dissolving it at 0.1 M concentration in 100 ml of methanol. The prepared aluminium dopant solutions were named as A (Aluminium acetylacetonate), B (Aluminium chloride), and C (Aluminium sulphate).

In dopant solution (0.2M) was prepared by dissolving indium (III) acetate ($In(OOCCH_3)_3$, Alfa Aesar, 99.99%) in a mixture of deionized water and acetic acid (1:1 volume proportion). This solution was labelled as ′I′.

3. 2. 2. AIZO thin films deposition

AIZO thin film depositions were carried out by using ultrasonic spray pyrolysis technique by using the appropriate Zn precursor and doping solutions (from section 3.2.1), Al and In co-doped ZnO thin films were deposited. List of AIZO film deposited were tabulated (Table 3.3). With these depositions, several parameters were optimized such as temperature, co-dopants concentration, acetic acid:water content, types of dopants precursors. The substrate temperature was maintained with the help of tin bath and Eurotherm temperature controller. The flow rate of the spraying solution was kept at 1ml/min. Nitrogen (from Infra) was used as carrier gas (90 psig). The distance between the nozzle and the substrate was 15 cm.

Table 3.3. Summary of AIZO thin film fabrication conditions

Sample ID	**Dopants type and (at.%)**		**Dep. Time (min)**	**Dep. Temp (°C)**	**Solution condition (Zn)**	**Effect studied**
	Al	In				
ALAC-T400	A (1.5)	I (1.5)	10	400	S50	Temperature
ALAC-T425	A (1.5)	I (1.5)	10	425	S50	
ALAC-T450	A (1.5)	I (1.5)	10	450	S50	
ALAC-T475	A (1.5)	I (1.5)	10	475	S50	
S0.5	A (0.5)	I (0.5)	10	425	S50	Dopants concentration
S1	A (1)	I (1)	10	425	S50	
S1.5	A (1.5)	I (1.5)	10	425	S50	
S2	A (2)	I (2)	10	425	S50	
S3	A (3)	I (3)	10	425	S50	
A-0	A (1.5)	I (1.5)	10	425	A0	Acetic acid & water content
A-25	A (1.5)	I (1.5)	10	425	A25	
A-50	A (1.5)	I (1.5)	10	425	A50	

A-75	A (1.5)	I (1.5)	10	425	A75	
A-100	A (1.5)	I (1.5)	10	425	A100	
S25	A (1.5)	I (1.5)	10	425	S25	Equal variations of acetic acid and water content
S50	A (1.5)	I (1.5)	10	425	S50	
S100	A (1.5)	I (1.5)	10	425	S100	
S150	A (1.5)	I (1.5)	10	425	S150	
ALCL-T425	B (2)	I (2)	10	425	S50	Temperature
ALCL-T450	B (2)	I (2)	10	450	S50	
ALCL-T475	B (2)	I (2)	10	475	S50	
ALCL1	B (1)	I (1)	10	450	S50	Dopants concentration of aluminium chloride precursor
ALCL1.5	B (1.5)	I (1.5)	10	450	S50	
ALCL2	B (2)	I (2)	10	450	S50	
ALCL3	B (3)	I (3)	10	450	S50	
ALS-T425	B (2)	I (2)	20	425	S50	Temperature
ALS-T450	B (2)	I (2)	20	450	S50	
ALS-T475	B (2)	I (2)	20	475	S50	
ALS1	C (1)	I (1)	20	425	S50	Dopants concentration of aluminium sulphate precursor
ALS1.5	C (1.5)	I (1.5)	20	425	S50	
ALS2	C (2)	I (2)	20	425	S50	
ALS3	C (3)	I (3)	20	425	S50	
ALAC	A (1.5)	I (1.5)	10	425	S50	Type of aluminium precursor
ALCL	B (2)	I (2)	10	450	S50	
ALSP	C (2)	I (2)	20	425	S50	
U10	A (1.5)	I (1.5)	10	475	S50	Ball milling effect
M10	A (1.5)	I (1.5)	10	475	S50	

(at.% – atomic percentage, dep.time – deposition time, and dep. Temp – deposition temperature)

3. 2. 3. Ball milling conditions

Prior to the preparation of starting solution, zinc precursor was milled for an hour in a Pulverissette 7 (Fritsch) planetary ball milling equipment, using the following conditions: volume of the vessel- 250 ml, ball to powder ratio- 5:1 and angular speed- 300 rpm. The sample id is M10 (Table 3.3). One unmilled sample (U10) was prepared for the comparison purpose. Both the depositions were carried out at 475°C for 10 min.

3. 3. Undoped ZnO thin film deposition by sputtering

3. 3. 1. Fabrication of undoped ZnO thin films at a target-substrate distance of 14 cm

Undoped ZnO thin films were deposited on glass substrates at room temperature by reactive radio frequency (RF) sputtering at different powers 50, 75, 100, and 125 W. The ZnO target was 99.999% pure (Kurt J. Lesker). The target-substrate distance was 14 cm. The pressure in the chamber maintained at 31mTorr with the controlled flow rate (50 sccm) of argon (99.999%, Praxair). The deposition was carried out for 2 h. The samples were identified based on power magnitudes LD50, LD75, LD100, and LD125.

3. 3. 2. Fabrication of undoped ZnO thin films at a target-substrate distance of 7 cm

Undoped ZnO thin films were deposited on glass substrates at room temperature by reactive radio frequency (RF) sputtering at different powers 50, 75, 100, and 125 W. The ZnO target was 99.999% pure (Kurt J. Lesker). The target-substrate distance was 7 cm. The pressure in the chamber maintained at 7.3mTorr with the controlled flow rate (20 sccm) of argon (99.999%, Praxair). The deposition was carried out for 2 h. The samples were identified based on power magnitudes SD50, SD75, SD100, and SD125.

3. 3. 3. Fabrication of undoped ZnO thin films at different substrate rotation speeds

Undoped ZnO thin films were deposited on glass substrates at room temperature by reactive radio frequency (RF) sputtering at 100 W. The Zn metal target of 99.993-99.995% pure (Kurt J. Lesker) was used. The target-substrate distance was 7 cm. The pressure in the chamber maintained at 13mTorr with the controlled flow rates of argon (99.999% pure, Praxair) and oxygen (99.999% pure, Praxair) were 10 and 7.5 sccm, respectively. The deposition was carried out for 2 h without substrate rotation, and with substrate rotation at different speeds (20, 40, 60, and 80 rpm). The samples were identified with their speed magnitudes, namely, R0, R20, R40, R60, and R80.

3. 4. In and Ga co-doped ZnO thin film deposition by co-sputtering

In and Ga co-doped ZnO thin films (IGZO) were deposited on glass substrates at room temperature by co-sputtering. We have placed Zinc Oxide/Gallium Oxide target (ZnO/Ga_2O_3,95/5 wt%, Kurt J. Lesker) in direct current magnetron and Indium target (99.99% pure, Lesker) in radio frequency magnetron and set the parameters as shown in below Table 3.4. The argon gas (99.999%, Praxair) flow was maintained at 15 sccm.

Table 3.4. Summary of IGZO thin film fabrication conditions

Thin film ID	Pressure (mTorr)	ZnO/Ga_2O_3 power (Watts)	In power (Watts)	Time (h)	Effect studied
I3	7.1	40	3	1	Power
I5	7.1	40	5	1	
I10	7.1	40	10	1	
I15	7.1	40	15	1	

3. 5. Characterization

3. 5. 1. Crystallite size and preferential orientation analysis

The X-ray diffraction (XRD) patterns of ZnO thin films were obtained from an X'Pert PRO PANalytical instrument using CuKα (λ=1.5406 Å) radiation. The crystallite size (D) of the films was estimated using the Schrerrer´s formula [2],

$$D = 0.9\lambda/\beta\cos\theta,$$

where λ (1.54Å) is the wavelength, β is the full width half maximum (FWHM) and θ is the angle of diffraction. Further, preferential orientation of the films were identified by estimating the texture coefficient (TC) of the planes by using the below formula [3],

$$TC_{(hkl)} = \frac{I(hkl)/I_0(hkl)}{\frac{1}{n}\sum_{i=1}^{i=n} I(hkl)/I_0(hkl)},$$

where $I(hkl)$ is the obtained intensity of the plane, $I_0(hkl)$ is the reference intensity of the plane (JCPDS of ZnO: 01-070-8070) and n is the number of the planes obtained in the spectra.

3. 5. 2. Surface morphology analysis

Thin film morphologies were observed through Zeiss-Auriga High Resolution Scanning Electron Microscope (HRSEM). Images were obtained using an accelerating voltage of 1kV for the incident electron beam. From the obtained image the size of the nanostructures were estimated using the scale bar.

3. 5. 3. Optical transmittance and sheet resistance measurements

The optical transmittances of ZnO thin films, in the UV-vis region were obtained using a Shimadzu 2401 spectrophotometer. We used a reference glass slide to measure the transmittance of the deposited thin films. From the spectra, the average transmittance (at 550nm) of each film, was obtained. The band gap energy, E_g, of the AIZO films were estimated from the extrapolation of $(\alpha h\gamma)^2$ versus $h\gamma$ plot, where $h = 6.624 \times 10^{-34}$ J-s, α is optical absorption constant, and γ is radiation frequency.

The sheet resistance values of ZnO thin films were obtained using Veeco 4 point probe instrument. We have measured sheet resistance at different locations (including edges and center) on the ultrasonically deposited thin films (5x2.5cm). Similarly for sputtered samples (2.5x1.7cm)The figure of merit (FOM) of the films was estimated using G. Haacke´s formula [4], which is a well balanced equation between optical and electrical properties. This helps to check the quality of the thin films for TCO applications,

$$FOM(\Phi_{TC}) = T^{10}/R_{s,}$$

where, T is the transmittance at 550nm, and R_s is the sheet resistance of the thin films.

3. 5. 4. Thickness measurements

The thickness of the films were measured with KLA Tencor P15 model profilometer. In order to measure the thickness, it is necessary to have step in the substrate containing the film. The step was obtained by immersing the substrate in the beaker which contains a mixture of hydrochloric acid and water (1:5). This immersion was kept for one minute and dried by blowing nitrogen gas. The thickness values of ultrasonically sprayed films were with ± 20-40nm error variations. The thickness values of sputtered films were with ± 15-30 nm error variations.

3. 5. 5. Quantitative analysis

Presence of dopants was confirmed by depth analysis through IMS-6F CAMECA Secondary Ion Mass Spectroscopy (SIMS). In this work, we have performed this analysis for the films prepared with co-dopants concentrations variations (S0.5, S1.5 and S3), since S1.5 showed the highest figure of merit ($8.3\pm0.55x10^{-3}/\Omega$), among other samples.

3. 6. References

[1] T. Young Ma, S. H. Kim, H. Y. Moon et al. Substrate temperature dependence of ZnO films prepared by ultrasonic spray pyrolysis, Jpn. J. Appl. Phys. Vol. 35 (1996) pp. 6208-6211.

[2] L. Alexander, H. P. Klug, L. Alexander, H. P. Klug, Determination of Crystallite Size with the X-Ray Spectrometer Determination of Crystallite Size with the X-Ray Spectrometer, Journal of Applied Physics. 21 (1950) 1–7.

[3] J. Gao, W. Jie, Y. Yuan, T. Wang, G. Zha, J. Tong, et al., Dependence of film texture on substrate and growth conditions for CdTe films deposited by close-spaced sublimation Dependence of film texture on substrate and growth conditions for CdTe films deposited by close-spaced sublimation, J. Vac. Sci. Technol. A 29 (2011) 051507.

[4] G. Haacke, New figure of merit for transparent conductors, J. Appl. Phys. 47 (1976) 4086–4089.

CHAPTER 4

RESULTS AND DISCUSSION – ULTRASONIC SPRAY PYROLYSIS

In this chapter, the structural, morphological, optical, electrical, and compositional characteristics of ultrasonically sprayed undoped and co-doped ZnO thin films as a function of deposition variables, is presented. Further, a correlation among the different characterization is discussed. Optimization of deposition variables based on the Haacke´s Figure of Merit are also mentioned.

4. 1. Undoped ZnO thin film deposition

The effect of water content in the starting solution on the structural, morphological, optical and electrical characteristics of the undoped ZnO thin films is described below. These depositions were carried out for 12 min at 450°C.

4. 1. 1. Structural properties

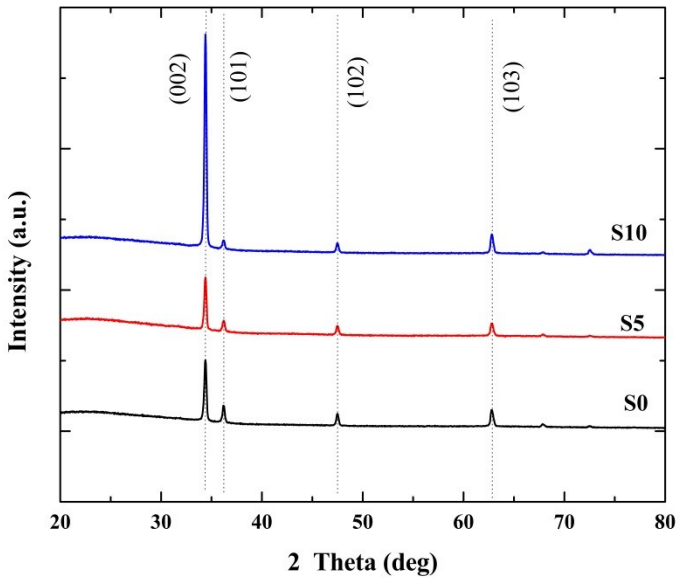

Fig. 4. 1. XRD of Undoped ZnO thin films deposited at 450°C with different water contents in the starting solution (S0-deposited with 0ml of water in the starting solution, S5-deposited with 5ml of water in the starting solution,S10- deposited with 10ml of water in the starting solution).

Fig. 4. 1. shows the XRD patterns of the deposited ZnO thin films deposited with different water contents in the starting solution. All the X-ray diffraction patterns fit well with the hexagonal wurtzite type ZnO structure according to the reported data in JCPDS file 01-089-0510. We can observe that all samples are polycrystalline with a (002) preferential orientation, and the other peaks presented are (101), (102), and (103). Identical polycrystalline nature for undoped ZnO is reported by several authors [1-3]. The intensity of (002) plane increases, as the water content increases from 0 ml to 10 ml, which in turn enhances the crystallinity of the films. From this result, it is believed that, the increase in water content changes the growth kinetics. The peak associated to the (002) plane was the basis for the estimation of the crystallite size (D) according to the Scherrer's formula [4]. The crystallite size of the samplesS0, S5, and S10 were found (estimated from the plane (002)) to be 23, 29, and 28 nm respectively. The thickness of the films S0, S5, and S10 were 515, 509, and 532 nm respectively.

4. 1. 2. Morphological properties

The effect of water content in the starting solution on the morphology of ZnO thin films is shown in Fig. 4. 2. The morphology (Fig.4.2 (a)) of S0 sample (without water), consists of grains with non definite geometries, perhaps resembling pyramids, tripods and few hexagonal slices. A water content of 5 ml per 100 ml, causes change in the morphology of the films, as features with hexagonal structures as seen in Fig. 4.2 (b).

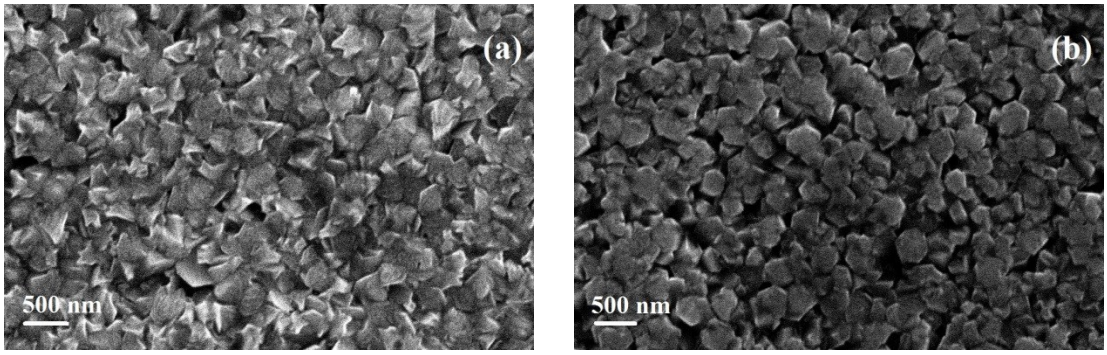

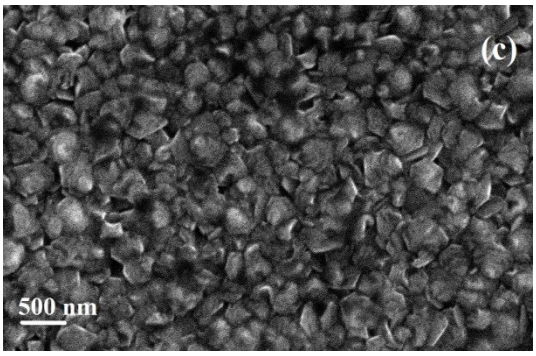

Fig. 4. 2. Scanning electron microscopy images of undoped ZnO thin films (a)Film prepared with 0ml water content (S0), (b) Film prepared with 5ml water content (S5), and (c) Film prepared with 10ml water content (S10).

The hexagonal grain size varies from 100-300 nm. Similar hexagonal features are reported by A. Smith et. al [5]. Further increase in the water content (10 ml) gives rise to a surface covered by overlapped and agglomerated hexagonal thin slices of size around 300 nm as can be seen in Fig. 4.2(c). Thus, a single variable, the water content, in the starting solution affects geometry shape and grain size characteristics of ZnO thin films.

4. 1. 3. Optical and electrical properties

Fig. 4. 3. shows the optical transmittance of the ZnO thin films deposited from starting solutions with different water content (0, 5, 10 ml/total volume). The samples showed a sharp decrease (absorption edge) in transmittance in the near ultraviolet region, around 375 nm. The measured transmittance at 550 nm for the samples S0, S5, and S10 were 59, 60, and 56%. The bandgap of the samples was around 3.28eV (bandgap estimation as in section 3.5.3). Undoped ZnO thin films showed high sheet resistance between $4x10^6$ and $5x10^6$ Ω/□, which is due to presence of oxygen vacancies [6]. In order to the enhance the electrical properties co-doping was carried out and those results are furnished in the following sections.

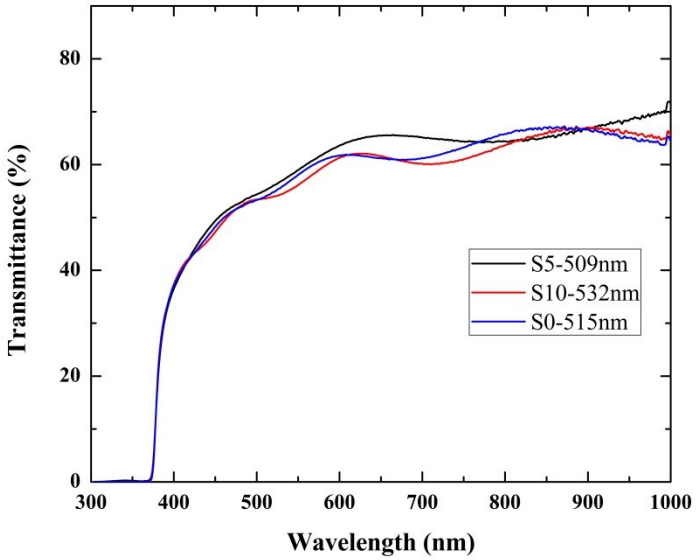

Fig. 4. 3. Optical transmittance of undoped ZnO thin films deposited at 450°C with 0ml (S0), 5ml (S5), and 10ml (S10) of water content in the starting solution.

4. 2. Characterization of Al and In co-doped ZnO

The need to manufacture ZnO thin films with low resistance and high transmittance leads to explore the depositon conditions including doping. As we have established in introduction, the lack of information in the co-doping route, for ZnO thin films, points the need for a detailed study on the effect of substrate temperature, change in the doping level, solvent proportions, type of doping precursors and milling of precursor. The study of these variables is now presented in the following sections, in such a way that main factors affecting transport and optical properties of ZnO thin films, are considered.

4. 2. 1. Optimization of substrate temperature

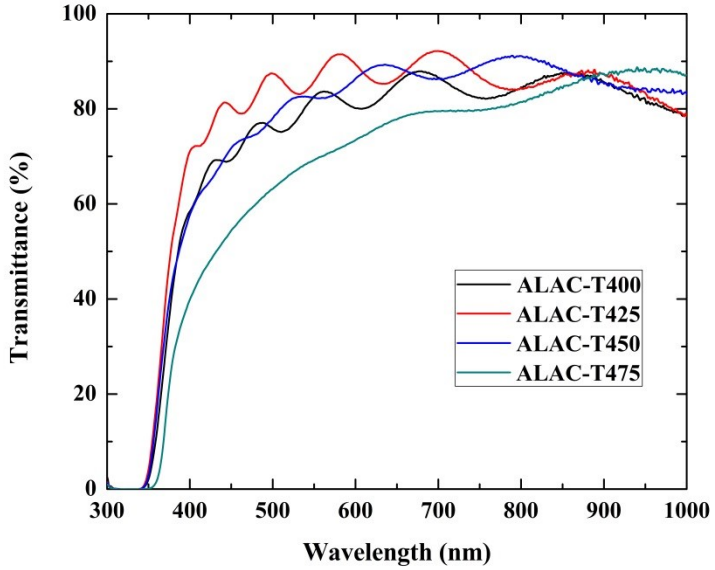

Fig. 4.4.1. Transmittance curves of AlZO thin films deposited at different substrate temperatures (400, 425, 450, and 475°C) with Al:In =1.5:1.5at.%.

This is a preliminary experiment in order to find a right temperature to obtain high figure of merit from range of substrate temperatures (400, 425, 450, and 475°C) using aluminium acetylacetonate as aluminium precursor. We have examined optical transmittance, sheet resistance, and figure of merit for the samples ALAC-T400, ALAC-T425, ALAC-T450 and ALAC-T475. The transmittance spectrum of the films is shown in Fig. 4.4.1.

Table 4.1. Optical transmittance (T_{550nm}), Sheet resistance (R_s), and Figure of Merit (FOM) of AlZO thin films deposited at 400, 425, 450, and 475°C .

Sample ID	**T_{550nm} (%)**	**R_s (Ω/□)**	**FOM (x10^{-3}/Ω)**
ALAC-T400	*82*	*30-60*	*2.2-3.4*
ALAC-T425	*85*	*22-25*	*7.8-8.9*
ALAC-T450	*82*	*23-29*	*4.7-5.9*
ALAC-T475	*83*	*90-219*	*0.7-1.7*

All the samples show transmittance >80%. Further, figure of merit (FOM) estimation is performed (T^{10}/R_S) using Haacke's formula (3.5.3) and tabulated in Table 4.1. This shows highest FOM is achieved for the sample deposited at 425°C.

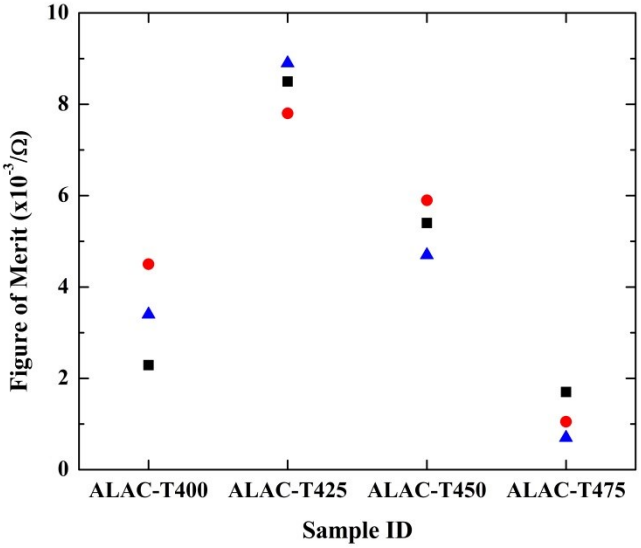

Fig. 4.4.2. Figure of merit of AIZO thin films deposited at different substrate temperatures (400, 425, 450, and 475°C) with Al:In =1.5:1.5at.%.

Below this temperature (<425°C), deposited films show an high value in the sheet resistance (47-50Ω/□), due to incomplete synthesis, while for high temperatures, in the order of 475°C, the occurrence of inhomogeneity reaction (in vapour phase) near the substrate (film surface appeared powdery), can degrade the quality of the films as well as increase the respective sheet resistance. Hence AIZO thin films were grown at 425°C since this temperature showed the higher figure of merit ($8.3\pm0.55 \times 10^{-3}/\Omega$) than others (Table 4.1).

4. 2. 2. Effect of co-dopants concentration

The effect of the variation of doping concentration on the structural, morphological, optical, electrical characteristics, and figure of merit of the AIZO thin films is presented. In order to simplify the exploration, same Al:In proportions were tested, namely 0.5:0.5 (S0.5), 1:1 (S1), 1.5:1.5 (S1.5), 2:2 (S2), and 3:3 (S3).

4. 2. 2. 1. Structural properties

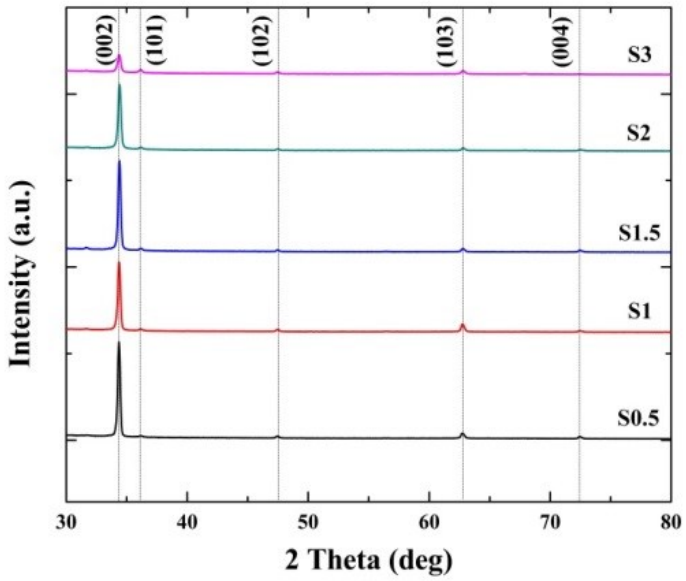

Fig. 4.5. XRD of AIZO thin films deposited with different co-dopants concentrations (S0.5 =0.5at.%Al:0.5at.%In, S1 =1at.%Al:1at.%In, S1.5 =1.5at.%Al:1.5at.%In, S2 =2at.%Al:2at.%In, and S3 =3at.%Al:3at.%In).

The XRD of AIZO thin films, with different doping concentration in the solution, and deposited at 425°C is shown in Fig. 4.5. All the films are polycrystalline and confirmed the formation of hexagonal wurtzite structure, irrespective of dopants proportions [7]. The preferential orientation is (002), confirms the growth of the films is along c-direction. No other peaks belong to either aluminium or indium phases, including metallic segregation, were observed in the XRD patterns, in turn indicate that both Al and In are incorporated well into the ZnO lattice [8].

In addition, the intensity of the peak (002) reduces as the dopants concentration increases, which is a result of reduction in thickness (Table 4.2). Similar intensity variations with respect to thickness have been previously reported by other authors [9,10]. It is worth to mention that reduction in thickness affects the values of full width at half maximum (FWHM), in turn affects the crystallinity. The estimated crystallite sizes (D) of the samples

S0.5, S1, S1.5, S2 and S3 were 49, 49, 35, 29, and 24 nm, respectively, using Scherrer's formula [4].

4. 2. 2. 2. Morphological properties

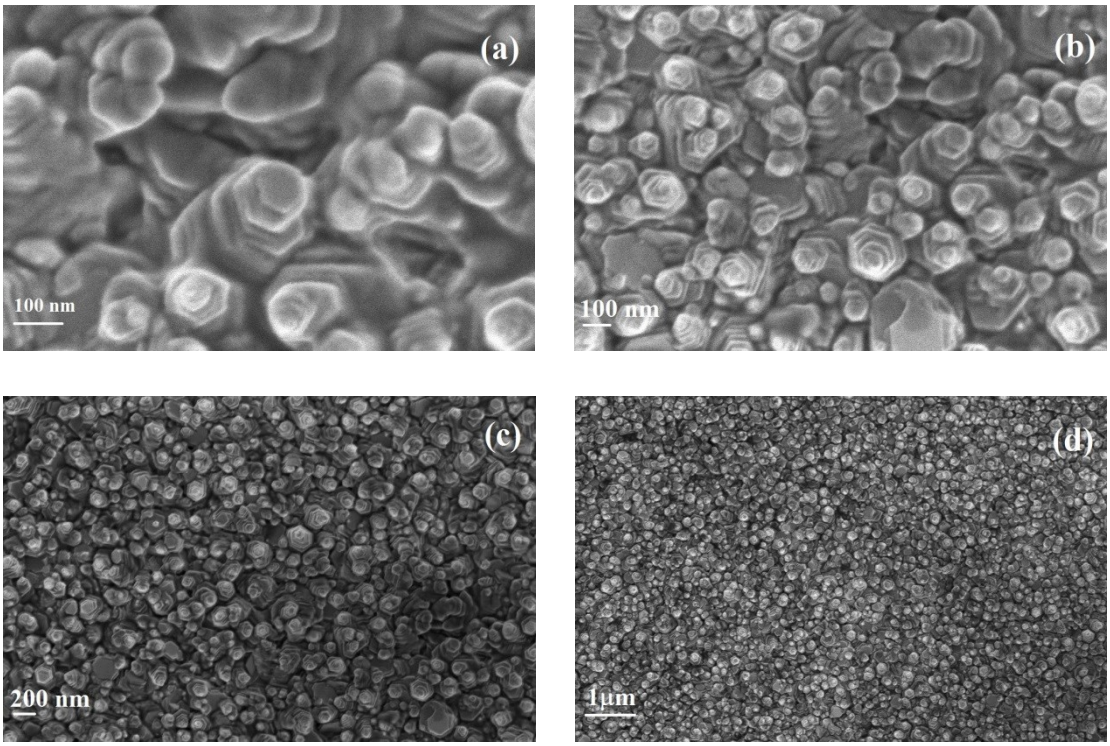

Fig. 4.6.1. Surface morphology of AIZO (S0.5) thin films deposited with 0.5at.% of Al, and 0.5 at.% of In, at 425°C, at different magnifications (a)100KX, (b)50KX, (c)20KX, and (d)10KX.

The morphologies of AIZO samples, S0.5, S1.5 and S3, are shown in the Fig. 4.6. Well defined hexagonal nanopyramids, are observed for S0.5 sample in Fig. 4.6.1 (a-d). These pyramidal structures are found to be uniformly distributed throughout the film. The estimated diameters show a wide distribution, ranging from 50 to 250 nm. The diameter of basal hexagon is around 100-120 nm. As the stacks of hexagons grow on the basal hexagon, the diameter of the hexagons is reduced to around 10 nm. From this, we can confirm that, low level doping results in forming hexagonal nanopyramids. Similar nanostructures were observed by A. Smith et. al. for undoped ZnO, sprayed using chlorine free solution [5]. When the concentration level of the dopants is increased (Al:In = 1.5 at.%:1.5 at.%), surface morphology changes as elongated grains with average dimensions

~200nm x 100nm as shown in Fig. 4.6.2 (a-d). It is worth to note that grains are wider ranging from ~40 to 550nm. These grains are densely packed structures and have stacks of slices. This change in morphology from hexagons (S0.5) to elongated grains (S1.5) is due to the successful diffusion of dopants.

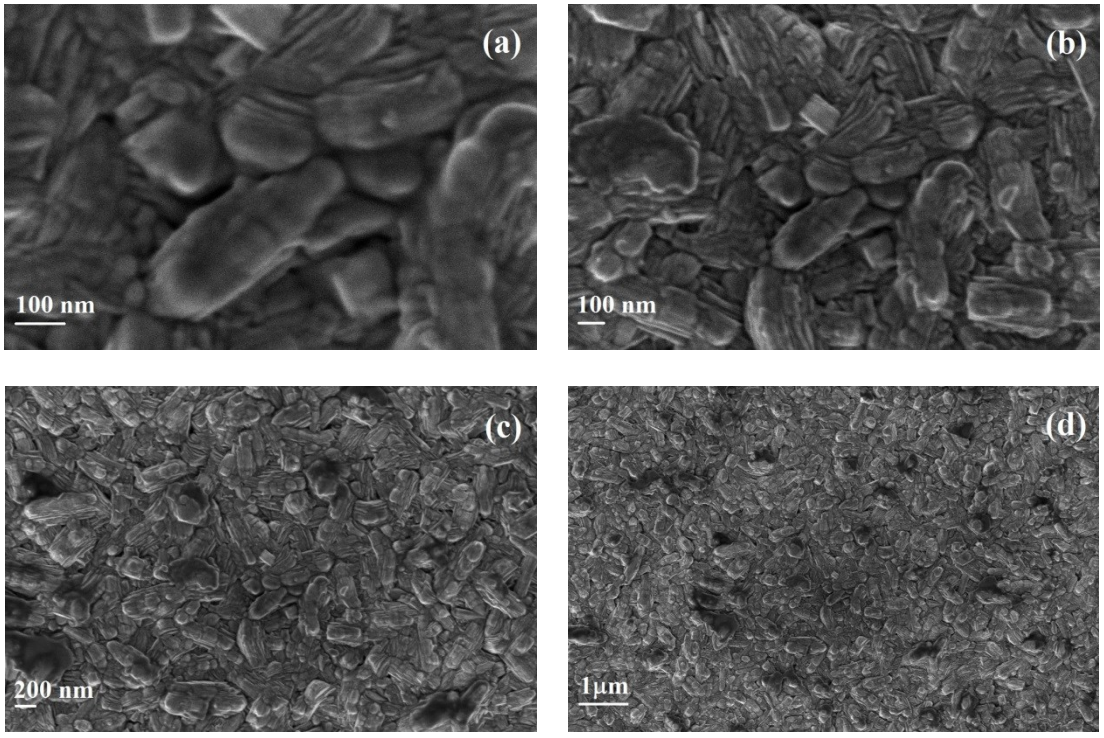

Fig. 4.6.2. Surface morphology of AIZO (S1.5) thin films deposited with 1.5at.% of Al, and 1.5 at.% of In, at 425°C, at different magnifications (a)100KX, (b)50KX, (c)20KX, and (d)10KX.

When doping level is further increased (Al:In =3 at.%:3 at.%) the surface of film (S3) is covered with irregular structures of trigonals of different sizes as shown in Fig. 4.6.3 (a-d). Identical morphology was found for the Al-doped ZnO thin films by spray pyrolysis, earlier reported by Crossay's group [11]. For low doping concentration, the effect of doping cations is not observed due to the small quantity incorporated into the lattice as occurs in films doped with Al and In at 0.5:0.5 at.%. However, the crystallographic characteristics of ZnO structure, based in the polar or less polar character of the planes exposed during the growth process, causes difference in the shape of the grains as the doping concentration

increases. Thus the dopant concentration plays a vital role in changing the morphology of co-doped films.

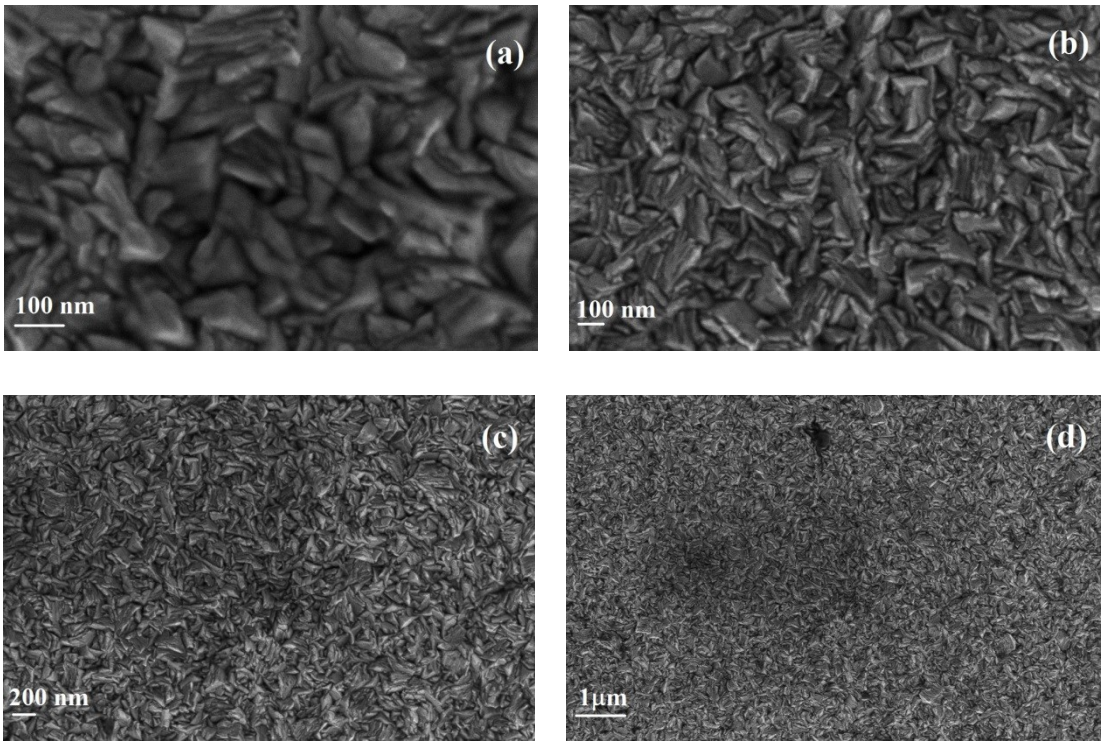

Fig. 4.6.3. Surface morphology of AIZO (S3) thin films deposited with 3 at.% of Al, and 3 at.% of In, at 425°C, at different magnifications (a)100KX, (b)50KX, (c)20KX, and (d)10KX.

4. 2. 2. 3. Optical and electrical properties

The estimated films thickness, transmittance, band gap, sheet resistance, and figure of merit of AIZO thin films doped with different concentrations, are furnished in Table 4.2. The optical transmittance in the visible region of AIZO thin solid films for all deposited films is shown in Fig. 4.7. We have measured sheet resistance at different locations (including edges and center) on the thin films (5x2.5 cm) and the range of values were included in the Table 4.2.

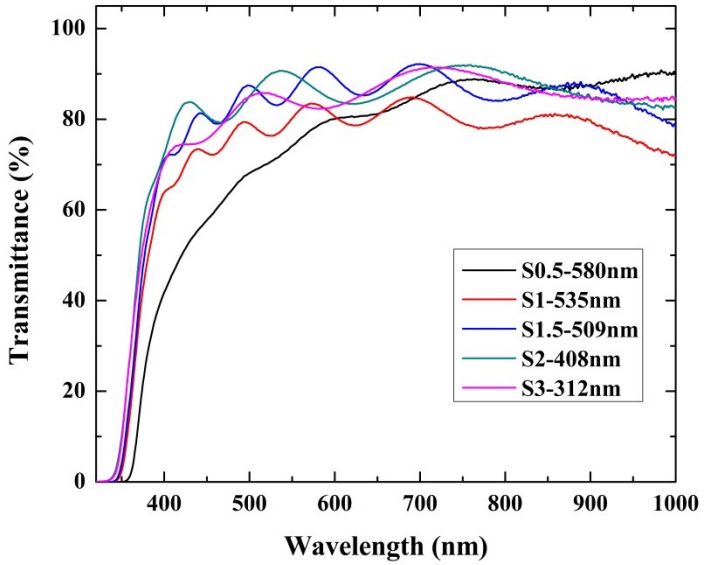

Fig. 4.7. Optical transmittance of AIZO thin films deposited with different co-dopants concentrations (S0.5 =0.5at.%Al:0.5at.%In, S1 =1at.%Al:1at.%In, S1.5 =1.5at.%Al:1.5at.%In, S2 =2at.%Al:2at.%In, and S3 =3at.%Al:3at.%In).

It is worthy to mention that the film thickness variation due to a lack of control during the growth process. As a matter of fact, in pneumatic spray pyrolysis, it is possible to control films thickness in a reliable way by observing the change in color of the film during deposition. In the case of ultrasonically sprayed films the wall of the reaction chamber is covered by a dense, white depositions. Deposition time is the only way to control to certain extent, the film thickness, but some uncertainty is present in every deposition. This is the reason why the S0.5 sample, presents the highest thickness (average value of thicknesses of is given in Table 4.2, there were variations in the thickness with ±20-40nm), showed the lowest average transmittance (74%) in the 400-700 nm interval, whereas all other samples exhibited higher trasmittance, >80%. The band gap values varied between 3.44 and 3.50 eV (bandgap estimation as in section 3.5.3). This increase in the band gap of the AIZO films can be the result of the increase in carrier concentration, known as Burstein-Moss effect [12]. Our band gap results are in good agreement with those reported by Tohsophon´s work on sputtered AIZO films [13].

Table 4.2. Thickness, Optical and electrical characteristics of AIZO films deposited with co-dopants concentration variations (S0.5 =0.5at.%Al:0.5at.%In, S1 =1at.%Al:1at.%In, S1.5 =1.5at.%Al:1.5at.%In, S2 =2at.%Al:2at.%In, and S3 =3at.%Al:3at.%In).

Characteristics	**Sample ID**				
	S0.5	**S1**	**S1.5**	**S2**	**S3**
Thickness (nm)	580	535	509	408	312
Transmittance at 550nm (%)	74	80	85	90	83
Band gap (eV)	3.44	3.48	3.49	3.50	3.50
Sheet resistance (Ω/□)	91-164	38-45	22-25	66-83	50-90
Figure of Merit (10^{-3}/Ω)	0.3-0.5	2.3-2.8	7.8-8.9	4.2-5.2	1.7-3.1

The reason for variations in the sheet resistance can be explained as follows.

(a) The samples S0.5 and S1 films presented high resistance values could be due to very low level doping.

(b) The sample S1.5 exhibited the lowest sheet resistance. A brief discussion is necessary to explain these results. Altamirano et al. [14] have deposited Al and F co-doped ZnO thin films by solgel technique. In the discussion of the results, they have encountered that decrease in the resistivity of AZO thin films can be due to the presence of Al_2O_3 crystallites at the ZnO grain boundaries, i.e. these crystals have an effect of passivation of the traps present in the material, according to photodecay measurements they also reported. Further increase in Al content, increases the number of Al_2O_3 aggregates at the grain boundaries, which may act as dispersion centers causing that resistivity of AZO films increases. As with solgel technique, in the ultrasonic spray technique the formation of Al_2O_3 is also favored in the present case, due to the great affinity of aluminum for oxygen under the high temperature synthesis. As a result, it is considered that the incorporation of the dopant as ‘free’ aluminum, which could act as electron donor, is unlikely to occur. On the other

hand, the In doping can be proceed by replacement of Zn into the ZnO lattice, as is usually accepted.

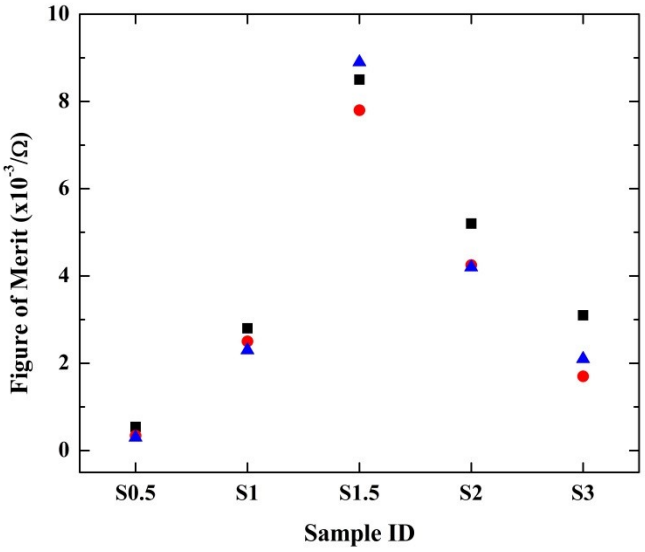

Fig. 4.8. Figure of merit of AIZO thin films deposited with co-dopants concentration variations (S0.5 =0.5at.%Al:0.5at.%In, S1 =1at.%Al:1at.%In, S1.5 =1.5at.%Al:1.5at.%In, S2 =2at.%Al:2at.%In, and S3 =3at.%Al:3at.%In).

(c) The samples S2 and S3 showed higher sheet resistance than S1.5, could be resulted from the reduction of carrier concentration. Excess doping of Al and In forms non-conducting Al_2O_3/In_2O_3 clusters at grain boundaries, leading to high sheet resistance. Researchers previously claimed that high doping concentration causes an increase in sheet resistance [15].

The optical and electrical quality can be examined with the help of a well-balanced equation (section 3.5.3), called as Haacke's figure of merit (T^{10}/R_s). As expected, S1.5 thin film presented (Fig. 4. 8) the highest figure of merit, $8.3\pm0.55x10^{-3}/\Omega$.

4. 2. 2. 4. SIMS analysis

In order to confirm the incorporation of dopants, depth analysis is carried out by SIMS. Based on the relative sensitive factors the elements were identified.

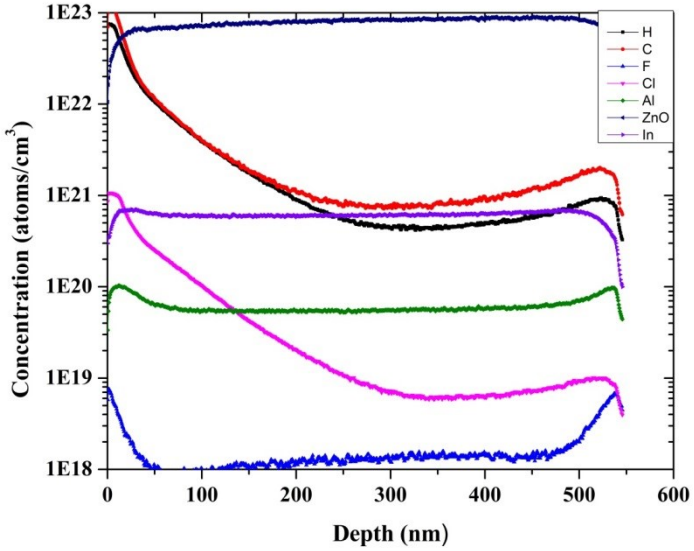

Fig. 4.9 (a). SIMS depth profile of AIZO thin films deposited with co-dopants concentration variations [S0.5 =0.5at.%Al:0.5at.%In].

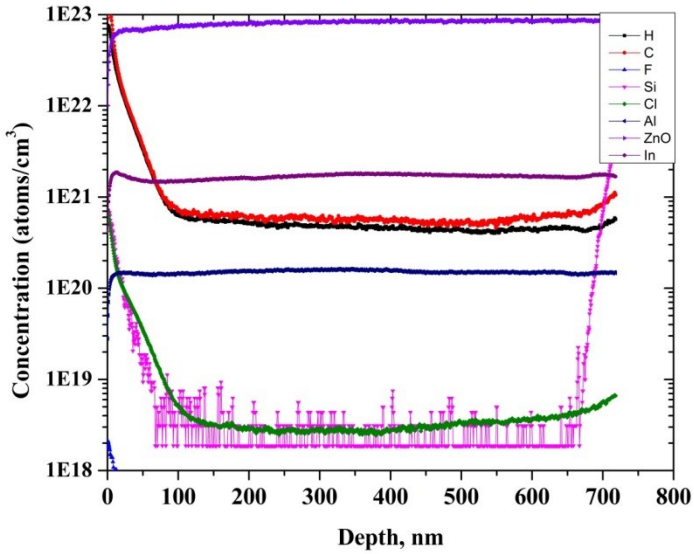

Fig. 4.9 (b). SIMS depth profile of AIZO thin films deposited with co-dopants concentration variations [S1.5 =1.5at.%Al:1.5at.%In].

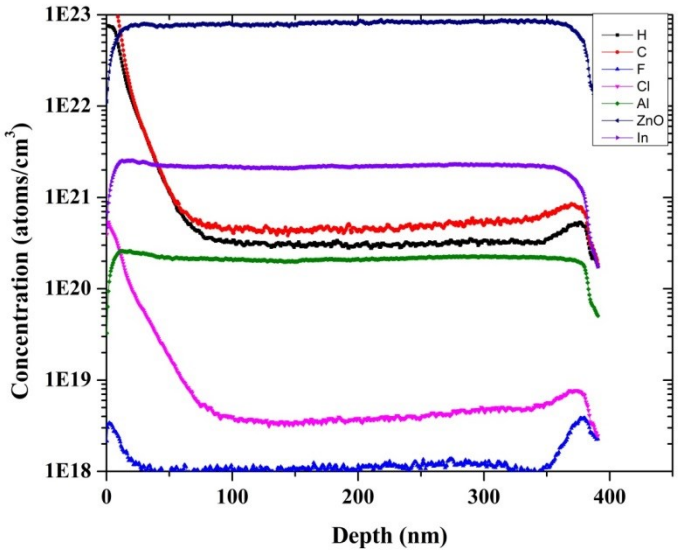

Fig. 4.9 (c). SIMS depth profile of AIZO thin films deposited with co-dopants concentration variations [S3 =3at.%Al:3at.%In]

Depth profiles of S0.5 (Fig. 4.9a), S1.5 (Fig. 4.9b) and S3 (Fig.4.9c) clearly show that Al and In are well embedded into the lattice, presenting almost constant concentration profiles. It is important to notice that the concentration of Al is lower than In in all the cases. This could be due to the difference in the vapor pressures of aluminium and indium. Additionally, it could be due to the difference in the volatilities of the dopant precursors. Aluminium acetylacetonate presents high volatility because of its lower melting point, 192-194°C, than indium (III) acetate, 270°C. Further, substrate elements such as Cl, and Si are also found. However, some contaminants like F, and C are also observed.

4. 2. 3. Effect of acetic acid and water content

From the above study, we observed that 1.5 at.% of Al and 1.5 at.% of In helps in achieving high figure of merit. So we further investigated by varying the acetic acid (0, 25, 50, 75, 100 ml/L) and water content (100, 75, 50, 25, 0 ml/L) in the zinc precursor solution (Zinc acetate dihydrate). These AIZO thin films were deposited at 425°C for 10 minutes using (Al:In =1.5%:1.5%). The aluminium and indium precursors were aluminium acetylacetonate and indium acetate respectively.

4. 2. 3. 1. Structural properties

XRD patterns of AIZO thin films fabricated from different acetic acid and water contents are shown in Fig.4.10. All the films were polycrystalline and confirmed the formation of hexagonal wurtzite structure, irrespective of solvent proportions. According to the position of the peaks, the wurtzite structure was confirmed in all AIZO deposited films. The intensity of the (002) plane dominates in films deposited from starting solutions with an acetic acid content until 50 ml, indicating that films grow with the c-axis perpendicular to the substrate. In the case of the AIZO films deposited from higher than 50 ml of acetic acid, the intensity of the peaks associated with the (002) and (101) planes, are similar. In addition, no other peaks belong to dopants are found in the patterns confirm that dopants are well integrated into the ZnO lattice [8].

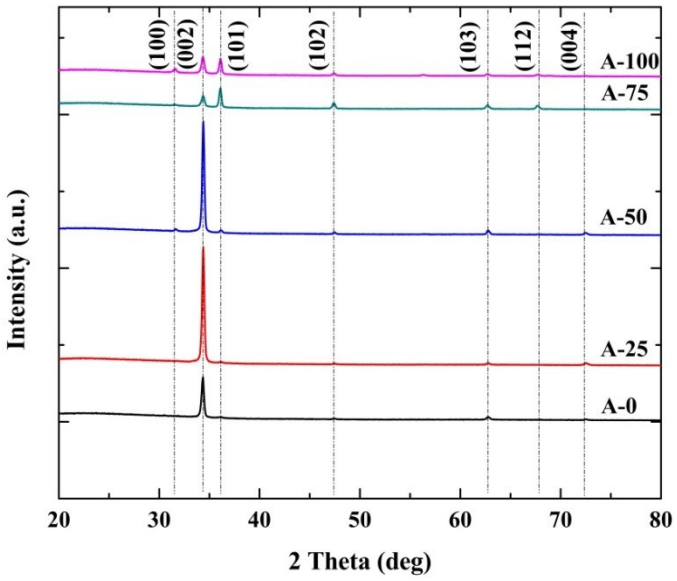

Fig. 4. 10. XRD patterns of AIZO thin films with different solvent proportions (A-0 deposited with 0 ml of acetic acid and 100 ml of water, A-25 deposited with 25 ml of acetic acid and 75 ml of water, A-50 deposited with 50 ml of acetic acid and 50 ml of water, A-75 deposited with 75 ml of acetic acid and 25 ml of water, A-100 deposited with 100 ml of acetic acid and 0 ml of water).

Further, preferential orientation is identified by estimating the texture coefficient (TC) [16]. For all the films, (002) plane texture coefficient appears to be greater than 1 (Table 4.3). Hence the preferential orientation of the grown AIZO thin films is (002). Later the crystallite size (D) of the films were calculated using Schrerrer´s formula [4], The obtained TC, D and thickness values are reported in Table 4.3.

Table 4.3. Thickness and structural parameters of AIZO thin films grown with different acetic acid and water content.

Sample ID	Thickness (nm)	TC	D (nm)
A-0	294	2.94	49
A-25	293	3.59	41
A-50	509	4.09	35
A-75	566	1.36	20
A-100	503	2.39	26

4. 2. 3. 2. Morphological properties

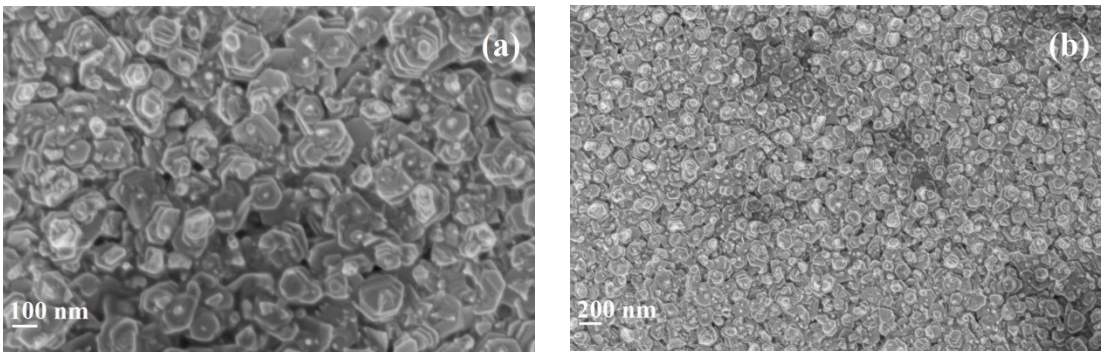

Fig. 4.11.1. Surface morphology of AIZO thin films (A-0) deposited with a zinc precursor solution contains 0ml acetic acid and 100ml of water, with (Al:In = 1.5:1.5at.%) doping concentration, at 425°C, at different magnifications (a)50KX, and (b)20KX.

Fig. 4.11 (1-5) show the variation in the morphology of AIZO thin films as a function of the acetic acid and water content in the zinc precursor solution. The morphology of the films deposited with a solution containing 0 ml acetic acid and 100 ml water were conformed of hexagonal tower structures as can be seen in Fig. 4.11.1. The size distribution of the top layer of hexagonal tower ranges from ~74 to 100 nm. When the

acetic acid content (A-25) is increased in the starting solution, we can observe a mixture of hexagonal and widely expanded flower structures (Fig. 4.11.2 (a-b)).

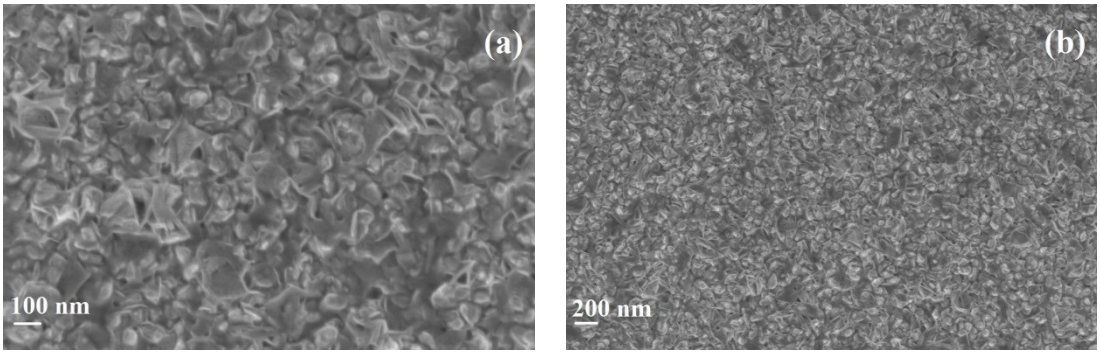

Fig. 4.11.2. Surface morphology of AIZO thin films (A-25) deposited with a zinc precursor solution contains 25ml acetic acid and 75ml of water, with (Al:In = 1.5:1.5at.%) doping concentration, at 425°C, at different magnifications (a)50KX, and (b)20KX.

When the acetic acid and water content are used equally (A-50) in the solution, the surface consists of densely packed elongated grains (or bundles) of size varying from 40 nm to 550 nm (Fig.4.11.3.(a-b)). Further, when there is an increase in the acetic acid content (A-75), the film surface has nano chisels and star like nano structures of different sizes (Figure 4.11.4.(a-b)). When the solution is free of water content (A-100), the AIZO thin films consists of crescent moon nanostructures (Fig. 4.11.5. (a-b)).

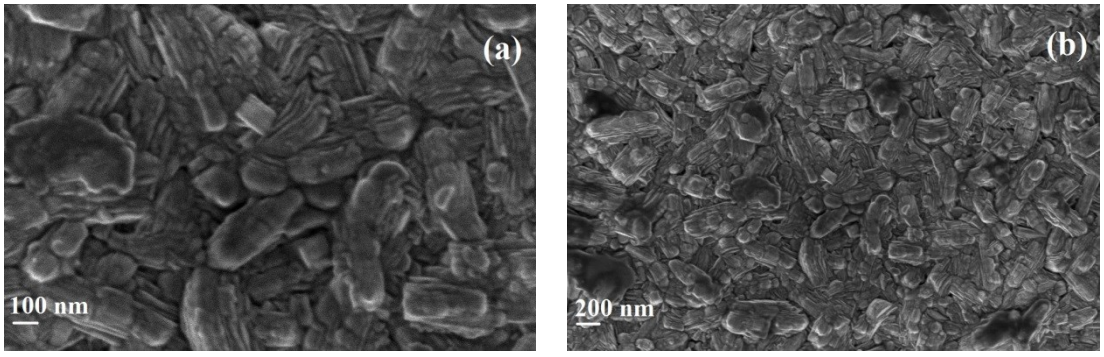

Fig. 4.11.3. Surface morphology of AIZO thin films(A-50) deposited with a zinc precursor solution contains 50ml acetic acid and 50ml of water, with (Al:In = 1.5:1.5at.%) doping concentration, at 425°C, at different magnifications (a)50KX, and (b)20KX.

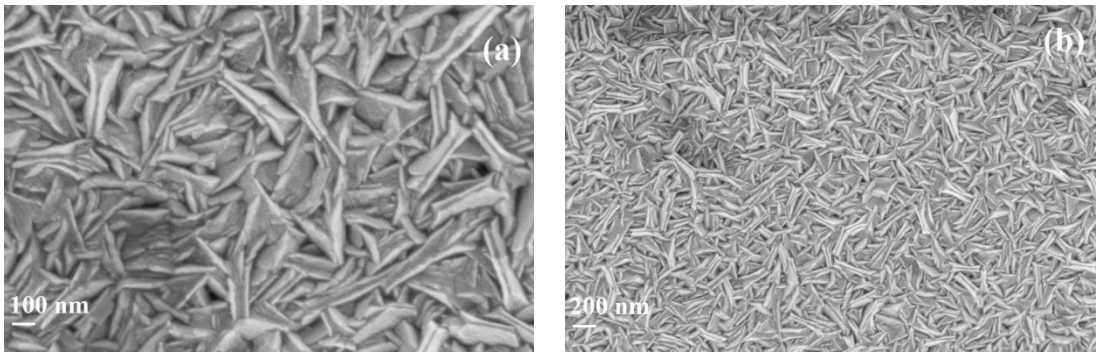

Fig. 4.11.4. Surface morphology of AIZO thin films(A-75) deposited with a zinc precursor solution contains 75ml acetic acid and 25ml of water, with (Al:In = 1.5:1.5at.%) doping concentration, at 425°C, at different magnifications (a)50KX, and (b)20KX.

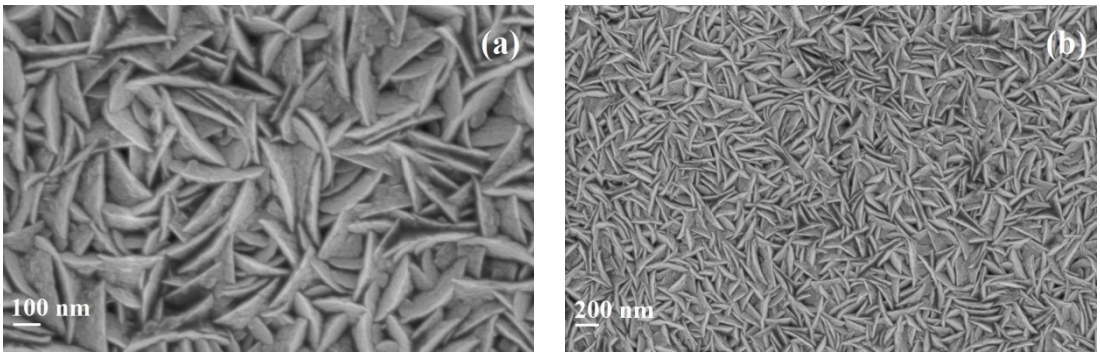

Fig. 4.11.5. Surface morphology of AIZO thin films (A-100) deposited with a zinc precursor solution contains 100ml acetic acid and 0ml of water, with (Al:In = 1.5:1.5at.%) doping concentration, at 425°C, at different magnifications (a)50KX, and (b)20KX.

From these results, where the change of water content in the starting solution leads to dramatic changes in the morphology of micro grains in AIZO thin films, we can assure that solvent proportion is an important deposition variable to be optimized in the spraying solution to achieve grains with different shapes and sizes. As a consequence, the performance of the material or device based in AIZO films will be affected according to the corresponding microstructure.

4. 2. 3. 3. Optical and electrical properties

The optical transmittance characteristics of AIZO thin films with variations with acetic acid content are given in Figure 4.12. Irrespective of sample preparation conditions, thin films showed an average transmittance (550nm) greater than 80%. However, there is a little

variation in the transmittance (Table 4.4) which is a result of change in thickness of the films (average value of thicknesses of is given in Table 4.3, there were variations in the thickness with ±20-40nm). Prasad et al. also found transmittance changes as thickness changes [17]. Almost all the films present the transmittance spectrum with interference fringes in turn indicates that films present good quality.

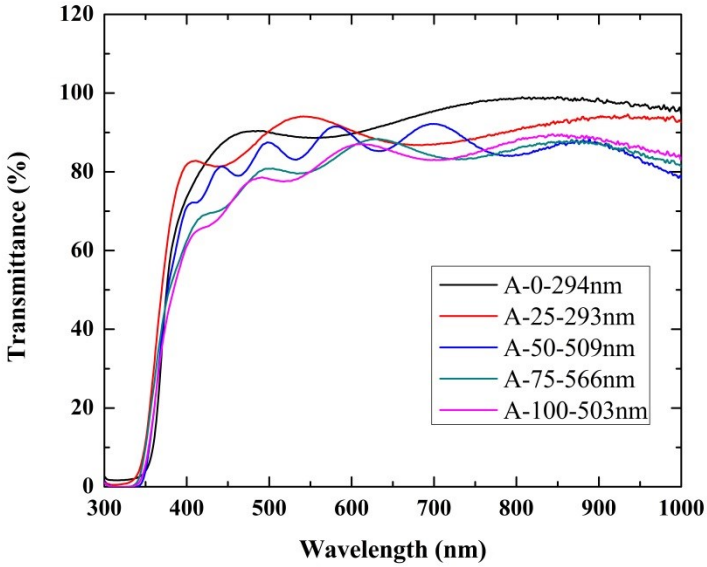

Fig. 4.12. Optical transmittance spectra of AIZO thin films deposited with different solvent proportions using (Al:In =1.5:1.5at.%) at 425°C (A-0 deposited with 0 ml of acetic acid and 100 ml of water, A-25 deposited with 25 ml of acetic acid and 75 ml of water, A-50 deposited with 50 ml of acetic acid and 50 ml of water, A-75 deposited with 75 ml of acetic acid and 25 ml of water, A-100 deposited with 100 ml of acetic acid and 0 ml of water).

Table 4.4. Optical and electrical parameters AIZO thin films deposited with different solvent proportions using (Al:In =1.5:1.5at.%) at 425°C.

Sample ID	**Transmittance (T) at 550 nm (%)**	**Sheet resistance (R_s) (Ω/□)**	**Figure of Merit ($x10^{-3}$/Ω)**	**Thickness (nm)**
A-0	88	1275-4500	0.06-0.21	294
A-25	93	299-319	1.5-1.6	293
A-50	85	22-25	7.8-8.9	509
A-75	79	110-119	0.79-0.86	566
A-100	80	362-405	0.26-0.29	503

Ilican's group stated that interference fringes represent the uniformity of the films [18]. The spectra present a clear absorption edge shift that induces variation in band gap values. The bandgap values varied between 3.3 and 3.5eV. Table 4.4 shows the variations in electrical sheet resistance and optical transmittance with respect to the acetic acid and water contents. The values of the sheet resistance suggest that co-dopants In substitutes the Zn lattice, and Al occupies grain boundaries which in turn increases the carrier concentration [14].

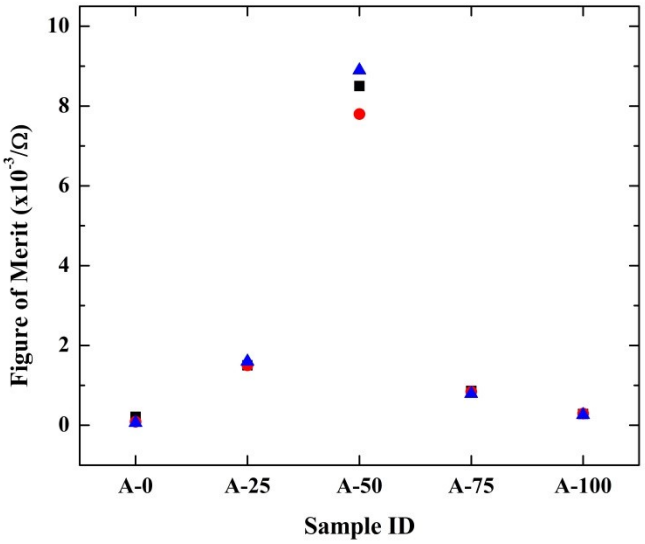

Fig. 4.13. Figure of merit of AIZO thin films (A-0 deposited with 0 ml of acetic acid and 100 ml of water, A-25 deposited with 25 ml of acetic acid and 75 ml of water, A-50 deposited with 50 ml of acetic acid and 50 ml of water, A-75 deposited with 75 ml of acetic acid and 25 ml of water, A-100 deposited with 100 ml of acetic acid and 0 ml of water).

However among all other samples, A-50 film showed the lowest sheet resistance, ~25Ω/□ could be due to its well-connected morphology, whereas other film morphologies are found with high porosity and irregular structures. The quality of the films can be examined by estimating the figure of merit. The film A-50 (Fig. 4.13) presented the highest figure of merit (Fig.4.13), whereas all other films presented less than $2x10^{-3}$/Ohm. This value indicates that films prepared with a 50:50 proportion of acetic acid and water results in good quality thin films.

4. 2. 4. Effect of equal variations of acetic acid and water content

From the above studies, we observed that Al:In = 1.5:1.5% concentration and 50ml acetic acid:50ml water proportions help to achieve high figure of merit. So we further investigated by varying the acetic acid (25, 50, 100, 150 ml/L) and water (25, 50, 100, 150 ml/L) in the zinc precursor solution (Zinc acetate dihydrate). These AIZO thin films were deposited at 425°C for 10 minutes using (Al:In =1.5%:1.5%). The aluminium and indium precursors were aluminium acetylacetonate and indium acetate respectively. (Sample description e.g. S25 thin film was deposited using 25ml of acetic acid and 25ml of water in the zinc precursor solution). The structural, morphological, optical, electrical characteristics, and figure of merit of the AIZO thin films are reported with respect to equal variations of the acetic acid and water content in the Zn precursor solution.

4. 2. 4. 1. Structural properties

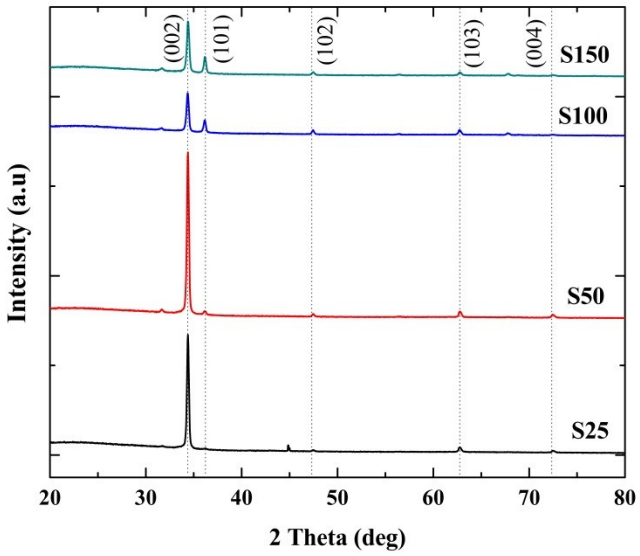

Fig. 4.14. X-ray diffraction patterns of AIZO thin films deposited with equal variations of acetic acid and water (S25 deposited from a zinc precursor solution containing 25ml of acetic acid and 25ml of water, S50 deposited from a zinc precursor solution containing 50ml of acetic acid and 50ml of water, S100 deposited from a zinc precursor solution containing 100ml of acetic acid and 100ml of water, S150 deposited from a zinc precursor solution containing 150ml of acetic acid and 150ml of water).

The XRD diffraction patterns of AIZO films deposited using equal variations of acetic acid and water content are shown in Fig. 4.14. All films presented a strong diffraction for (002) plane. The other peaks observed are (101), (102), (103), and (004). In addition, patterns fit well with ZnO wurtzite type structure (JCPDS card no:01-089-0510). Peaks belong to neither Al nor In are found confirm that co-dopants are well occupied into the ZnO lattice. It is worth to note that thickness of the nanostructured AIZO films decreases with respect to change in solvents content. These thickness variations affect the FWHM (Full width at half maximum) in turn changes the crystallinity. Prasad's research group also reported that thickness influences the crystallinity [17]. The AIZO film (S25), presented the least FWHM and hence its crystallinity is high. The crystallite sizes of the samples are calculated using Scherrer's formula [4] and reported in Table 4.5.

4. 2. 4. 2. Morphological characteristics

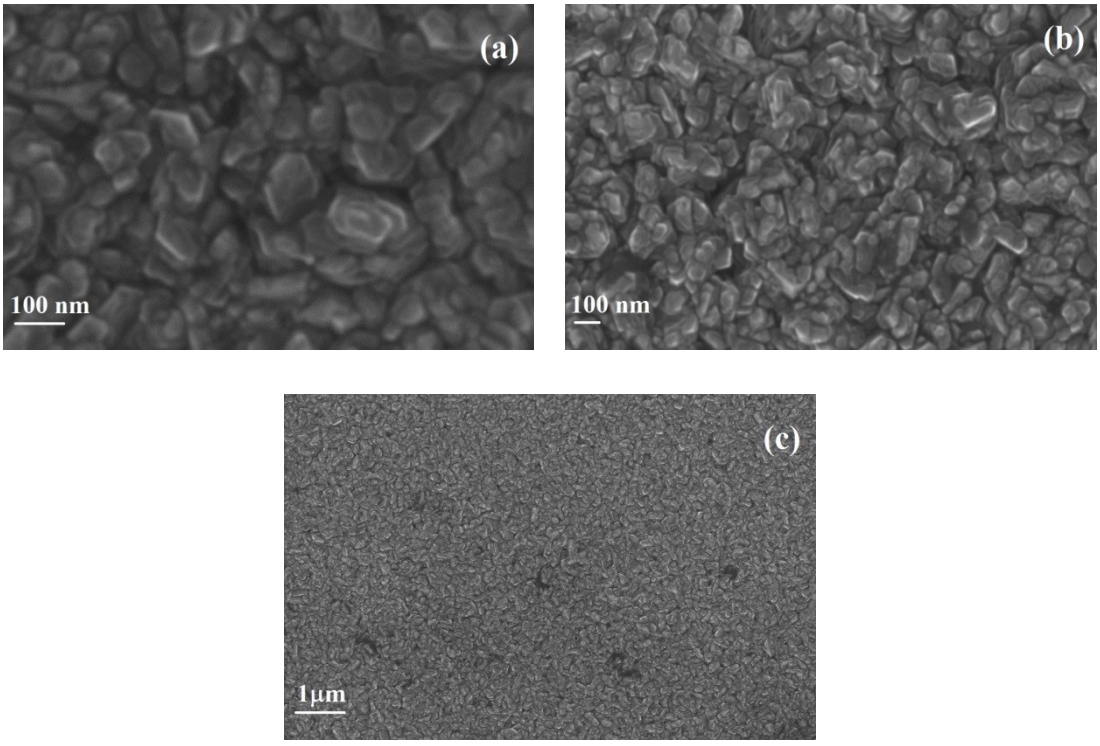

Fig. 4.15.1. Surface morphology (at different magnifications) of AIZO thin film (S25) deposited using 25ml of acetic acid and 25ml of water in the zinc precursor solution (a)100KX, (b)50KX, and (c)10KX.

The scanning electron microscopy images of AIZO samples deposited using equal variations of acetic acid and water content are shown in Fig. 4.15. The Fig. 4.15.1(a-c) shows the hexagonal pyramids with diameter varying from 40 to 100 nm approximately when the deposition is carried out with low content of acetic acid (25ml) and water (25ml). The film surface has gaps of size 10-30nm between the pyramids. However this morphology seems to be poor growth might be due to the low level content of acetic acid. Low acetic acid in the spraying solution results in precipitation of Zn-OH in turn affects the growth of nanostructures [19]. Elongated grains are grown (Fig. 4.15.2(a-d)) when the content of acetic acid (50ml) and water (50ml) is increased. The grains are well connected without any porosity on the film surface. The average dimensions of the grains are found to be ~200 nm x 100 nm.

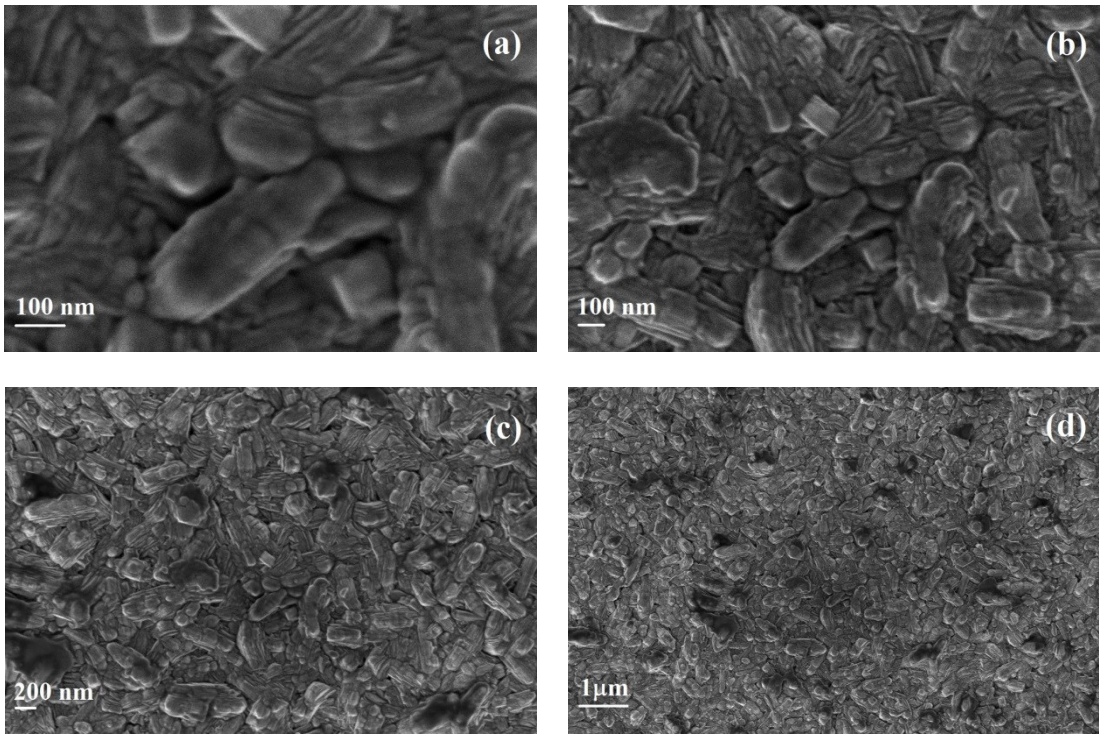

Fig. 4.15.2. Surface morphology (at different magnifications) of AIZO thin film (S50) deposited using 50ml of acetic acid and 50ml of water in the zinc precursor solution (a)100KX, (b)50KX, (c)20KX, and (d)10KX.

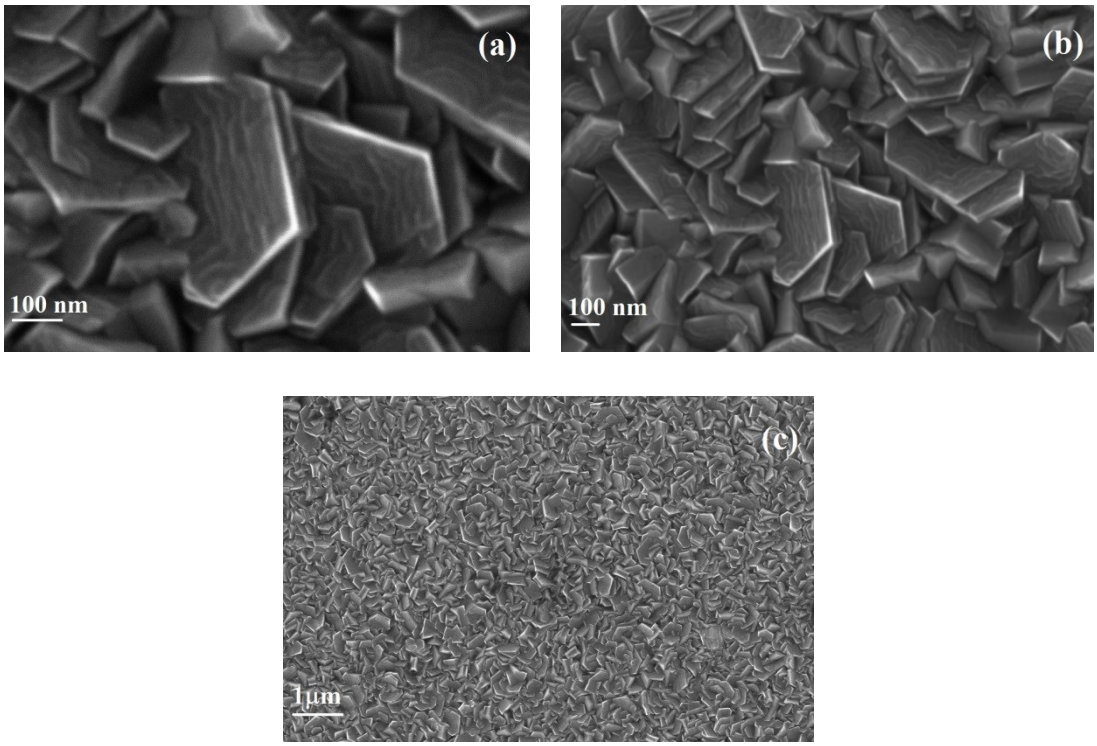

Fig. 4.15.3. Surface morphology (at different magnifications) of AIZO thin film (S100) deposited using 100ml of acetic acid and 100ml of water in the zinc precursor solution Surface morphology of S100 at different magnifications (a)100KX, (b)50KX, and (c)10KX.

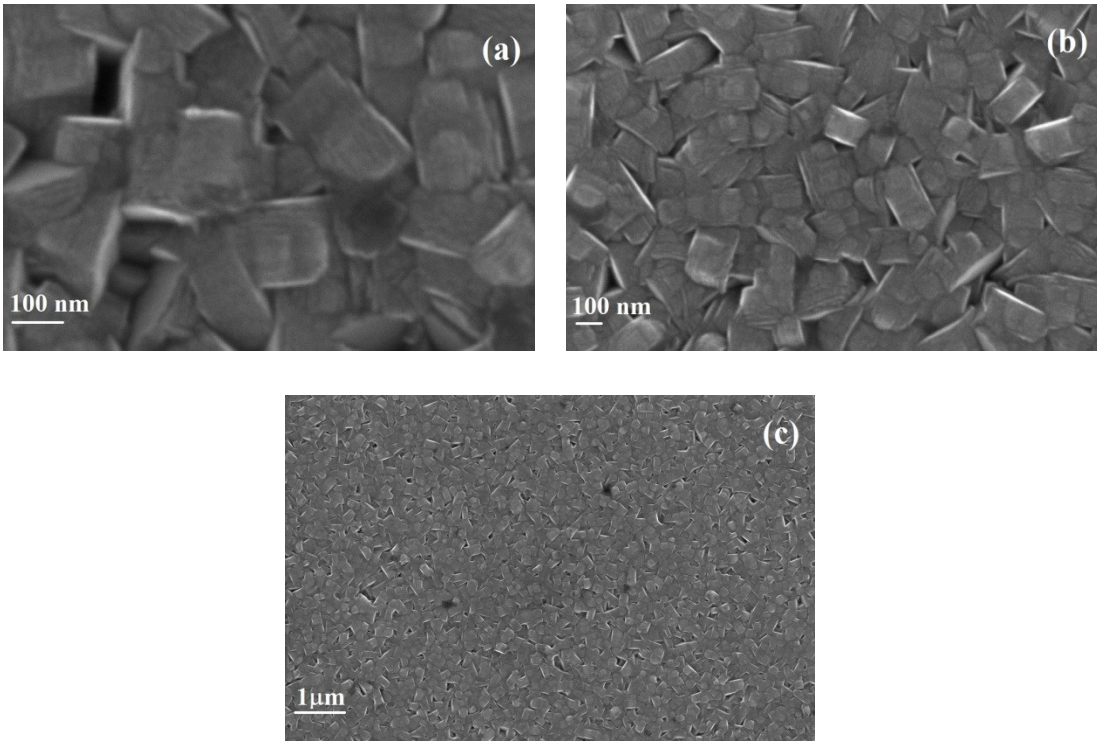

Fig. 4.15.4. Surface morphology (at different magnifications) of AIZO thin film (S150) deposited using 150ml of acetic acid and 150ml of water in the zinc precursor solution (a)100KX, (b)50KX, and (c)10KX.

Further increasing solvents quantity, lead to super grown hexagons Fig.4.15.3 (a-c). The diameter of these hexagons are in the range of ~200-500nm. Similar hexagon flakes were obtained by Jiao research group for indium doped ZnO thin films [20]. Increasing the content of acetic acid (150ml) and water (150ml) in the precursor solution results in formation of woven nanostructures with dimensions ~150x550 nm as in Fig.4.15.4 (a-c). These nanostructures are inter-connected, and have some squared patterns on their superficial of size ~100nm.

4. 2. 4. 3. Optical and electrical characteristics

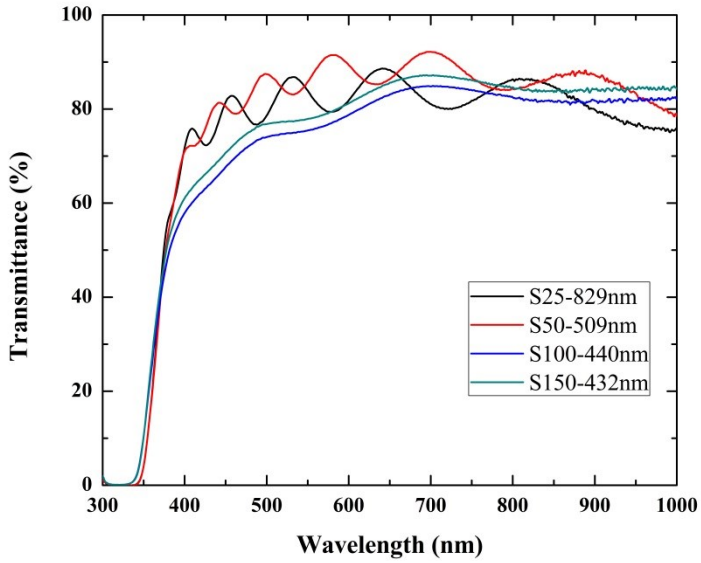

Fig. 4.16. Optical transmittance of AIZO thin films (S25, S50, S100, and S150) deposited with equal variations of acetic acid and water content in the zinc precursor solution.

The optical transmittance of S25, S50, S100, and S150 is shown in Fig. 4.16. All the films showed a transmittance >75%. The absorption edges of the nanostructures are found in between 338 and 342nm. S25 and S50 presented transmittance with more interference fringes than S100 and S150 nanostructures which imply that S25 and S50 are with good

quality. Ilican also stated that interference fringes play a vital role in identifying the homogeneity and quality [18]. The bandgap (E_g) values of the samples are varied between 3.49 and 3.52eV Tohsophon´s research group also observed similar E_g values for their sputtered AIZO thin films [13]. The shift in bandgap value of AIZO from the bandgap of undoped ZnO (3.37eV) indicates that co-dopants are successfully incorporated in the ZnO lattice. This effect is referred as Burstein-Moss effect [12].

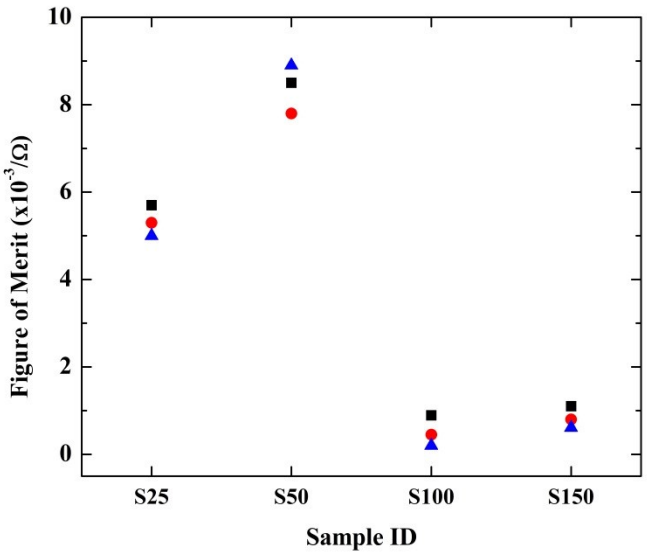

Fig. 4.17. Figure of Merit of AIZO thin films (S25, S50, S100, and S150) deposited with equal variations of acetic acid and water content in the zinc precursor solution.

Table 4.5. shows the sheet resistance of AIZO thin films. All the thin films exhibited sheet resistance less than 100Ω/□. The values of the sheet resistance suggest that co-dopants In substitutes the Zn lattice, and Al occupies grain boundaries which in turn increases the carrier concentration [14]. Among all samples, S50 is well connected without any porosity consequently resulted in the lowest sheet resistance (Table 4.5). Further, Fig. 4.17 shows the FOM of AIZO thin films, in which S50 presented the highest FOM, since it presented the lowest resistance and the highest transmittance.

Table 4.5. Structural, optical, electrical parameters and the figure of merit of AIZO thin films (S25, S50, S100,and S150) deposited with equal variations of acetic acid and water content in the zinc precursor solution.

Characteristics	Sample ID			
	S25	**S50**	**S100**	**S150**
Thickness, t (nm)	829	509	440	432
FWHM (deg)	0.1851	0.2356	0.2861	0.3534
Crystallite size, L (nm)	44	35	29	23
Transmittance at 550nm (%)	83	85	75	77
Optical bandgap, E_g (eV)	3.49	3.49	3.52	3.52
Sheet resistance, R_s (Ω/□)	27-31	22-25	63-274	64-120
Figure of Merit (10^{-3}/Ω)	5-5.7	7.8-8.9	0.81-0.86	0.6-1.1

4. 3. Characterization of Al and In co-doped ZnO fabricated using aluminium chloride

From the above studies, we observed that 50ml of acetic acid, and 50ml of water content in the zinc precursor solution shows high figure of merit. So, we have with same proportions and deposited AIZO films using different aluminium precursor. The aluminium and indium precursors were aluminium chloride and indium acetate respectively.

4. 3. 1. Optimization of substrate temperature

This is a preliminary experiment in order check which temperature (425, 450, and 475°C) gives high figure of merit. We have examined optical transmittance, sheet resistance and figure of merit for the samples ALCL-T425, ALCL-T450, and ALCL-T475. The transmittance spectrum of the films is shown in Fig. 4.18. All the samples show transmittance >80%.

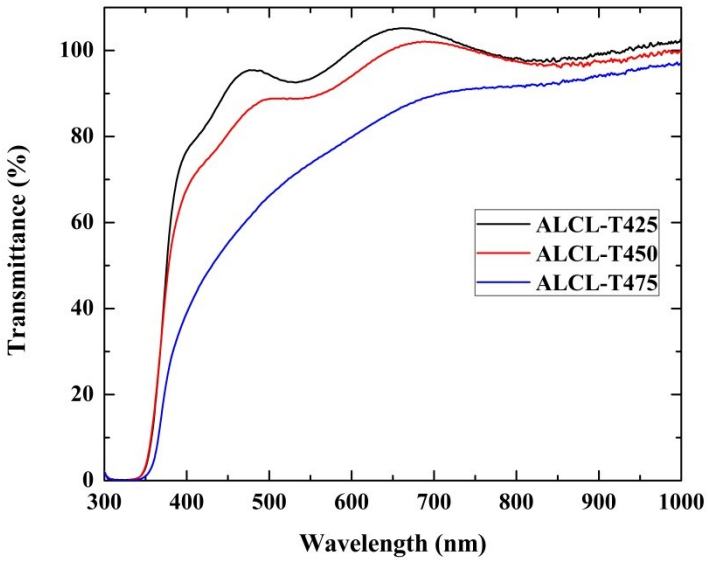

Fig. 4.18.1. Transmittance curves of AIZO thin films (ALCL-T425, ALCL-T450, and ALCL-T475) deposited at different temperatures (425, 450, and 475°C) for 10min.

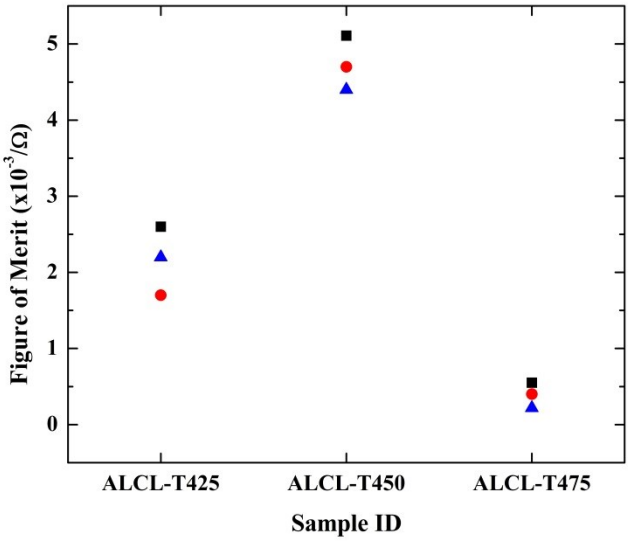

Fig. 4.18.2. Figure of Merit of AIZO thin films (ALCL-T425, ALCL-T450, and ALCL-T475) deposited at different temperatures (425, 450, and 475°C) for 10min

Further, figure of merit (FOM) estimation is performed (T^{10}/R_S) using Haacke's formula and tabulated in Table 4.6. This shows highest FOM is achieved for the sample deposited at 450°C for 10min. Hence further studies are proceeded with depositions at 450°C.

Table 4.6. Tabulation of transmittance, sheet resistance, and Figure of Merit of AIZO thin films deposited at different temperatures 425,450, and 475°C using aluminium chloride as aluminium dopant.

Sample ID	**T_{550nm} (%)**	**R_s (Ω/□)**	**FOM ($x10^{-3}$/Ω)**
ALCL-T425	*93*	*181-284*	*1.7-2.6*
ALCL-T450	*89*	*61-70*	*4.4-5.1*
ALCL-T475	*73*	*78-194*	*0.2-0.5*

4. 3. 2. Effect of co-dopants concentration

In order to simplify the exploration, same Al:In proportions were tested, namely 1:1 (ALCL1), 1.5:1.5 (ALCL1.5), 2:2 (ALCL2), and 3:3 (ALCL3). In addition, we should remember that optimum total doping value is below the solubility limit into ZnO lattice. These depositions were carried out at 450°C for 10 min.

4. 3. 2. 1. Structural properties

The Fig.19. shows the XRD patterns of thin films prepared using aluminium chloride precursor. Here we can observe that films are polycrystalline and fit well with JCPDS data (01-089-0510) card of ZnO. The films ALCL1, ALCL1.5 and ALCL2 present (002) preferential orientation confirmed from texture co-efficient estimations. In addition confirms the growth of hexagonal wurtzite structure [7]. In contrast, the film ALCL3 show texture co-efficient near to 1 for many planes confirms that ALCL3 is randomly oriented. Nora et. al. also obtained ZnO thin films with random orientation [21]. The peaks of the samples are slightly shifted from the In addition peaks belonging to Al and In are not observed, which confirms that the dopants are incorporated into the lattice of ZnO.

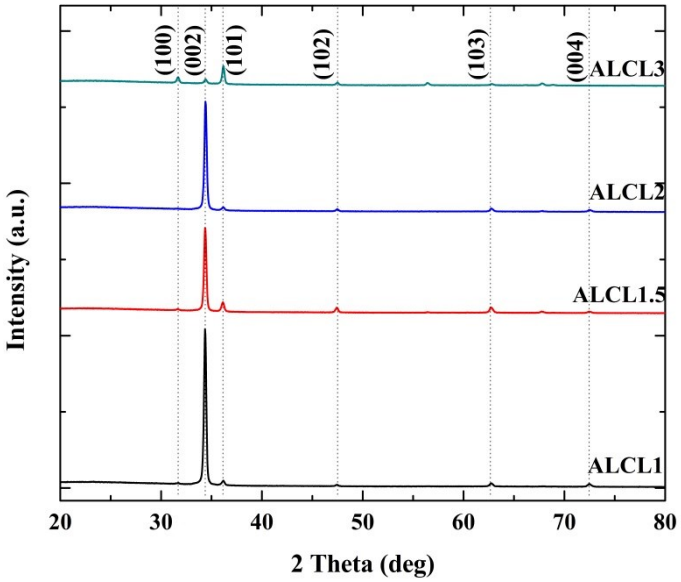

Fig. 4.19. XRD patterns of AIZO thin films deposited with different co-dopants concentration (ALCL1=1at.%Al:1at.%In, ALCL1.5=1.5at.%Al:1.5at.%In, ALCL2=2at.%Al:2at.%In, ALCL3=3at.%Al:3at.%In).

However, there are variations in intensity and full width half maximum with respect to change in dopants concentration, which is a result of variation in thickness. This in turn affects the crystallinity of the thin films. The crystallite size and FWHM of the films are given in Table 4.7. The crystallite sizes (D) of the AIZO films are estimated using Schrerrer´s formula [4].

Table 4.7. Thickness and structural characteristics of AIZO films deposited with different co-dopants concentrations (ALCL1=1at.%Al:1at.%In, ALCL1.5=1.5at.%Al:1.5at.%In, ALCL2=2at.%Al:2at.%In, ALCL3=3at.%Al:3at.%In).

Thin film ID	Thickness (nm)	FWHM (deg)	Crystallite size from the (002) plane (nm)
ALCL1	690	0.1683	49
ALCL1.5	570	0.1683	49
ALCL2	447	0.2356	35
ALCL3	461	0.2357	35 (for the plane (101)

4. 3. 2. 2. Morphological properties

The morphologies of AIZO thin films deposited using aluminium chloride as aluuminium dopant precursor with different concentration are given in Fig. 4.20. ALCL1(Fig. 4.20.1(a-c)) and ALCL1.5 (Fig. 4.20.2 (a-c)) films present a layered hexagonal morphology of different sizes. The sizes vary in between ~50 to 350nm.

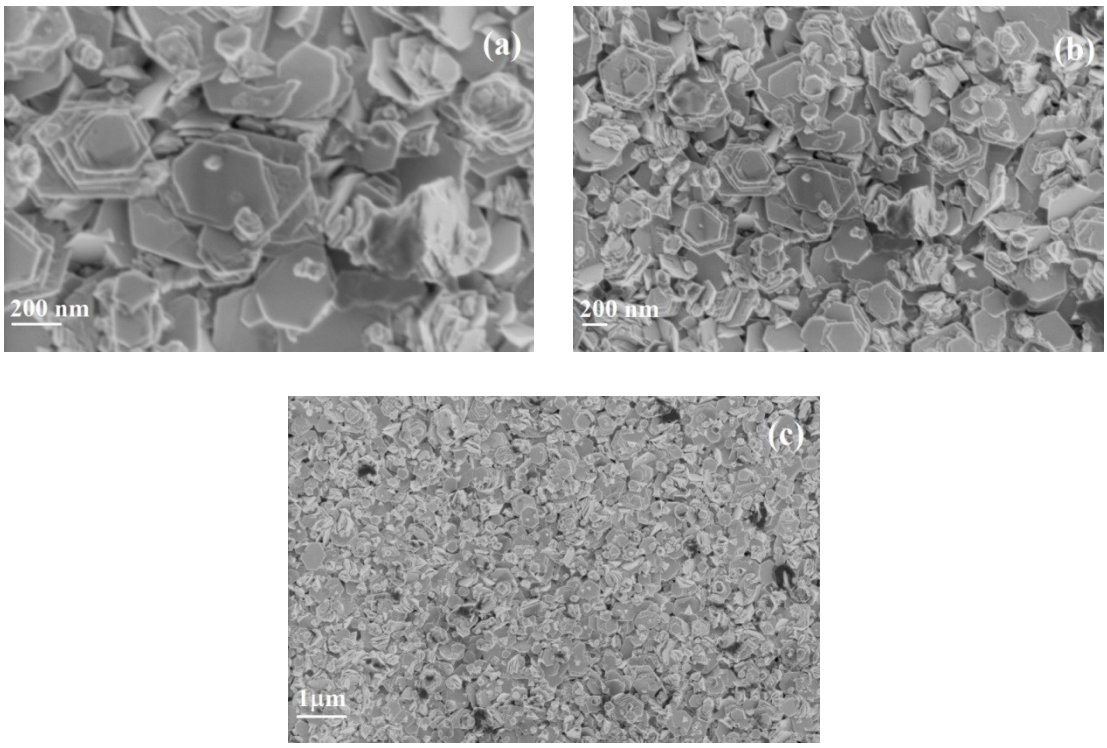

Fig. 4.20.1. Surface morphology at different magnifications of AIZO thin films (ALCL1) deposited with Al:In=1:1at.% (a)50KX, (b)25KX, and (c)10KX.

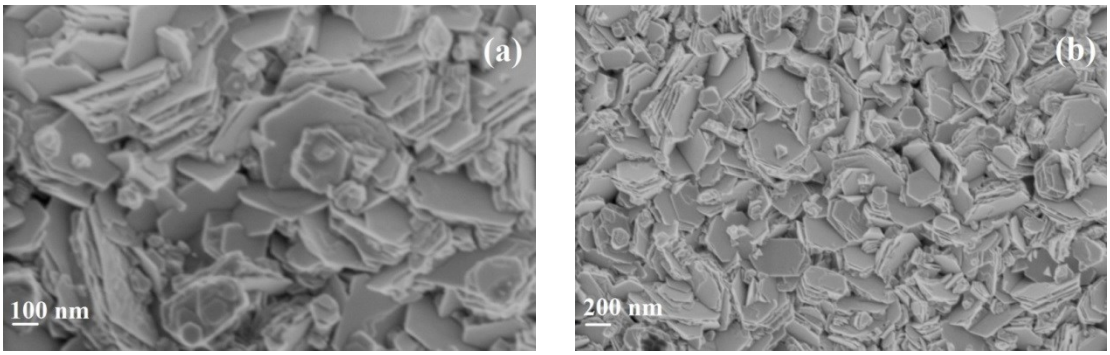

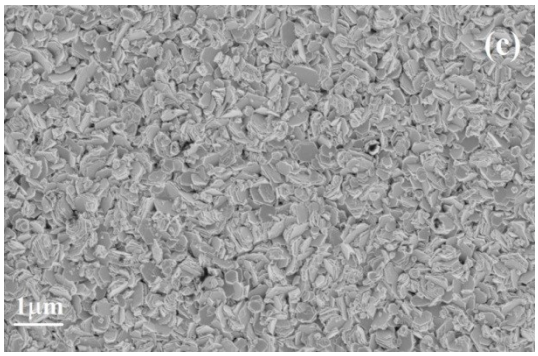

Fig. 4.20.2. Surface morphology at different magnifications of AIZO thin films (ALCL1.5) deposited with Al:In=1.5:1.5at.% (a)50KX, (b)25KX, and (c)10KX.

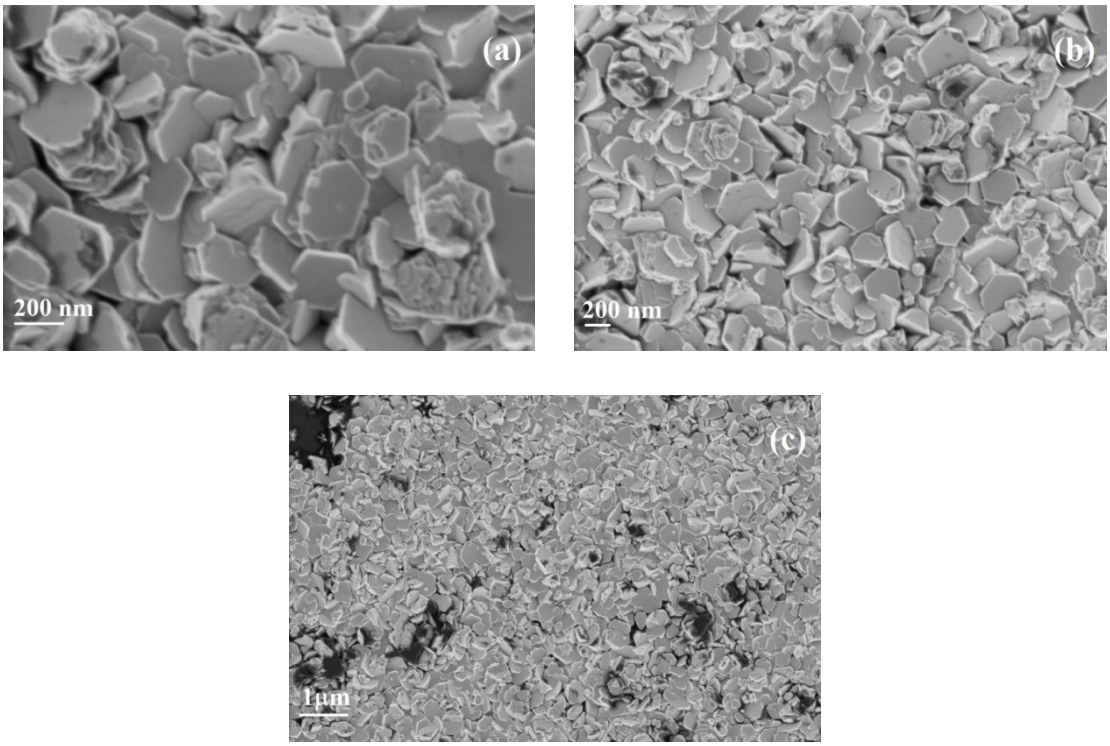

Fig. 4.20.3. Surface morphology at different magnifications of AIZO thin films (ALCL2) deposited with Al:In=2:2at.% (a)50KX, (b)25KX, and (c)10KX.

However, when dopants concentration increases, ALCL2 (Fig.4.20.3 a-c) shows a surface consists of individual hexagons of different sizes (~100-400nm). Further increase in dopants concentration (Fig. 4.20.4 (a-c)) results in compact of leaves like structures. From, Fig. 4.20.4. it is clear that as co-dopants concentrations increases, compactness also increases in film surface.

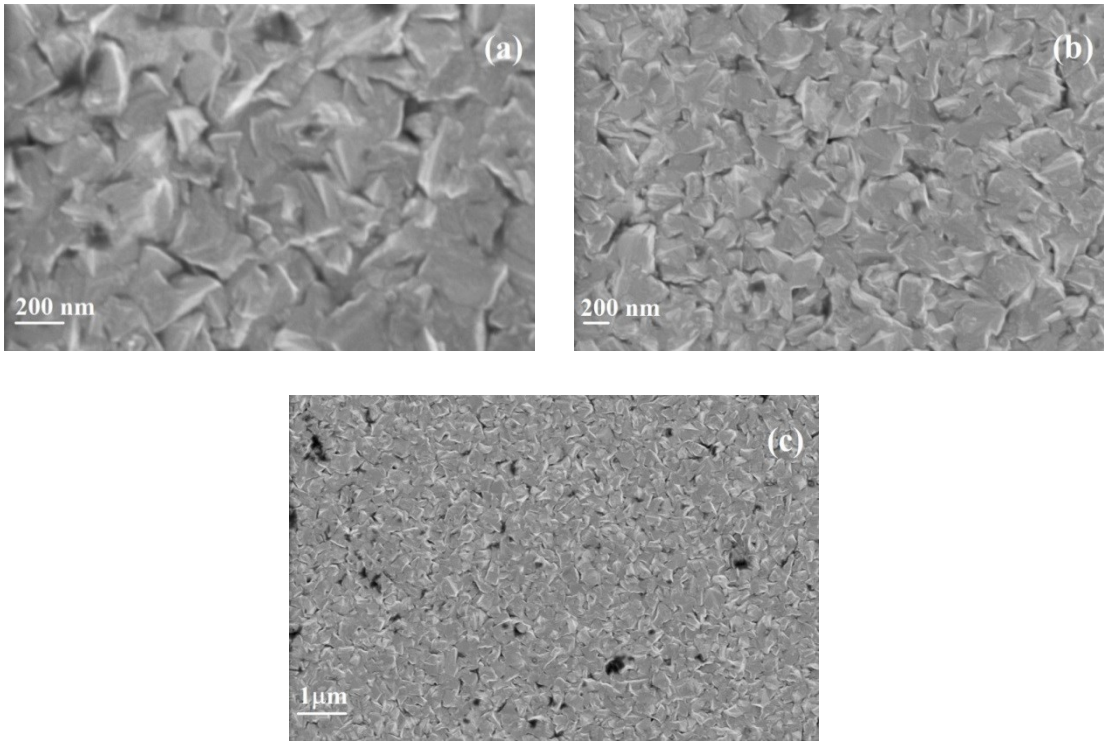

Fig. 4.20.4. Surface morphology at different magnifications of AIZO thin films (ALCL3) deposited with Al:In=3:3at.% (a)50KX, (b)25KX, and (c)10KX.

4. 3. 2. 3. Optical and electrical properties

Fig. 4.21.1. shows the optical transmittance spectra of AIZO thin films deposited with different co-dopants concentration. From the spectra, following conclusions can be derived.

a) Films (ALCL1, & ALCL1.5) doped with low concentration result in very low transmittances.
b) Film (ALCL2) co-doped with 2at.% show high transmittances (>80%).
c) The bandgap (E_g) values are found to be oscillating between 3.41 to 3.42eV.

However, Eg is shifted little from bulk ZnO (Eg=3.3eV), results due to increase in carrier concentration, which is called Burstein-Moss effect [13].

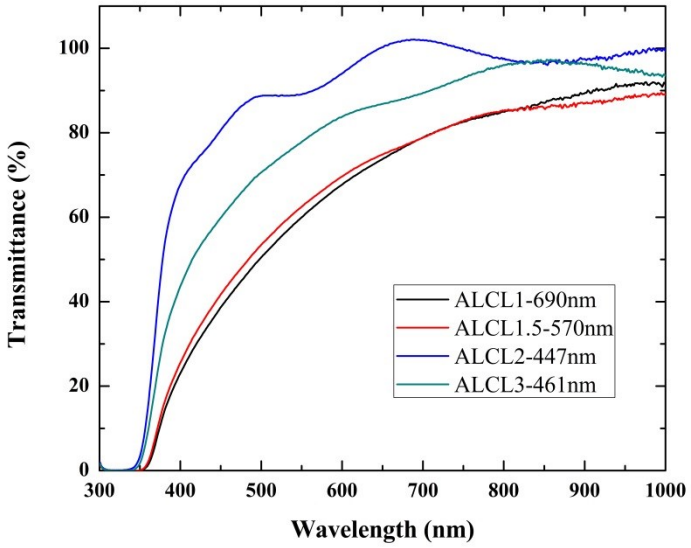

Fig. 4.21.1. Optical transmittance AIZO thin films deposited with different co-dopants concentration (ALCL1=1at.%Al:1at.%In, ALCL1.5=1.5at.%Al:1.5at.%In, ALCL2=2at.%Al:2at.%In, ALCL3=3at.%Al:3at.%In).

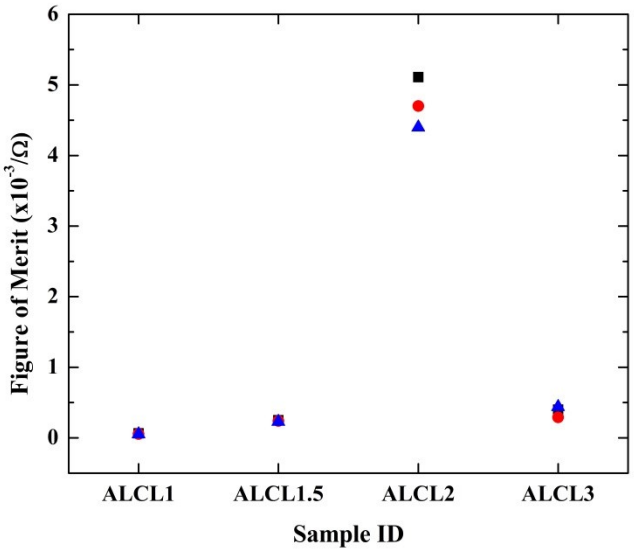

Fig. 4.21.2. Figure of Merit of AIZO thin films deposited with different co-dopants concentration (ALCL1=1at.%Al:1at.%In, ALCL1.5=1.5at.%Al:1.5at.%In, ALCL2=2at.%Al:2at.%In, ALCL3=3at.%Al:3at.%In).

In addition, when we observe electrical characteristics from Table 4.8, films show sheet resistance in between 33.54 to 154.40 Ω/□, which in turn suggest that In substitutes the Zn lattice, and Al occupies grain boundaries which in turn increases the carrier concentration [14]. In both the cases, high level doping (3at.% of Al and 3at.% of In) leads to high resistance, which could be due to the aggregation of Al_2O_3 or In_2O_3 at grain boundaries. The film ALCL2 appears to be best since it shows the highest FOM as in Table 4.8.

Table.4.8. Optical and electrical parameters of AIZO thin films deposited with different co-dopants concentration (ALCL1=1at.%Al:1at.%In, ALCL1.5=1.5at.%Al:1.5at.%In, ALCL2=2at.%Al:2at.%In, ALCL3=3at.%Al:3at.%In).

Thin film ID	**Thickness (nm)**	**T_{550} (%)**	**R_s (Ω/□)**	**FOM ($x10^{-3}$ /Ω)**
ALCL1	690	59	79-98	0.05-0.06
ALCL1.5	570	62	33-36	0.23-0.25
ALCL2	447	89	61-78	*4.4-5.1*
ALCL3	461	77	154-245	0.2-0.4

4. 4. Characterization of Al and In co-doped ZnO fabricated using aluminium sulphate

We have used 50ml of acetic acid and 50ml of water content in the zinc precursor solution and deposited AIZO films for 20min using different aluminium precursor. The aluminium and indium precursors were aluminium sulphate and indium acetate respectively.

4. 4. 1. Optimization of substrate temperature

This is a preliminary experiment in order check which temperature (425, 450, and 475°C) gives high figure of merit. We have examined optical transmittance, sheet resistance and figure of merit for the samples ALS-T425, ALS-T450, and ALS-T475. The transmittance spectrum of the films is shown in Fig. 4.22.1. All the samples show transmittance >80%.

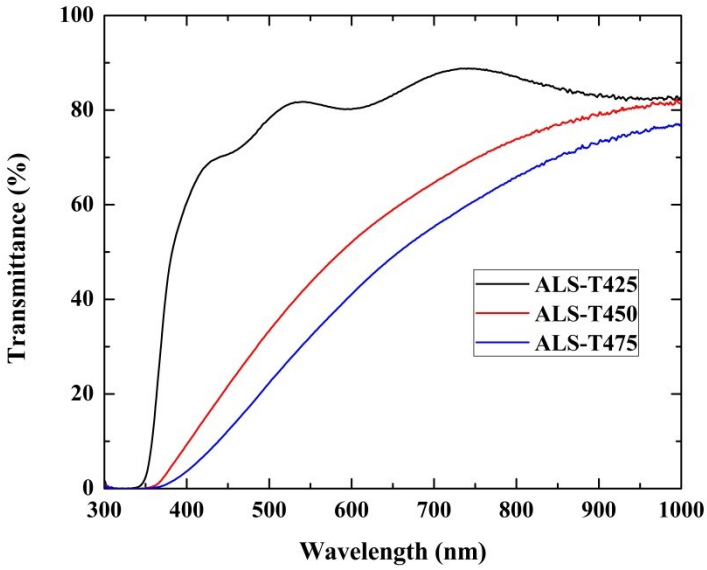

Fig. 4.22.1. Optical transmittance curves of AIZO thin films (ALS-T425, ALS-T450,and ALS-T475) deposited at 425, 450, and 475°C.

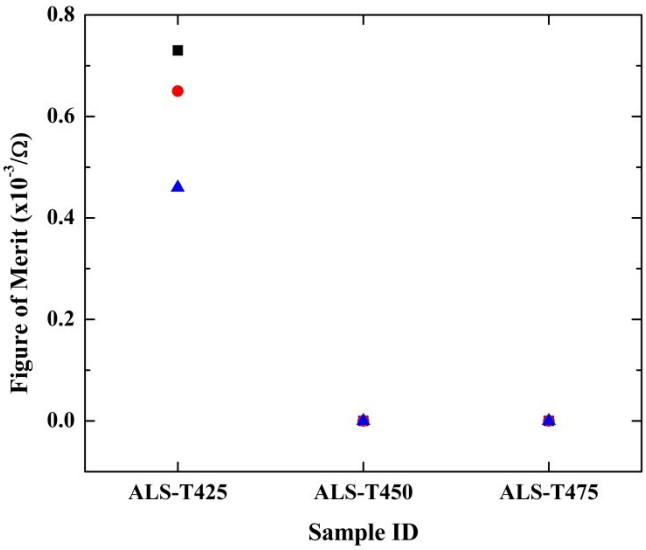

Fig. 4.22.2. Figure of Merit of AIZO thin films (ALS-T425, ALS-T450,and ALS-T475) deposited at 425, 450, and 475°C.

Further, figure of merit (FOM) estimation is performed (T^{10}/R_S) and tabulated in Table 4.6. This shows highest FOM is achieved for the sample deposited at 425°C. Hence further studies are proceeded with depositions at 425°C.

Table 4.9. Tabulation of transmittance (T), sheet resistance(R_s), and Figure of Merit (FOM) of AIZO thin films deposited using aluminium sulphate at different temperatures.

Sample ID	T_{550nm} (%)	R_s (Ω/□)	FOM ($x10^{-3}$/Ω)
ALS-T425	81	169-259	0.46-0.73
ALS-T450	43	293-547	$3.9x10^{-4}$-$7.37x10^{-4}$
ALS-T475	32	90-251	$6.1x10^{-5}$ -$1.24x10^{-4}$

4. 4. 2. Effect of co-dopants concentration

In order to simplify the exploration, same Al:In proportions were tested, namely 1:1 (ALS1), 1.5:1.5 (ALS1.5), 2:2 (ALS2), and 3:3 (ALS3). In addition, we should remember that optimum total doping value is below the solubility limit into ZnO lattice. These depositions were carried out at 450°C for 10 min.

4. 4. 2. 1. Structural properties

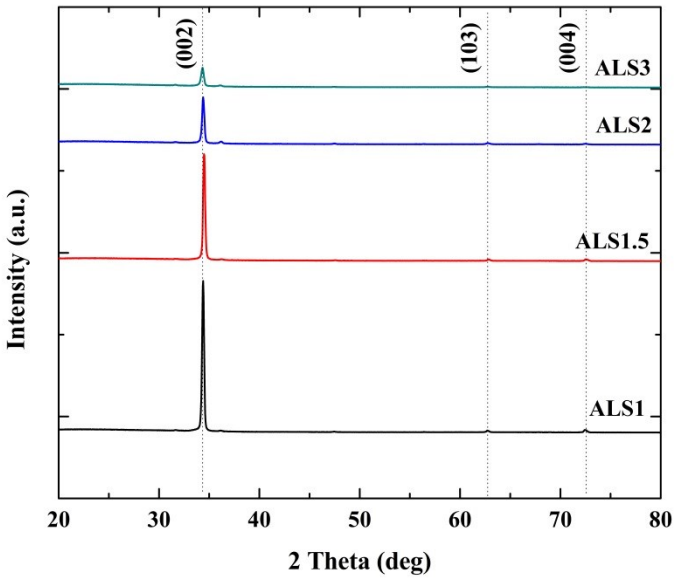

Fig. 4.23.XRD patterns of AIZO thin films deposited with different co-dopants concentrations (ALS1=1at.% Al:1at%.In, ALS1.5=1.5at.% Al:1.5at%.In, ALS2=2at.% Al:2at%.In, ALS3=3at.% Al:3at%.In).

The Fig. 4.23. shows the XRD diffraction patterns of the Al and In co-doped ZnO thin films fabricated using aluminium sulphate as Al precursor (with different co-dopants concentration). All the ALS films show (002) as preferential orientation, in addition

confirms the growth of hexagonal wurtzite structure. The peaks of the samples are fit well with JCPDS data (01-089-0510) card of ZnO. In addition peaks belonging to Al and In are not observed, which confirms that the dopants are incorporated into the lattice of ZnO [8]. The patterns show a dominating peak along (002) plane indicating that AIZO thin films are grown along c-direction of hexagonal wurtzite structure.

Table 4.10. Thickness and structural characteristics of AIZO films deposited using different doping concentrations (ALS1=1at.% Al:1at%.In, ALS1.5=1.5at.% Al:1.5at%.In, ALS2=2at.% Al:2at%.In, ALS3=3at.% Al:3at%.In).

Thin film ID	Thickness (nm)	FWHM (deg)	(002) plane crystallite size (nm)
ALS1	763	0.1851	44
ALS1.5	585	0.1683	49
ALS2	451	0.2019	41
ALS3	265	0.3029	27

However, there are variations in intensity and full width half maximum with respect to change in dopants concentration, which is a result of variation in thickness [9]. This in turn affects the crystallinity of the thin films. The crystallite size and FWHM of the films are given in Table 4.10. The crystallite sizes (D) of the AIZO films are estimated using Schrerrer´s formula [4].

4. 4. 2. 2. Morphological properties

When AIZO films are prepared using aluminium sulphate, the film morphologies are appeared as shown in Fig. 4.24. Hexagonal pyramidal like structures (Fig. 4.24.1 and Fig. 4.24.2) are formed when the co-dopants concentration is very low (1 and 1.5at.%) of size ~200 to 400nm. Inclusion of 2at.% of co-dopants results in the formation or irregular hexagonal features along with few pyramids (Fig.4.24.3). Addition of 3at.% of co-dopants leads to the growth of hexagonal flakes and some trigonals of different sizes between ~180nm to 400nm (Fig.4.24.4).

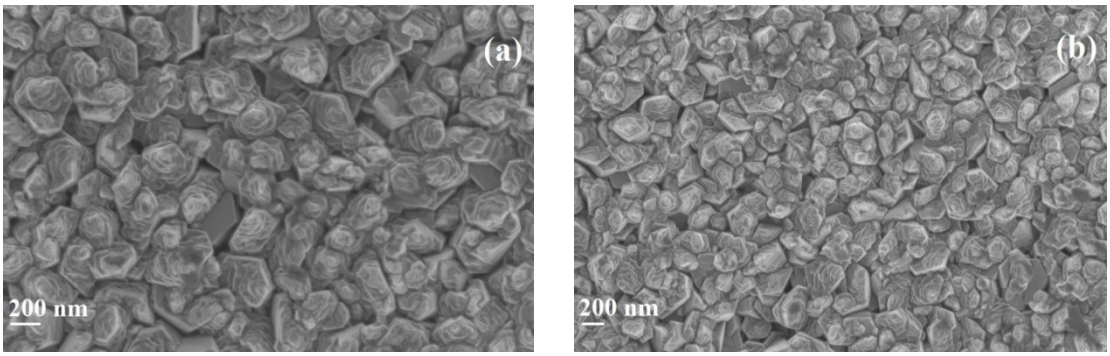

Fig. 4.24.1. Surface morphology at different magnifications of AIZO thin films (ALS1) deposited with Al:In=1:1at.% (a)30KX, (b)10KX.

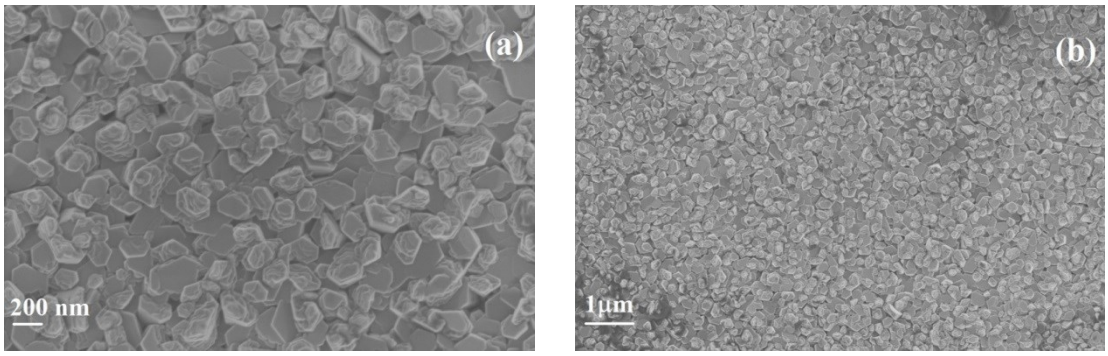

Fig. 4.24.2. Surface morphology at different magnifications of AIZO thin films (ALS1.5) deposited with Al:In=1.5:1.5at.% (a)30KX, (b)10KX.

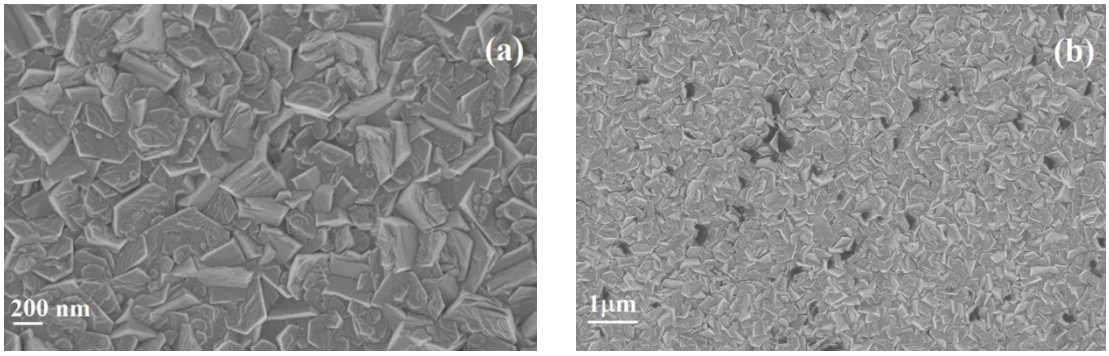

Fig. 4.24.3. Surface morphology at different magnifications of AIZO thin films (ALS2) deposited with Al:In=2:2at.% (a)30KX, (b)10KX.

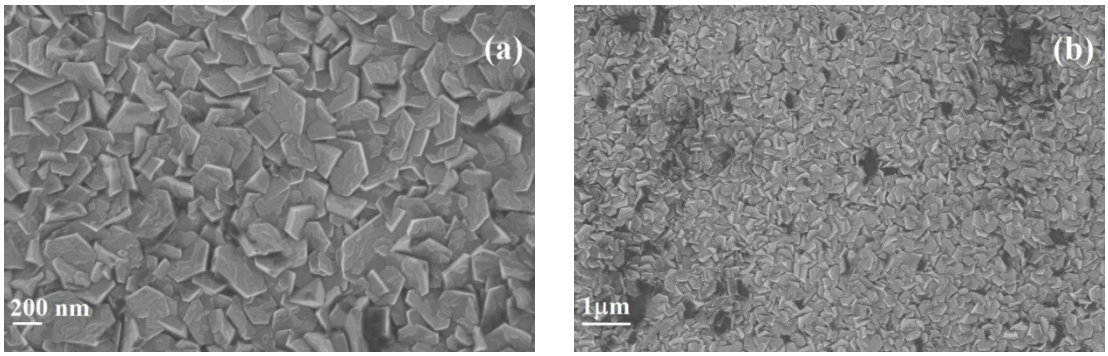

Fig. 4.24.4. Surface morphology at different magnifications of AIZO thin films (ALS3) deposited with Al:In=3:3at.% (a)30KX, (b)10KX.

4. 4. 2. 3. Optical and electrical properties

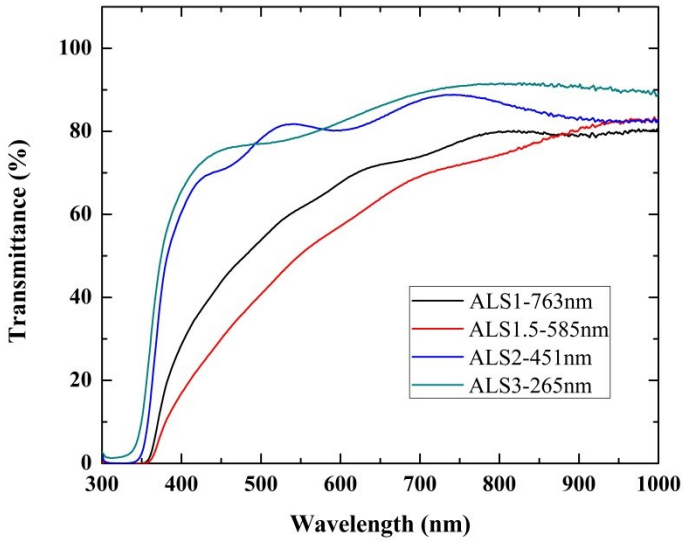

Fig. 4.25.1. Optical transmittance AIZO thin films deposited with different co-dopants concentration (ALS1=1at.% Al:1at%.In, ALS1.5=1.5at.% Al:1.5at%.In, ALS2=2at.% Al:2at%.In, ALS3=3at.% Al:3at%.In).

Fig. 4.25.1 shows the transmittance of deposited AIZO thin films prepared using aluminium sulphate as an aluminium precursor. From the Table 4.11 we can observe that there is a drastic change in transmittance values in turn is a result of change of thickness. However, ALS3 presents the lower transmittance than ALS2, though the thickness is low

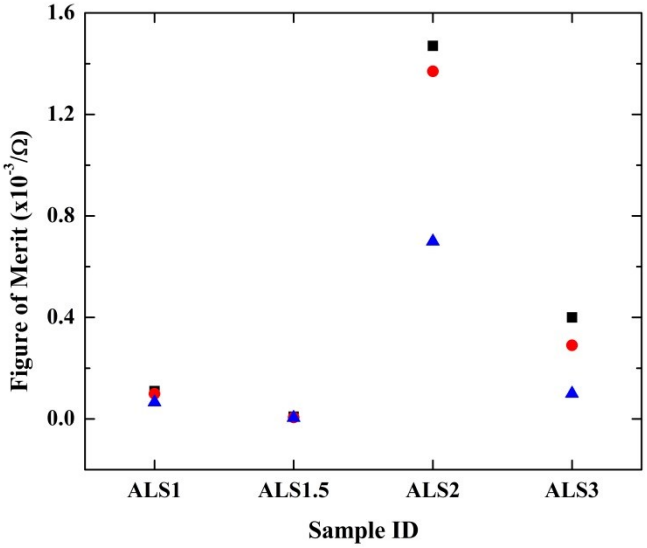

Fig. 4.25.2. Figure of Merit of AIZO thin films deposited with different co-dopants concentration (ALS1=1at.% Al:1at%.In, ALS1.5=1.5at.% Al:1.5at%.In, ALS2=2at.% Al:2at%.In, ALS3=3at.% Al:3at%.In).

for ALS3. This behavior could be due to type of nanostructure formed on the thin film surface. From the spectra, following conclusions can be derived.

1) Films (ALS1, & ALS1.5) doped with low concentration result in very low transmittances.
2) Film (ALS2) co-doped with 2at.% show high transmittances (>80%).
3) The bandgap (E_g) values are found to be oscillating between 3.41 to 3.48eV.

However, Eg is shifted little from bulk ZnO (Eg=3.3eV), results due to increase in carrier concentration, which is called Burstein-Moss effect [12]. In addition, when we observe electrical characteristics from Table 4.11, films show sheet resistance in between 72.6 to 309.2 Ω/□, which in turn assures that In substitutes the Zn lattice, and Al occupies grain boundaries which in turn increases the carrier concentration [14]. In the case high level doping (3at.% of Al and 3at.% of In) leads to high resistane, which could be due to the aggregation of Al_2O_3 or In_2O_3 at grain boundaries.

Table.4.11. Optical transmittance (T) and electrical parameters of AIZO thin films (ALS1=1at.% Al:1at%.In, ALS1.5=1.5at.% Al:1.5at%.In, ALS2=2at.% Al:2at%.In, ALS3=3at.% Al:3at%.In).

Thin film ID	**Thickness (nm)**	**Transmittance T_{550} (%)**	**Sheet Resistance R_s (Ω/□)**	**Figure of Merit ($x10^{-3}$ /Ω)**
ALS1	763	62	73-120	0.06-0.11
ALS1.5	585	51	129-256	0.004-0.009
ALS2	451	82	93-187	0.7-1.4
ALS3	265	79	217-515	0.1-0.4

4. 5. Summary of the effect of different type of aluminium precursor

From Table 4.12 we can observe how the type of aluminium precursor helps in achieving good quality AIZO thin films. Among those three aluminium precursors, ALAC (aluminium acetylacetonate) requires less deposition time and less co-dopants concentration to grow films with high figure of merit.

Table.4.12. Comparison of the experimental conditions on the preparation of AIZO thin films using different aluminium precursors (ALAC-Aluminium acetylacetonate, ALCL-aluminium chloride, ALS-aluminium sulphate)

Conditions	**ALAC**	**ALCL**	**ALS**
Substrate temperature (°C)	425	450	450
Deposition time (min)	10	10	20
Dopants concentration of Al and In (at.%)	1.5:1.5	2:2	2:2

From Table 4.13 we can see that ALAC presented the lowest sheet resistance as well as good transmittance. Thus these results confirm that choosing a proper type of dopant precursor is an important factor to get high quality AIZO thin films.

Table.4.13. Comparison on the electrical and optical results of AIZO thin films prepared using different aluminium precursors (ALAC-Aluminium acetylacetonate, ALCL-aluminium chloride, ALS-aluminium sulphate)

Parameter	**ALAC**	**ALCL**	**ALS**
FOM (x10^{-3}/Ω)	7.8-8.9	4.4-5.1	0.7-1.47
Transmittance at 550nm (%)	85	87	81
Sheet resistance (Ω/□)	22-25	61-78	93-187

4. 6. Effect of precursor milling

Prior to the preparation of starting solution, zinc precursor (zinc acetate dihydrate) was milled for an hour in a planetary ball milling equipment at a speed of 300 rpm. Later the AIZO thin film (M10) deposition was carried out for 10min at 475°C using aluminium acetylacetonate, and indium acetate as Al and In precursors respectively. For comparison purpose, one AIZO film (U10) was deposited using un milled zinc precursor (other conditions are same as above).

4. 6. 1. Structural properties

The X-ray diffraction patterns of the Al and In co-doped ZnO thin films (M10 and U10) are shown in Fig. 4.26. The peaks of the samples are slightly shifted from the JCPDS data (01-089-0510) card of ZnO. This shift might be attributed to strain in the films. In addition peaks belonging to Al and In are not observed in the which confirms that the dopants are incorporated into the lattice of ZnO. The patterns show a dominating peak along (002) plane indicating that AIZO thin films are grown along c-direction of hexagonal wurtzite structure.

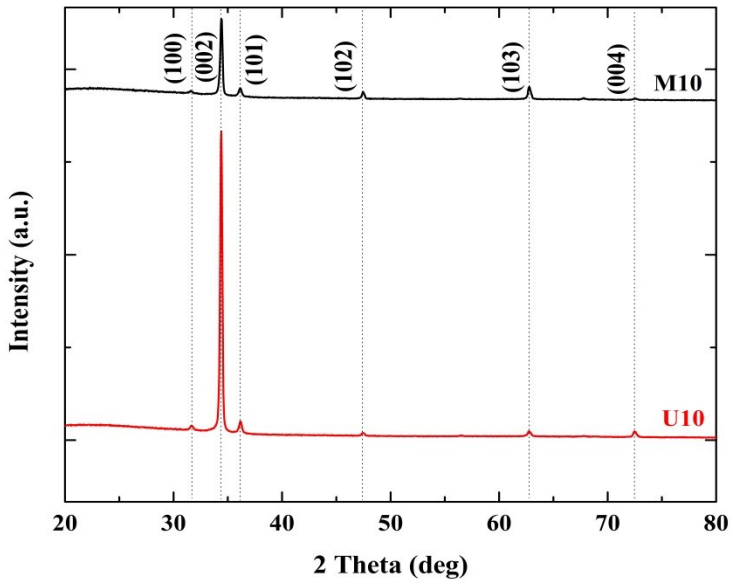

Fig. 4.26. XRD patterns of AIZO thin films with the effect of milling (U10-AIZO film deposited using unmilled zinc precursor, M10-AIZO film deposited using milled precursor).

The films present other weak peaks, corresponding to the planes (100), (101), (102), (103) and (004). There is a variation in intensity which is a result of change in thickness of the films. The thickness of U10 and M10 are 659 and 360 nm respectively. The estimated crystallite size of the U10 and M10 are 41 and 49 nm respectively using Schrerrer´s formula [4].

4. 6. 2. Morphological properties

In the case of film (U10) deposited with unmilled precursor, the surface is covered with hexagonal pyramids. The size of base of the pyramids is in the range ~50 to 250 nm (Fig. 4.27.1). And also, this sample is not closely packed like ball milled sample. M10 surface appears compact with small and half-grown hexagonal structures (Fig. 4.27.2), of size oscillating between 100 and 200 nm.

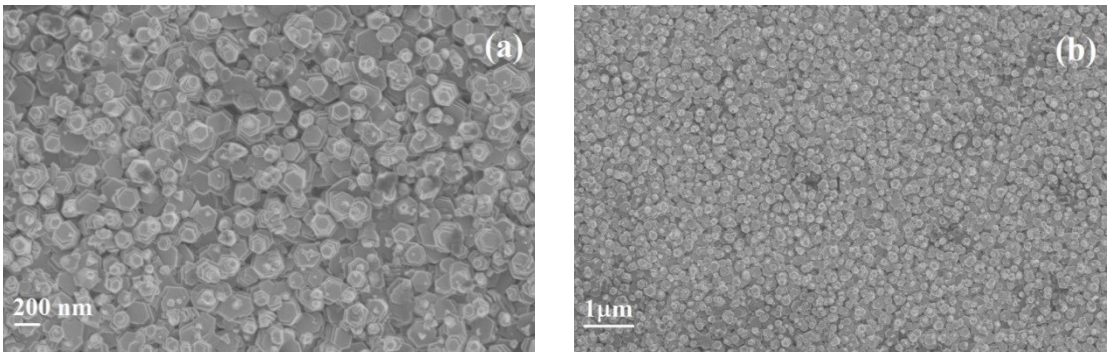

Fig. 4.27.1. Surface morphology at different magnifications of AIZO thin films deposited using unmilled zinc precursor (U10) with Al:In=1.5:1.5at.% (a)25KX, and (b)10KX.

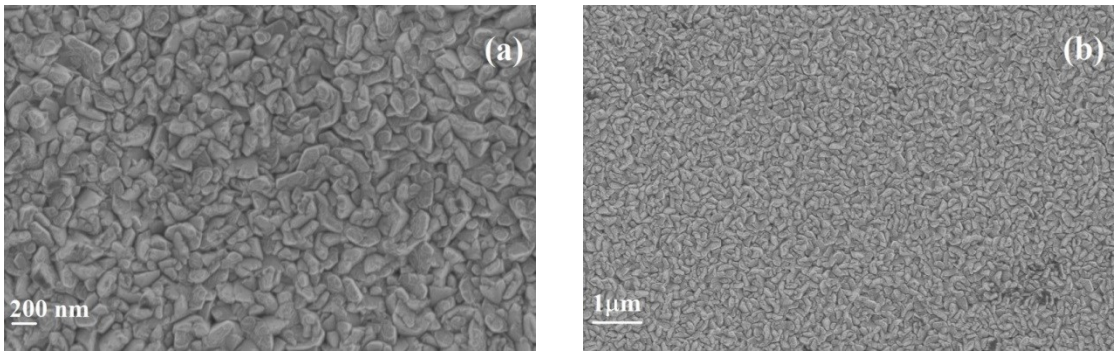

Fig. 4.27.2. Surface morphology at different magnifications of AIZO thin films deposited using milled zinc precursor (M10) with Al:In=1.5:1.5at.% (a)25KX, and (b)10KX.

4. 6. 3. Optical and electrical properties

When we compare the average transmittances of milled and unmilled samples, lesser transmittance is observed for U10 than M10. This would have occurred due to the size of the grains (Fig. 4.27.1 and 4.27.2) and change in thickness (Table 4.13). In addition, U10 doesn't present interference fringes like M10, in turn assures that surface of the film is not uniform. Earlier, Ilican expressed the quality of indium doped ZnO films based on interference fringes [18]. The E_g values of U10 and M10 3.48 and 3.53eV respectively. The shift in bandgap with respect to the bandgap undoped ZnO (E_g = 3.37 eV) suggests that dopants are incorporated into the ZnO lattice. This optical phenomenon is referred as Burstein-Moss effect [12]. In the end, when we correlated the milled precursor results with the AIZO film deposited using unmilled precursor, we observed drastic changes in the properties.

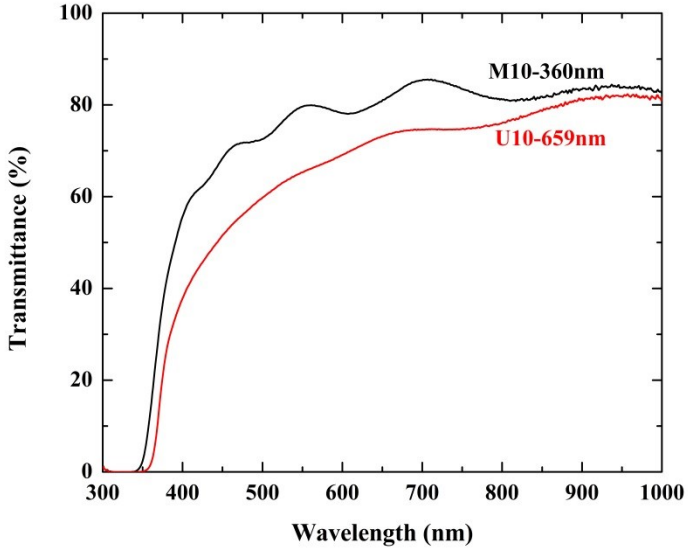

Fig. 4.28.1. Optical transmittance of M10 (deposited using milled zinc precursor) and U10 (deposited using unmilled zinc precursor) AIZO thin films.

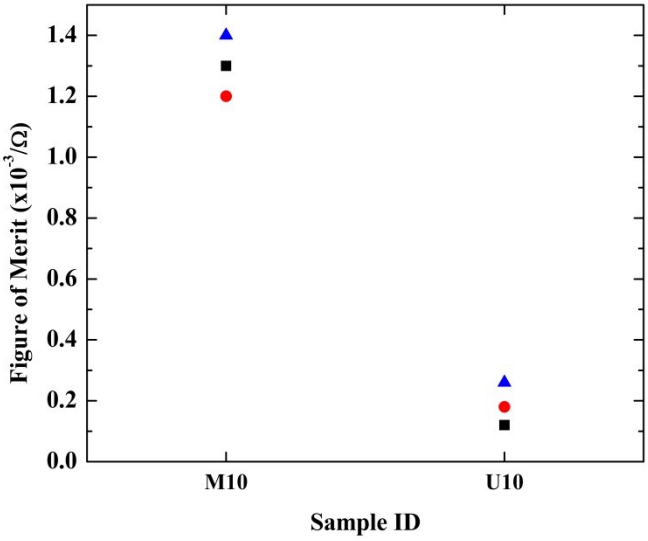

Fig. 4.28.2. Figure of Merit of M10 (deposited using milled zinc precursor) and U10 (deposited using unmilled zinc precursor) AIZO thin films.

The figure of merit (FOM) is increased by an order when we used milled Zn precursor (Table 4.14). From our results, we noticed that ball milling of a precursor before thin film fabrication enhances the optical and electrical properties; thereby AIZO films can be highly suitable for TCO applications.

Table.4.14.Optical and electrical parameters of M10 (deposited using milled zinc precursor) and U10 (deposited using unmilled zinc precursor) AIZO thin films.

Characteristics	**M10**	**U10**
Thickness (nm)	*360*	*659*
Transmittance (%)	*80*	*66*
Sheet resistance (Ω/□)	*76-88*	*60-122*
FOM (x10^{-3}/Ω)	*1.1-3.3*	*0.12-0.26*

4. 7. Conclusions

The physical properties such as structural, morphological, optical and electrical properties of the fabricated undoped ZnO and AIZO (Al and In co-doped ZnO) thin films prepared by ultrasonic spray pyrolysis were analyzed in detail. The physical characteristics were examined with respect to changes in temperature, solvents proportions, type of dopant precursor, and milling conditions. We have obtained the highest figure of merit (8.3±0.55x10^{-3}/Ω**)** for the AIZO thin films deposited at 425°C for 10 min using aluminium acetyl acetonate as aluminium precursor, indium acetate as indium precursor and zinc acetate as zinc precursor. The optimized dopants concentrations were 1.5 at.% of Al and 1.5 at.% of In.

4. 8. REFERENCES

[1] J. Li, H. Fan, X. Jia, J. Chen, Z. Cao, X. Chen, Electrostatic spray deposited polycrystalline zinc oxide films for ultraviolet luminescence device applications, Journal of alloys and compounds. 481 (2009) 735–739. doi:10.1016/j.jallcom.2009.03.094.

[2] G. Zou, W. Chen, R. Liu, Z. Xu, Orientation enhancement of polycrystalline ZnO thin films through thermal oxidation of electrodeposited zinc metal, Materials Letters. 61 (2007) 4305–4308. doi:10.1016/j.matlet.2007.01.092.

[3] O. Dimitrov et. al., Ultrasonically sprayed ZnO films : optical , electrical and gas sensing properties, Journal of physics, conference series, 398 (2012) 012022 (n.d.). doi:10.1088/1742-6596/398/1/012022.

[4] L. Alexander, H.P. Klug, L. Alexander, H.P. Klug, Determination of Crystallite Size with the XRay Spectrometer, Journal of applied physics. 137 (1950) 1–7. doi:10.1063/1.1699612.

[5] A. Smith, R. Rodriguez-Clemente, Morphological differences in ZnO films deposited by the pyrosol technique: Effect of HCl, Thin Solid Films. 345 (1999) 192–196. doi:10.1016/S0040-6090(99)00167-4.

[6] J. Anderson, G. Chris, Fundamentals of ZnO as a semiconductor, Rep. Prog. Phys. 72 (2009) 126501 (29pp).

[7] A.E.T.S. Tlemc, Structural , electrical and optical properties of sprayed Nd – F codoped ZnO thin films, Journal of sol-gel sci technology. (2015) 557–562. doi:10.1007/s10971-014-3518-y.

[8] S.Y. Lim, S. Brahma, C.P. Liu, R.C. Wang, J.L. Huang, Effect of indium concentration on luminescence and electrical properties of indium doped ZnO nanowires, Thin Solid Films. 549 (2013) 165–171. doi:10.1016/j.tsf.2013.09.001.

[9] R. Swapna, M. Ashok, G. Muralidharan, M.C.S. Kumar, Journal of Analytical and Applied Pyrolysis Microstructural , electrical and optical properties of ZnO : Mo thin films with various thickness by spray pyrolysis, J. Anal. Appl. Pyrolysis. 102 (2013) 68–75. doi:10.1016/j.jaap.2013.04.001.

[10] C. Baek, D.H. Kim, H.H. Kim, K. Lim, Processing Research Effect of thickness on properties of ZnO film prepared by direct current reactive magnetron sputtering method, Journal of ceramics processing Research. 13 (2012) 403–406.

[11] A. Crossay, S. Buecheler, L. Kranz, J. Perrenoud, C.M. Fella, Y.E. Romanyuk, et al., Spray-deposited Al-doped ZnO transparent contacts for CdTe solar cells, Sol. Energy Mater. Sol. Cells. 101 (2012) 283–288. doi:10.1016/j.solmat.2012.02.008.

[12] A.P. Roth, J.B. Webb, D.F. Williams, Band-gap narrowing in heavily defect-doped ZnO, Phys. Rev. B. 25 (1982) 7836–7839. doi:10.1103/PhysRevB.25.7836.

[13] T. Tohsophon, N. Wattanasupinyo, B. Silskulsuk, N. Sirikulrat, Effect of aluminum and indium co-doping on zinc oxide films prepared by dc magnetron sputtering, Thin Solid Films. 520 (2011) 726–729. doi:10.1016/j.tsf.2011.06.079.

[14] G. Torres-delgado, D.C. Altamirano-ju, O. Jim, S. Jim, R. Castanedo-p, Low-resistivity ZnO : F : Al transparent thin films, Sol. Energy Mater. Sol. Cells. 82 (2004) 35–43. doi:10.1016/j.solmat.2004.01.003.

[15] G. Kenanakis, N. Katsarakis, E. Koudoumas, Influence of precursor type, deposition time and doping concentration on the morphological, electrical and optical properties of ZnO and ZnO:Al thin films grown by ultrasonic spray pyrolysis, Thin Solid Films. 555 (2014) 62–67. doi:10.1016/j.tsf.2013.10.015.

[16] J. Gao, W. Jie, Y. Yuan, T. Wang, G. Zha, J. Tong, et al., Dependence of film texture on substrate and growth conditions for CdTe films deposited by close-spaced sublimation Dependence of film texture on substrate and growth conditions for CdTe films deposited by close-spaced sublimation, Journal of vacuum science and technology. 051507 (2016). doi:10.1116/1.3610177.

[17] T. Prasada Rao, M.C. Santhoshkumar, Effect of thickness on structural, optical and electrical properties of nanostructured ZnO thin films by spray pyrolysis, Appl. Surf. Sci. 255 (2009) 4579–4584. doi:10.1016/j.apsusc.2008.11.079.

[18] S. Ilican, M. Caglar, Y. Caglar, Determination of the thickness and optical constants of transparent indium-doped ZnO thin films by the envelope method, Mater. Sci. 25 (2007) 709–718.

[19] M.D.L. Olvera, A. Maldonado, R. Asomoza, M. Mel, Effect of the substrate temperature and acidity of the spray solution on the physical properties of F-doped ZnO thin films deposited by chemical spray, Sol. Energy Mater. Sol. Cells. 71 (2002) 61–71.

[20] B.C. Jiao, X.D. Zhang, C.C. Wei, J. Sun, Q. Huang, Y. Zhao, Effect of acetic acid on ZnO:In transparent conductive oxide prepared by ultrasonic spray pyrolysis, Thin Solid Films. 520 (2011) 1323–1329. doi:10.1016/j.tsf.2011.04.152.

[21] N.S. Portillo-vélez, M. Bizarro, Sprayed Pyrolyzed ZnO Films with Nanoflake and Nanorod Morphologies and Their Photocatalytic Activity, Journal of Nanomaterials. 5981562 (2016). http://dx.doi.org/10.1155/2016/5981562.

CHAPTER 5

RESULTS AND DISCUSSION - SPUTTERING

To obtain high quality homogeneous films, addition to spray pyrolysis we used sputtering. The characteristics of undoped ZnO and IGZO (indium and gallium co-doped) thin films deposited by the sputtering technique are presented in this chapter, according to the experiments presented in Chapter 3. The characteristics of the films presented were: structural, morphological, optical and electrical. Additionally, the quality of the films was examined using a well-known formula (Haacke's) to check the suitability for transparent conductive oxide applications.

5. 1. Undoped ZnO thin film properties

Undoped ZnO thin films were deposited on sodacalcic glass substrates with variations in target to substrate distance, power, and substrate rotation speed. Here we have included experimental results comprehending the effect of substrate rotation speed on the quality of ZnO films. The variation in substrate rotation speed was carried out for the first time in the scientific community, in order to obtain highly homogeneous ZnO thin films.

5. 1. 1. Effect of power on film thickness at large target-substrate distance

The effect of power on the growth of ZnO thin films (at large distance, 14 cm) is a mandatory study in order to explore how the film thickness is influenced. In this respect, we have carried out depositions during 2 h at four different powers, namely, 50, 75, 100, and 125W.

Optical transmittance spectra of undoped ZnO thin films with respect to variations in the sputtering power at larger distance are presented in Fig. 5.1. The average transmittance of the samples LD50, LD75, LD100, and LD125 were 90, 78, 74, and 84%, respectively. The variations in the transmittance could have attributed to the variations in the thickness values. Though the films were deposited for 2 hours, the films presented very low thickness values. The thickness values of LD50, LD75, LD100, and LD125 were 15, 26, 39, and 32 nm, respectively. Since the thicknesses of these films were less than 100 nm, we can refer these films as "ultrathin films". From this, we can understand that, a low yield causes that the solid angle distribution density of sputtered particles coming from the target is also very

low; hence the growth rate is low as well. Henceforth, since the thicknesses of these films were less than 100 nm, the distance target-substrate was reduced to 7 cm for further experiments.

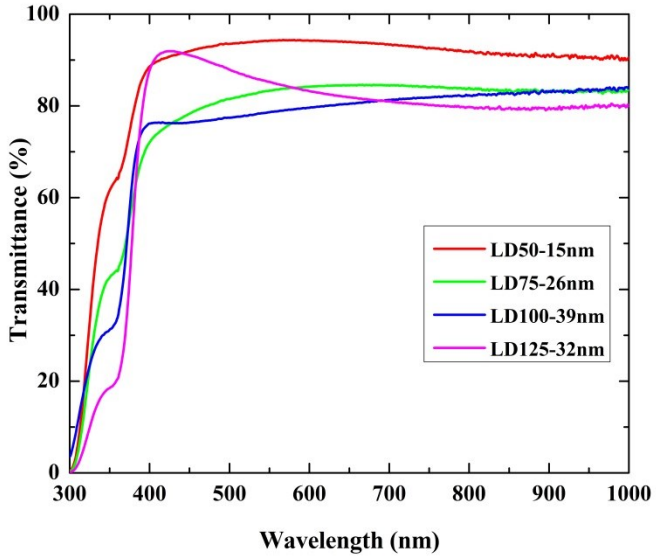

Fig. 5.1. Optical transmittance of undoped ZnO thin films (LD50-deposited at 50W, LD75-deposited at 75W, LD100-deposited at 100W, LD125-deposited at 125W) as a function of the sputtering power, at larger distance (14 cm).

5. 1. 2. Effect of power on film thickness at short target-substrate distance

The target-substrate distance (7cm) effect on ZnO films was studied in order to prove how the physical properties, such as structural, optical, morphological, and electrical, are affected. This study was developed as a function of the sputtering radio frequency (RF) power (50, 75, 100, and 125W).

5. 1. 2. 1. Structural properties

The XRD patterns of ZnO thin films deposited with different sputtering powers are shown in Fig. 5.2. The major two peaks are (002), and (103). All samples confirm the formation of the hexagonal wurtzite ZnO phase, irrespective of power magnitude. The plane (002),

which is the preferential orientation of ZnO, confirms the ZnO growth is along c-direction [1-3].

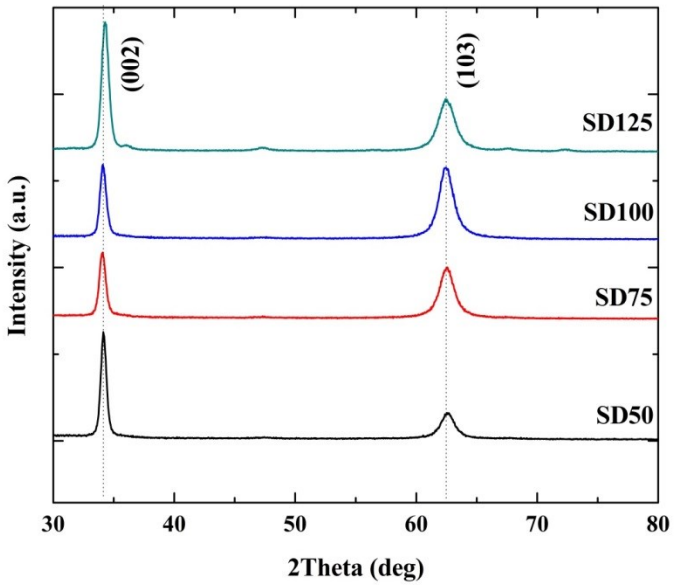

Fig. 5. 2. X-ray diffraction patterns of undoped ZnO thin films (SD50-deposited at 50W, SD75-deposited at 75W, SD100-deposited at 100W, SD125-deposited at 125W) with respect to variations in the sputtering power at short distance (7cm).

When power is increased from 50 to 75W, the intensity of (002) plane decreases which indicates that the crystallinity of the films is affected. When the power is increased to 100 and 125W the intensity of (002) plane increases, confirming the improvement of crystallinity of the thin films. As power increases, the number of collisions between sputtered particles decreases, which in turn increases their mobility; consequently the growth rate increases giving rise to thicker films [5]. The measured thicknesses of the films SD50, SD75, SD100, SD125 are 258, 519, 770, and 1262 nm, respectively. The crystallite sizes were estimated by using Scherrer's formula [6], the values are 16, 11, 12, and 14 nm for SD50, SD75, SD100, and SD125, respectively.

5. 1. 2. 2. Morphological properties

The morphology of the sputtered ZnO thin films as a function of the power are shown in Figs. 5.3.1-5.3.4 with the same magnifications. From these images, it is observed that the increase in the RF power causes an increase in grain size of ZnO. For the films deposited at powers 50 (Fig.5.3.1) and 75W (Fig. 5.3.2), uniform average size of sputtered particles around 25 and 40 nm were estimated, respectively. The reason for the uniform grain sizes can be explained as follows, at low deposition powers, the kinetic energy of bombarded particles was less thereby increasing collision time between particles, and consequently the long collision time enables the particles to reach the substrate and start the nucleation uniformly. Identical compact structures were also obtained by J. Lee group [7]. As we further increased the RF power to 100 and 125 W, the shape and size of the grains were less uniform. Films deposited at 100 W power (Fig. 5.3.3) presented a compact array of conical features of different sizes. The diameter of the conical structures oscillated around 40-100 nm. Films deposited with 125 W power (Fig. 5.3.4), presented the biggest grains as compared to the films sputtered at low powers. These samples show a pyramidal/conical and layered structures with smaller grains packed in between these structures. These different structures are resulted from the high sputtering powers leading to faster bombardment of particles due to their enhanced kinetic energy. Zhu et al also noticed that highly energized sputtered species increases the grain size [8].

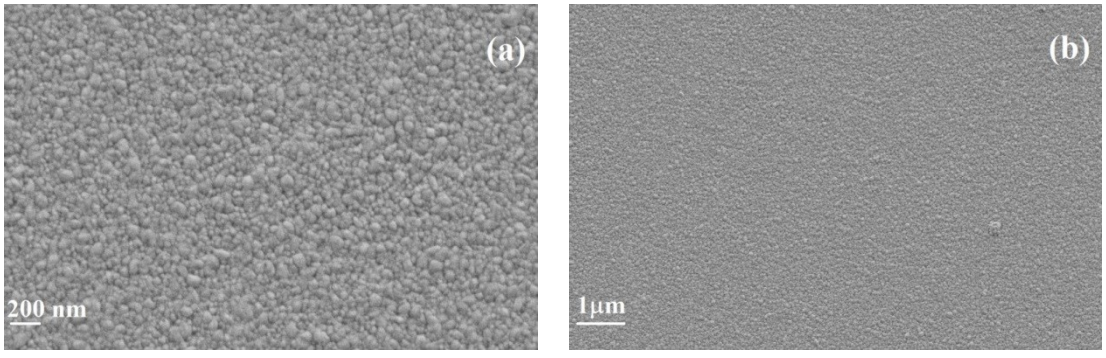

Fig.5.3.1. Surface morphology of ZnO thin film deposited with 50W power at a short target-substrate distance of 7cm (SD50) at different magnifications (a)30KX, and (b)10KX.

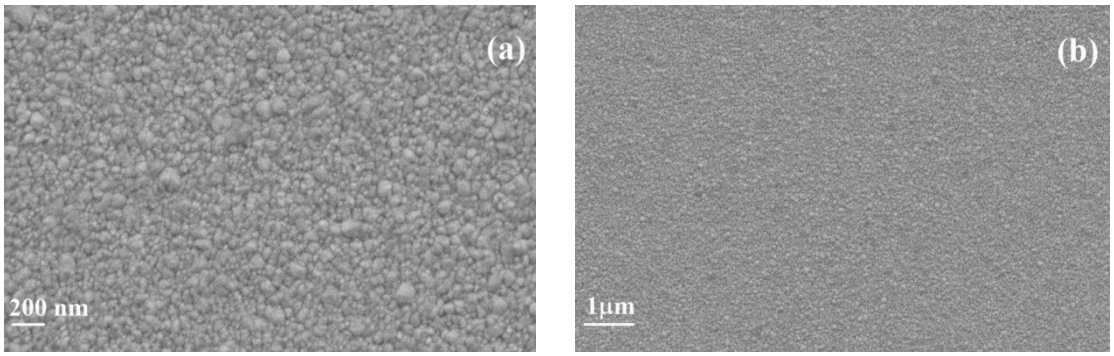

Fig.5.3.2. Surface morphology of ZnO thin film deposited with 75W power at a short target-substrate distance of 7cm (SD75) at different magnifications (a)30KX, and (b)10KX.

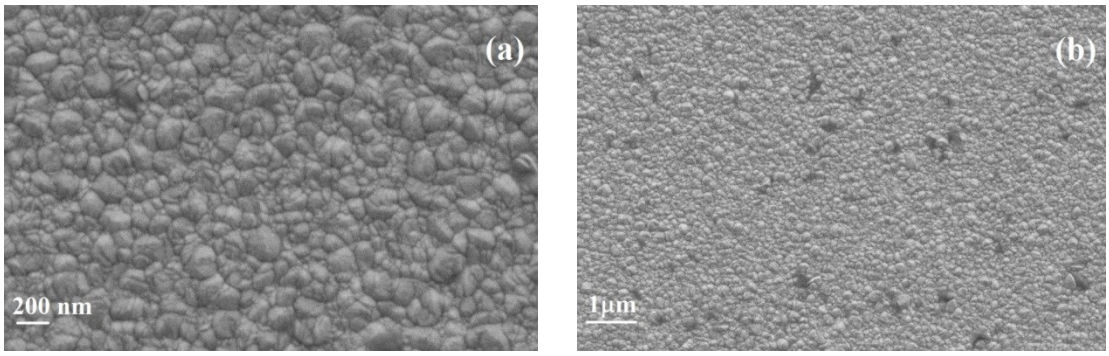

Fig.5.3.3. Surface morphology of ZnO thin film deposited with 100W power at a short target-substrate distance of 7cm (SD100) at different magnifications (a)30KX, and (b)10KX.

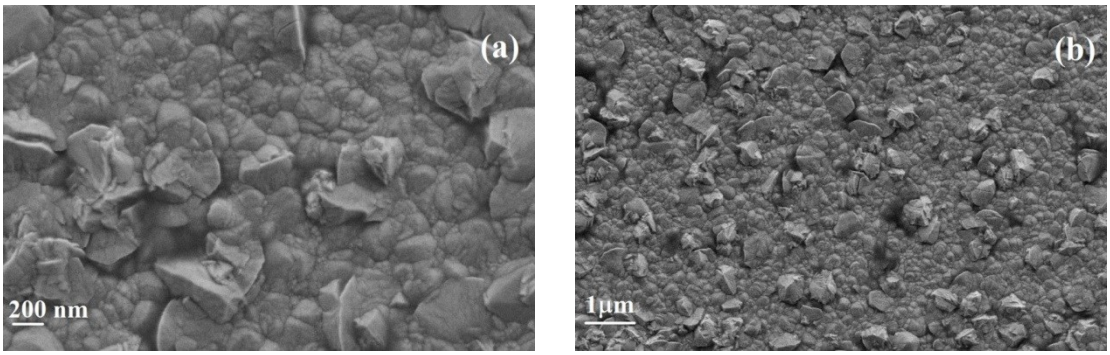

Fig.5.3.4. Surface morphology of ZnO thin film deposited with 125W power at a short target-substrate distance of 7cm (SD125) at different magnifications (a)30KX, and (b)10KX.

As a result, inhomogeneity in the films was caused by highly energized sputter particles. During the binding between any two particles on the substrate, there is always a possible interference by a third particle, thereby affecting homogeneity. As the deposition continues different nanostructures with different sizes are formed at high power sputtered films and thus bigger grains grew. From the SEM analysis, it is evident that the surface morphology (shape and grain size) of the sputtered ZnO films is strongly influenced by the rf power.

5. 1. 2. 3. Optical and electrical properties

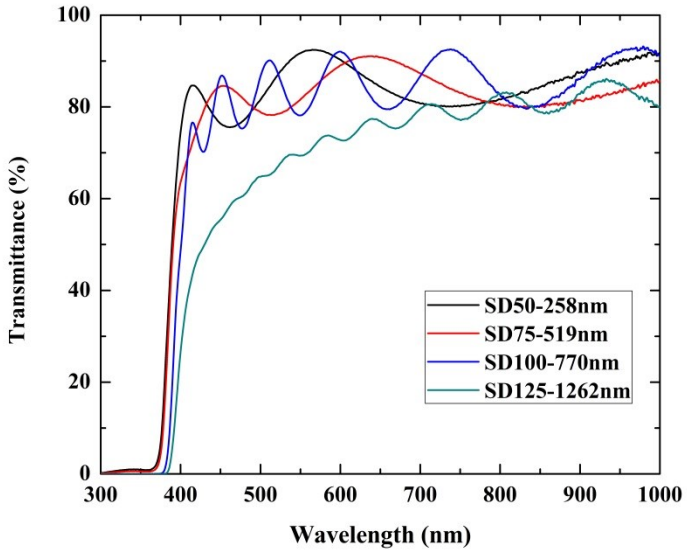

Fig.5.4. Optical transmittance of sputtered undoped ZnO thin films (SD50-deposited at 50W, SD75-deposited at 75W, SD100-deposited at 100W, SD125-deposited at 125W) at short distance (7cm) with variations in deposition power.

The optical transmittance of undoped ZnO thin films deposited with different sputtering powers is shown in Fig. 5.4. The presence of interferences indicates that the film thickness is very uniform and of high quality. The average transmittances in the visible region samples (400-700 nm) of the samples SD50, SD75, SD100, and SD125 are 91, 81, 78, and 69%, respectively. Transmittances varied according to their thickness magnitudes. The thickness values of SD50, SD75, SD100, and SD125 are 258, 519, 770, and 1262 nm, respectively. Increase in thickness is due to increase in kinetic energy of argon with power. Considering ZnO as a direct bandgap semiconductor, bandgap values were 3.25, 3.25, 3.23,

and 3.24 eV for the samples SD50, SD75, SD100, and SD125, obtained from the estimations as mentioned in Chapter 3 (section 3.5.3). The bandgap values estimated are in good accordance with reports of Ismail et al. in the literature [5].

Additionally, it was found that undoped ZnO thin films exhibited a high sheet resistance, between 4 and 6 x10^6 Ω/□. From these observations, it was confirmed that short distance between target and substrates enhances the film quality. Additionally, we can conclude that the deposition power plays a vital role in changing the structural, morphological, and optical characteristics of the undoped ZnO thin films.

5. 1. 3. Effect of substrate rotation speed

To obtain highly homogeneous, it is necessary to optimize the substrate rotation speed. In addition, this optimization is not found in the scientific literature. In this respect, we have varied the substrate rotation speeds from 0 to 80 rpm, with an interval of 20 rpm. The physical characteristics such as structural, morphological, optical are studied and the results are furnished below.

5. 1. 3. 1. Structural properties

In order to investigate, how the substrate rotation speed influences on structural characteristics, XRD characterization is performed. The diffraction patterns of ZnO thin films deposited at different rotation speeds is given in Fig. 5.5. Strong peak is observed at 34.04° and a very weak peak is observed at 62.46°, which correspond to (002) and (103) planes, respectively. Irrespective of the rotation speed, all the samples were grown with (002) preferential orientation. The full-width half maximum (FWHM) of the sample R40, presents the lowest value, indicating that, sample R40 is highly crystalline than others. Scherrer´s formula [6], was used to estimate the crystallite size of ZnO, The calculated crystallite sizes of the samples R0, R20, R40, R60, and R80 were 4, 3, 13, 4, and 4 nm, respectively.

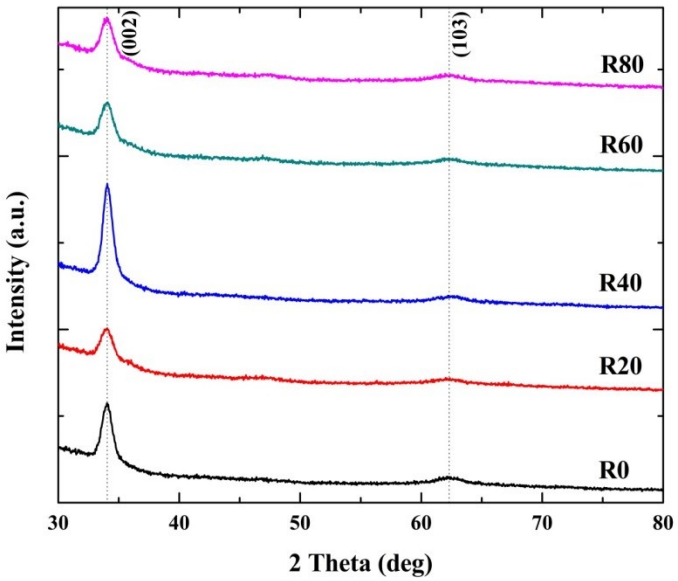

Fig. 5.5. X-ray diffraction patterns of undoped ZnO thin films fabricated at different substrate rotation speeds (0 to 80 rpm with an interval of 20 rpm).

5. 1. 3. 2. Morphological properties

The effect of substrate rotation speed on the morphological characteristics can be observed from the scanning electron microscopy images as shown in Fig. 5.6. From the fig. 5.6.1 we can observe that there are variations in the grain size of ZnO thin films between 50 to 200 nm. It is important to note that, when there is no substrate rotation agglomeration of grains on thin film surface took place. When the substrate rotation speed was increased to 20 rpm (Fig. 5.6.2), film surface looks uniform however some bigger grains of size ~200 nm were observed at random locations. Fig. 5.6.3 shows the surface of the ZnO film deposited at 40 rpm. This sample presents almost equally sized grains ~50 nm throughout the film surface without agglomeration. Further when we increase the speed from 60 to 80 rpm (Fig. 5.6.4 and 5.6.5) caused agglomerations as well as grain size variations from 50 to 100 nm. From the morphological results, we can confirm that speed of the substrate rotation having an effect in forming well defined nano grains on the film surface.

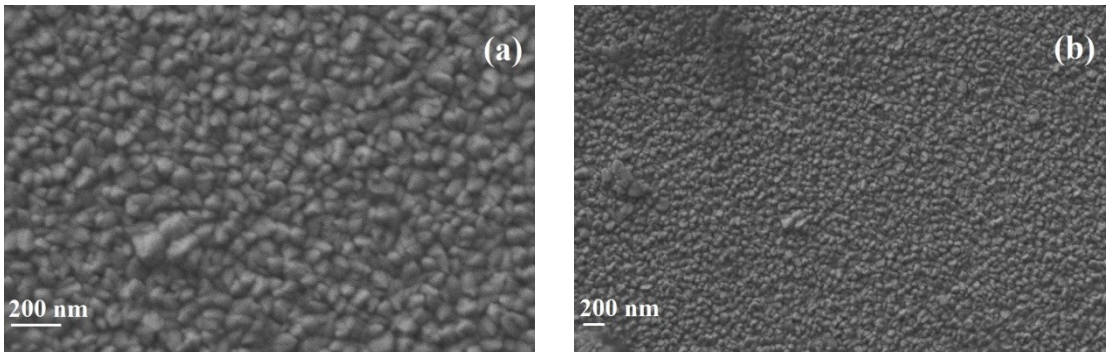

Fig. 5.6.1. Surface morphology of undoped ZnO thin film (R0) deposited without substrate rotation (a) 50KX, and (b) 20KX.

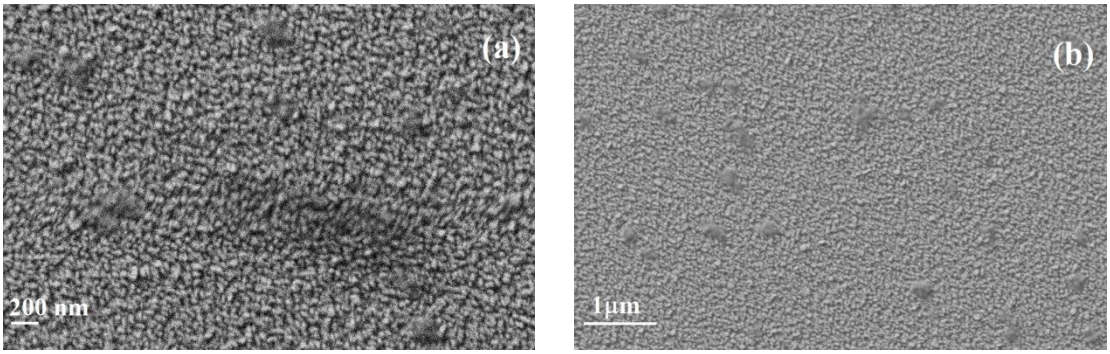

Fig. 5.6.2. Surface morphology of undoped ZnO thin film (R20) deposited with 20 rpm substrate rotation (a) 25KX, and (b) 15KX.

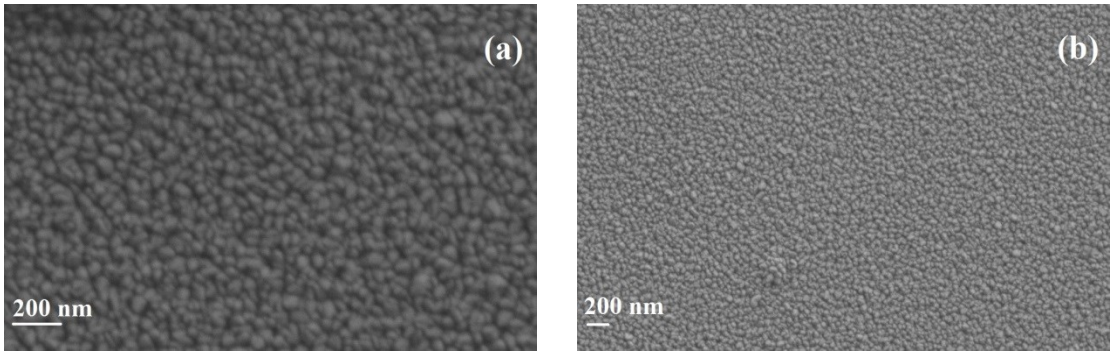

Fig. 5.6.3. Surface morphology of undoped ZnO thin film (R40) deposited with 40 rpm substrate rotation (a) 50KX, and (b) 20KX.

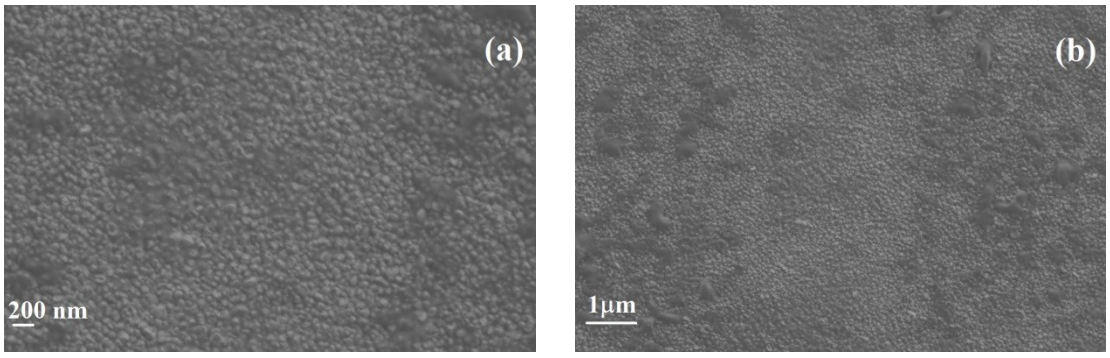

Fig. 5.6.4. Surface morphology of undoped ZnO thin film (R60) deposited with 60 rpm substrate rotation (a) 20KX, and (b) 10KX.

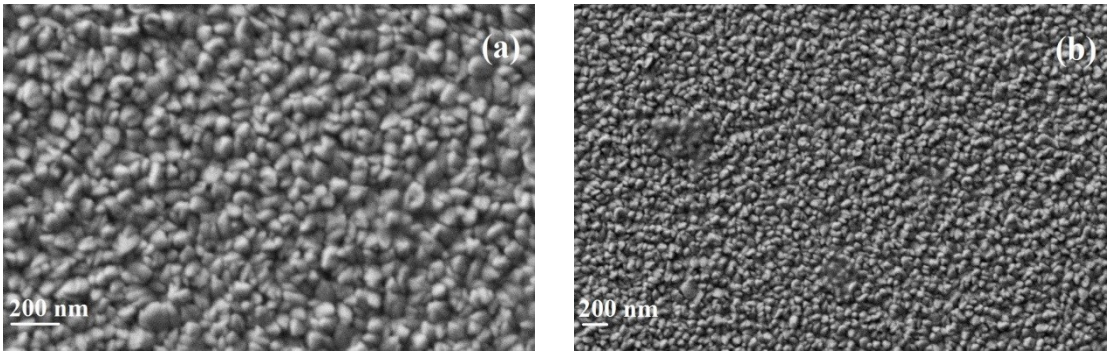

Fig. 5.6.5. Surface morphology of undoped ZnO thin film (R80) deposited with 80 rpm substrate rotation (a) 50KX, and (b) 25KX.

5. 1. 3. 3. Optical and electrical properties

Through naked eye, the films appear to be transparent. However, the optical transmittance of the undoped ZnO thin films is tested in the 300-1000nm region. The optical transmittance of ZnO thin films deposited at different substrate rotation speeds is shown in Fig. 5.7. The similar transmittance behaviour of all the samples proves that the films are with uniform thickness irrespective of substrate rotation speed. The average transmittances in the visible region samples (400-700nm) of the samples R0, R20, R40, R60, and R80 are 93, 89, 92, 91, and 90.0% respectively. The abrupt absorption edge with a high transparency presented confirms the high quality of the deposited films.

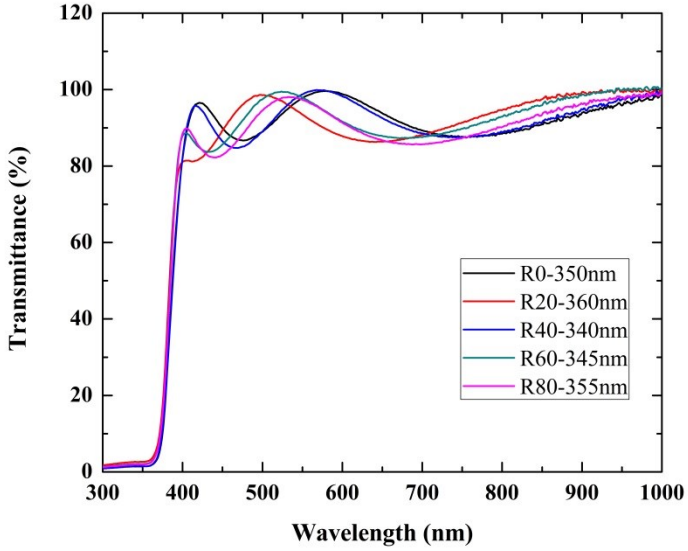

Fig. 5.7. Optical transmittance of undoped ZnO thin films deposited by sputtering with different substrate rotation speeds.

The estimated bandgap values were 3.23, 3.25, 3.24, 3.25, and 3.24 eV for the samples R0, R20, R40, R60, and R80, respectively (section 3.5.3). These bandgap values are in good agreement with the results reported by F. Chabouni et al. for ZnO [9].

Additionally, when we measured the electrical sheet resistance, we found that the undoped thin films exhibit high sheet resistance, between $4x10^6$ and $6x10^6$ Ω/□. We can conclude that though the obtained undoped ZnO thin films are homogeneous, films presented high sheet resistance. In order to enhance the electrical properties, doping was carried out and those results are furnished in the following sections.

5. 2. In and Ga co-doped ZnO thin film properties (Effect of power on In target)

Due to time restrictions and target limitations, we have carried out only few depositions for the preparation of IGZO thin films. In these experiments, the power of GZO source was set constant (40W), and the power of In source was varied as 3, 5, 10, and 15W (detailed experimental conditions are given in Chapter 3). Morphological, optical, and electrical characteristics of the IGZO thin films were studied.

5. 2. 1. Morphological properties

The effect of power of indium source was examined on morphological characteristics. Fig. 5.8.1, shows the surface morphology of IGZO thin films, which is grown at 3W of indium. From the Fig.5.8.1, we can see the grain size distribution of ZnO thin films varied between 16 to 55 nm. When the power of indium source was increased to 5W, the thin film (Fig. 5.8.2) surface appears to be more uniform. In this case, the size distribution of the grain narrowed between 17 to 32 nm. Further increase in the power of indium source (10W), increased the size distribution of the grains (Fig. 5.8.3) between 20 to 53 nm. When IGZO thin films were grown using 15W of power, the thin film surface ((Fig. 5.8.4) appears as non-uniform. Moreover, a significant increase in the grain size distribution between 17 nm to 92 nm was observed, with a prevalence of larger grains over smaller grains. From the morphology studies, it is evident that at variations in sputtering power results in IGZO surface morphologies with different sizes of grains.

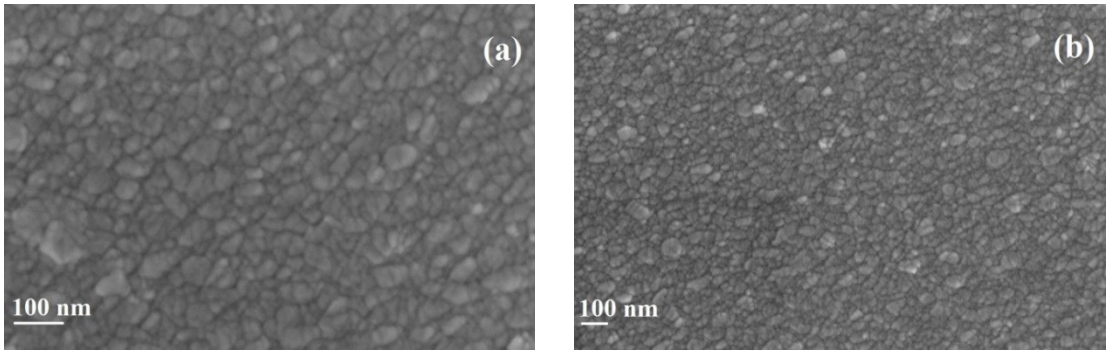

Fig. 5.8.1. Surface morphology of IGZO (I3) thin films deposited with 3W of indium at different magnifications (a) 100KX, and (b) 50KX.

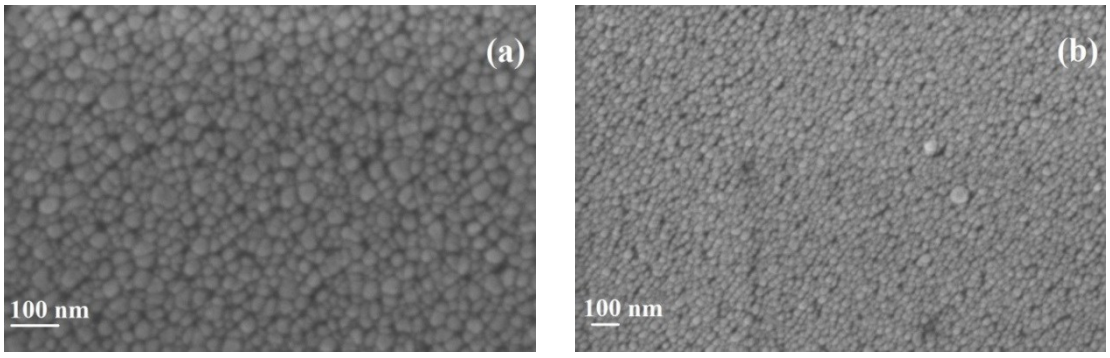

Fig. 5.8.2. Surface morphology of IGZO (I5) thin films deposited with 5W of indium at different magnifications (a) 100KX, and (b) 50KX.

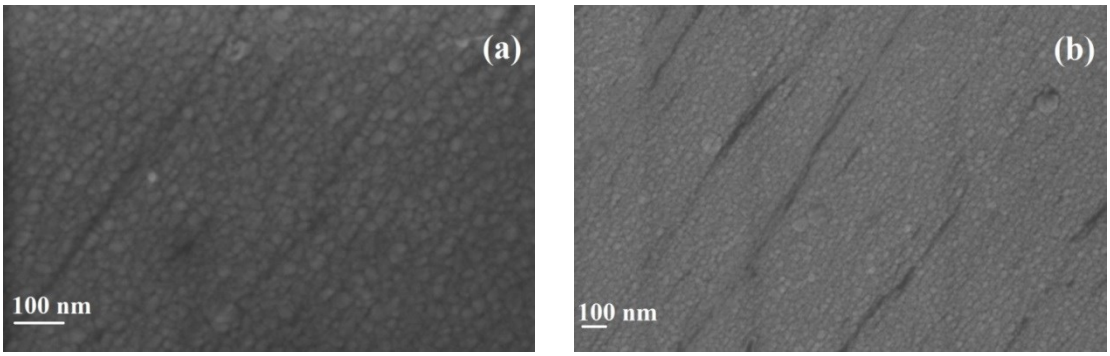

Fig. 5.8.3. Surface morphology of IGZO (I10) thin films deposited with 10W of indium at different magnifications (a) 100KX, and (b) 50KX.

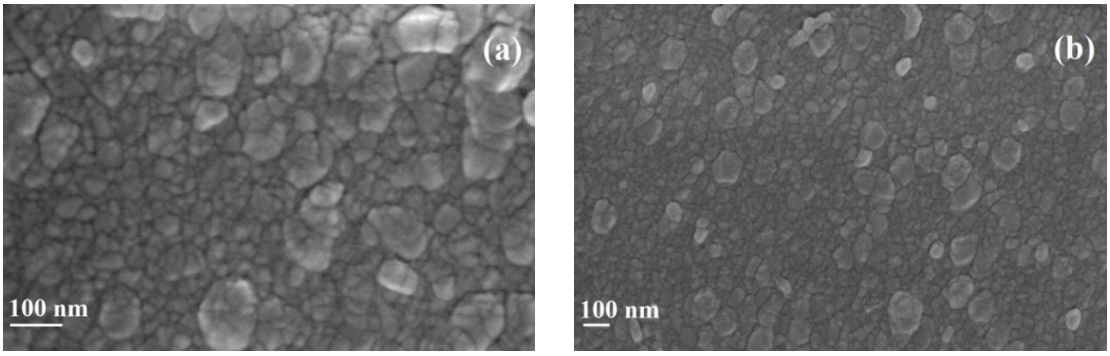

Fig. 5.8.4. Surface morphology of IGZO (I15) thin films deposited with 15W of indium at different magnifications (a) 100KX, and (b) 50KX.

5. 2. 2. Optical and electrical properties

The optical transmittance of IGZO thin films is shown in Fig. 5.9. Almost all the samples presented average transmittance (~90%) in the visible region samples (400-700 nm) except I15 sample. However, there are little variations in the transmittance, which might be due to differences in the grain size as given in the section 5.2.1.

The I15 film shows the lowest transmittance could be due the high thickness as well as large grains on the film. The abrupt absorption edge and high transparency presented confirms the good quality of the deposited films. The estimated bandgap values were 3.32, 3.35, 3.30, and 3.29 eV for the samples I3, I5, I10, and I15, respectively (section 3.5.3).

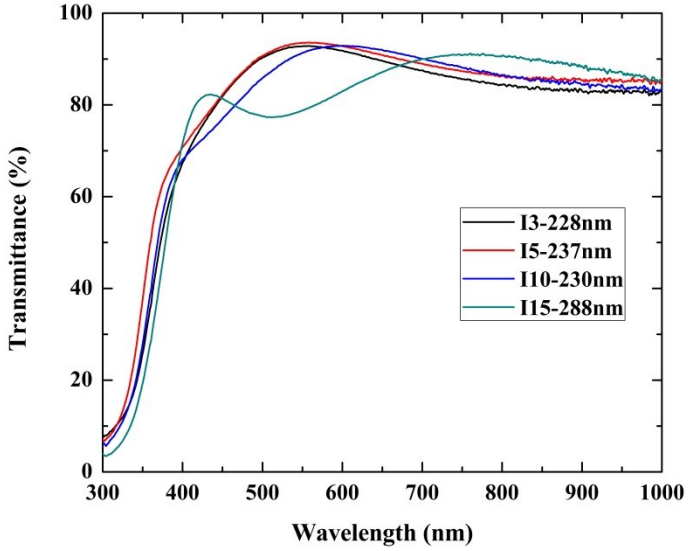

Fig. 5.9.1. Optical transmittance of IGZO thin films with variations in indium power (3,5,10 and 15W).

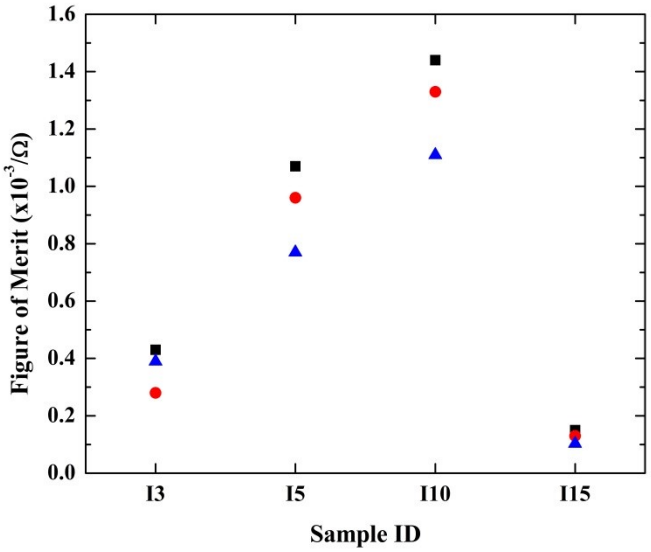

Fig. 5.9.2. Figure of Merit of IGZO thin films with variations in indium power (3,5,10 and 15W).

Table 5.1. Optical and electrical properties of IGZO thin films (with variations in power of indium)

Sample ID	Thickness (nm)	Transmittance at 550nm (T_{550})	Sheet Resistance (Ω/□)	Figure of Merit ($x10^{-3}/\Omega$)
I3	228	92	1003-1450	0.3-0.4
I5	237	93	450-627	0.7-1.1
I10	230	91	270-340	1.1-1.4
I15	288	78	533-808	0.10-0.15

The optical and electrical quality of sputtered IGZO thin films for TCO application was evaluated with Haacke´s figure of merit [10]. Among all the films, IGZO thin films (I10) presented the figure of merit in the range of $1.25\pm0.15x10^{-3}/\Omega$, since I10 presented transmittance >90% as well as showed lowest sheet resistance 270 Ω/□.

5. 3. Experience in the sputtering deposition process

We have faced some serious issues during the fabrication of ZnO thin films. The problems encountered and the solutions we employed are given below.

1) The actual velocity of the turbo molecular pump is 27000 rpm. Due to the failure in the internal circuit (frequency meter) of turbo controller, the velocity started to decrease without control. After the service given by the engineer of the distributor (tighten the frequency meter), the problem was resolved.

2) In the magnetron power unit, once the power value (75W) was set, a decrease in the power (20W) was observed after 5 minutes. This problem was raised due to the fault in the cable. This is a serious issue, because when there is a sudden change in the power to the target, it leads to cracks in the source material as occurred with the ($ZnO:Al_2O_3$) target.

3) The shutter is of up-down type in the vacuum chamber, due to this, the distance between the target and the substrate is long (14 cm) which leads to a very slow deposition process (3Å/min). In order to have better quality films, the substrate-target distance was kept at 7 cm, the growth rate is increased as 64 Å/min. However, this distance was still high for getting a significant increase in the growth rate deposition. We recommend using left-right shutter in the future.

4) After a certain number of depositions, a thick layer is formed on the substrate holder. However, this layer comes out after a certain period. Sometimes, during depositions, it has fallen on the target surface. This results in the formation of contaminated films. This is a serious issue if we are using our equipment, for multiple material depositions. In addition, it is worthy to note that this layer is not easily etched with isopropyl alcohol or acetone (These are recommended solvents for cleaning the chamber by the manufacturer (except O-ring). So before placing the substrate, it is mandatory to clean the substrate holder with isopropyl alcohol.

5) After two consecutive depositions, the magnetron as well as the target should be cleaned carefully. If the cleaning is not performed, the plasma during the growth process is not stable (suddenly the plasma goes off). This interrupts the growth of the thin film. The magnetron was cleaned with a laboratory soft cloth (Protec, Absorbent). The shield and the shutter of the magnetrons were cleaned with isopropyl alcohol. The target surface was cleaned by blowing nitrogen gas.

6) No consecutive deposition is possible with our equipment. After one deposition, when we try to restart the turbo pump for a new deposition immediately, the controller shows the error "PUMP CURRENT". In order to prevent this error, we have to cool down the turbo pump for minimum 2 hours. So this forced us to deposit maximum two films in a day.

7) Initially, we tried to fabricate AIZO (Al and In co-doped ZnO) thin films by co-sputtering. So, we tried to get conditions for Al-doped ZnO (AZO) growth. But, all our experimental conditions produced thin films with high sheet resistance (values in between 4 and $5x10^6$ Ω/□). List of experiments were given in appendix B.

5. 4. Comparison of films deposited with the ultrasonic spray pyrolysis and sputtering techniques

Based on our working experience and results obtained, we have compared the techniques ultrasonic spray pyrolysis (USP) and sputtering. Major observations were compared in Table 5.6.

1) USP technique is cost-effective, simple experimental setup and faster growth rate, whereas sputtering is costly, complicated experimental setup and lower growth rate.
2) Maintenance of the USP is easier than sputtering. Identifying the vacuum leaks is a really difficult issue.
3) Fabricating films for large scale applications are economic by spray, whereas large scale applications are difficult and costly by sputtering.
4) A high degree of contamination occurs in films deposited with USP than those deposited with sputtering process, because sputtering depositions are carried out in vacuum.
5) When we compare our obtained results, undoped ZnO thin film fabricated by both techniques showed high sheet resistance (Table 5.2).
6) When we compare figure of merit of the AIZO thin films fabricated by USP and the IGZO thin films fabricated by sputtering, USP results show higher values than sputtering. However it depends on the various parameters involved in the experiments. In our case, we have explored several parameters (temperature, solution conditions, ball milling conditions, precursor types) for USP, whereas in the case of IGZO thin films were fabricated by varying only power. However, the sputtering experiments were limited in our case, due to the time restrictions, non-availability of the targets on time, and the problems we faced as mentioned in section 5.3 of this chapter.

Table 5.2. Comparison of ultrasonic spray pyrolysis and sputtering

S. No.	Ultrasonic spray pyrolysis	Sputtering
1	Cost-effective experimental setup	Expensive experimental setup
2	Maintenance is easy	Maintenance is difficult
3	Higher deposition rate than sputtering (50 nm/min)	Low deposition rate (6 nm/min)
4	Undoped ZnO thin films were with high sheet resistance in the range of $4x10^6$– $5\ x10^6\ \Omega/\square$ and exhibited optical transmittance in the range 55-56%	Undoped ZnO thin films were with high sheet resistance in the range $4x10^6 – 6x10^6\ \Omega/\square$) and exhibited optical

		transmittance 69-90%
5	AIZO thin films with optical transmittance of 85% with minimum sheet resistance of (22-25 Ω/□) were obtained	AIZO thin films with optical transmittance of 91% with minimum sheet resistance of (270-340 Ω/□) were obtained
6	Highest figure of merit obtained was $8.3\pm0.55x10^{-3}/\Omega$.	Highest figure of merit obtained was $1.25\pm0.15x10^{-3}/\Omega$

5. 5. Conclusions

Structural, morphological, optical and electrical characteristics of both the undoped ZnO thin and the IGZO thin films were studied in detail. For the fabrication of undoped ZnO thin films, depositions of films by varying the substrate-target distance, sputtering power, and substrate rotation speed were done. From the results, it can be concluded that substrate rotation, is an important parameter for growing ZnO samples with good homogeneity. For the fabrication of IGZO thin films, we varied the sputtering power of indium source. In the case of IGZO thin films, the highest figure of merit of $1.25\pm0.15x10^{-3}/\Omega$ was achieved when the sputtering power of indium was 10W. The optical transmittance and electrical sheet resistance values of IGZO thin films make suitable candidates for transparent conductive oxide applications.

5. 6. REFERENCES

[1] H.A.N. Dedong, W. Yi, Z. Shengdong, S.U.N. Lei, H.A.N. Ruqi, S. Matsumoto, et al., Influence of sputtering power on properties of ZnO thin films fabricated by RF sputtering in room temperature, Science china, 55 (2012) 951–955. doi:10.1007/s11432-011-4347-z.

[2] N.D. Sin, M.Z. Musa, M. Rusop, Effect of R . F Power to the Properties of ZnO Thin Films Deposited by Magnetron Sputtering,Advanced Materials Research. 364 (2012) 119–123. doi:10.4028/www.scientific.net/AMR.364.119.

[3] X. Yu, J. Ma, F. Ji, Y. Wang, X. Zhang, Effects of sputtering power on the properties of ZnO : Ga films deposited by r . f . magnetron-sputtering at low temperature, J. Cryst. Growth. 274 (2005) 474–479. doi:10.1016/j.jcrysgro.2004.10.037.

[4] Y. Tsai, N. Wang, C. Tsai, Fluorine-doped ZnO transparent conducting thin fi lms prepared by radio frequency magnetron sputtering, Thin Solid Films. 518 (2010) 4955–4959. doi:10.1016/j.tsf.2010.03.086.

[5] A. Ismail, M.J. Abdullah, The structural and optical properties of ZnO thin films prepared at different RF sputtering power, J. King Saud Univ. - Sci. 25 (2013) 209–215. doi:10.1016/j.jksus.2012.12.004.

[6] L. Alexander, H.P. Klug, L. Alexander, H.P. Klug, Determination of Crystallite Size with the XRay Spectrometer, J. Appl. Phys. 137 (1950) 1–7. doi:10.1063/1.1699612.

[7] J. Lee, D. Lee, D. Lim, K. Yang, Structural, electrical and optical properties of ZnO:Al films deposited on flexible organic substrates for solar cell applications, Thin Solid Films. 515 (2007) 6094–6098. doi:10.1016/j.tsf.2006.12.099.

[8] B.L. Zhu, J. Wang, S.J. Zhu, J. Wu, D.W. Zeng, C.S. Xie, Optimization of sputtering parameters for deposition of Al-doped ZnO films by rf magnetron sputtering in Ar+H2 ambient at room temperature, Thin Solid Films. 520 (2012) 6963–6969. doi:10.1016/j.tsf.2012.07.049.

[9] F. Chabouni, J. B. Belgacem, M. Abaab, Physical Properties of TCO - ZnO Thin Films Sputtered from a Powder Target, Chinese journal of physics. 52 (2014) 272–285. doi:10.6122/CJP.52.272.

[10] G. Haacke, New figure of merit for transparent conductors, J. Appl. Phys. 47 (1976) 4086–4089. doi:10.1063/1.323240.

CHAPTER 6

CONCLUSIONS

Undoped and co-doped ZnO thin films with controlled characteristics, for applications as transparent conductive oxides, were deposited by chemical spray and sputtering techniques, separately. It is important to mention that we are the first research group to work on co-doped ZnO thin films in the section of solid state electronics.

In both techniques, undoped ZnO thin films were highly transparent, but exhibited high resistivity. For films deposited with the chemical spray technique, a non usual and novel chemical approach was proposed to dope ZnO with Al and In elements simultaneously. It was necessary to explore the effect of deposition variables on the characteristics of co-doped ZnO thin films. The sheet resistance of as-deposited ZnO thin films served for a quick feedback to guide the extent of the variation in each variable. In this way, as a first step, the best substrate temperature value was easily found ranging from 425 to 450°C. Based in the role that solvent plays in the transport properties, a study variation in the acetic acid:water proportions per liter of solution was done, and as a result, it was encountered that the 50:50 proportion per liter was the optimum. Finally, the role of the precursor aluminium salt was explored, finding that aluminium acetylacetonate is the best choice, as a minimum sheet resistance (22-25 Ω/□) with transmittance (85%), which in turn resulted in the highest figure of merit ($8.3\pm0.55x10^{-3}/\Omega$).

Additionally, for the first time, the ball milling of the precursor previous to solution preparation, was tested and reported for the deposition of transparent and conductive thin films deposited by ultrasonic spray pyrolysis technique. The results show that ball milling treatment produces chemical species in turn enhance the characteristics of ZnO thin films, opening the way to manufacture high quality materials. Its worth to mention the comment of a reviewer of a journal that the results were considered as extremely important topics, and deserved immediate publication. However, more exploratory work is necessary to gain knowledge in this new way of processing materials.

In the case of sputtering, undoped homogeneous ZnO thin films were obtained by optimizing several sputtering conditions such as target-substrate distance, power, and

substrate rotation speed. We found that the rotation speed of the substrate influences in fabricating highly homogeneous films. Further, we have performed IGZO through co-sputtering. In this case, we have used two targets, namely ZnO/Ga_2O_3 and In. The obtained figure of merit of IGZO is $1.25\pm0.15x10^{-3}/\Omega$.

By comparing, the characteristics of co-doped ZnO thin films deposited by either ultrasonic spray or sputtering, we end up with the following observations: 1) Highest figure of merit was achieved in AIZO thin films deposited by ultrasonic spray. However, the figure of merit obtained in co-doped ZnO thin films deposited by sputtering also appears to be competitive. In addition, changes in the vacuum chamber of the sputtering system are necessary in order to obtain ZnO thin films with higher figure of merit values. 2) By using ultrasonic spray we have obtained several nanostructures such as hexagonal towers/pyramids, elongated grains, trigonals, crescent moon structures, super grown hexagons, woven nanostructures, layered hexagons, etc., of sizes greater than 50 nm, whereas in sputtering we have obtained nanograined ZnO of sizes even less than 20nm. 3) We conclude that if we are interested in large scale applications, ultrasonic spray would be more convenient than sputtering, because ultrasonic spray is simple and cost-effective.

CHAPTER 7

FUTURE WORKS

Controlled chemical processes occurs during the synthesis of semiconductor materials are far from being satisfactorily explained and even the all variety of chemical routes involved have not exhausted in professional literature. Research has raised the role of certain deposition variables on the characteristics of the synthesized materials, but thoroughly and systematic work is still needed to discover, accidentally or systematically, new efficient ways in the manufacturing of quality materials. In the case of the chemical spray technique, the role of solution aging, grinding of the precursor previous to dissolution, and codoping, has not reported in literature.

In this work the role of co-doping of Al and In, and the optimization of deposition conditions for the manufacturing of quality TCOs were shown. Future work should be oriented to other systems, e.g. F and Al, In and F as made in this work. Based on our experience in the current work, we came to know, for the first time, that grinding the Zn precursor prior to solution preparation for the fabrication of thin films, helps in enhancing the transport properties. In the near future, we are interested in fabricating undoped ZnO, single element doped ZnO, and co-doped ZnO by using ball-milled precursor. There are several parameters involved in ball-milling such as milling time, milling speed, ball to powder ratio, and type of precursor that need a careful study. A lot of work will be generated as detailed evolution of chemical species during the grinding of the precursor has not yet been reported. It is expected to have enhanced properties in the applications of ZnO thin films in photocatalysis, TCO applications, and gas sensors devices.

Similarly, we have obtained only few competitive results by sputtering. We are interested in preparing targets through ball milling the precursors. In the literature, we have found that controlling the sputtering parameters is difficult for achieving high quality films through co-doping, and co-sputtering. In this respect, we have plans to fabricate undoped, single element doped, and co-doped ZnO thin films and to employ in different applications.

ANNEXURE A: PRECURSOR DETAILS

Table A.1. ULTRASONIC SPRAY PYROLYSIS – PRECURSOR/GAS DETAILS

S.NO	REACTIVE / GAS	CHEMICAL FORMULA	PURITY (%)	COMPANY
1	Zinc acetylacetonate	$C_{10}H_{14}O_4Zn.xH_2O$	98	Sigma Aldrich
2	Methanol	CH_3OH	99.8	J. T. Baker
3	Acetic acid	CH_3COOH	99.9	J. T. Baker
4	Zinc acetate dihydrate	$(Zn(OOCCH_3)_2.2H_2O$	98-101	Alfa Aesar
5	Aluminium acetylacetonate	$C_{15}H_{21}AlO_6$	99	Alfa Aesar
6	Aluminium chloride	$AlCl_3.6H_2O$	97-101	Alfa Aesar
7	Aluminium sulphate	$Al_2(SO_4)_3 \bullet xH_2O$ (x≈14-18)	97	Alfa Aesar
8	Indium (III) acetate	$In(OOCCH_3)_3$	99.99	Alfa Aesar
9	Nitrogen gas	N_2	99.99 (Industrial grade)	Infra

Table A.2. SPUTTERING –TARGET DETAILS (All targets were purchased from Kurt J. Lesker Company)

S.NO	TARGET NAME	CHEMICAL FORMULA	PURITY (%)	DIAMETER x THICKNESS (inches)
1	Zinc oxide	ZnO	99.999	2 x 0.25
2	Zinc	Zn	99.993-99.995	2 x 0.25
3	Zinc oxide/Alumina	ZnO/Al_2O_3	98/2 wt%	2 x 0.25

4	Indium	In	99.99	2 x 0.25
5	Zinc oxide/Gallium oxide	ZnO/Ga_2O_3	95/5 wt%	2 x 0.125
6	Indium gallium zinc oxide	InGaZnO4	99.99	2 x 0.125

Table A.3. SPUTTERING –GAS CYLINDER DETAILS

S.NO	**GAS**	**CHEMICAL FORMULA**	**PURITY (%)**	**COMPANY**
1	Argon	Ar	99.999 (Ultra high pure)	Infra
2	Oxygen	O_2	99.999 (Ultra high pure)	Praxair
3	Nitrogen	N_2	99.99 (Industrial grade)	Praxair
4	Nitrogen	N_2	99.998 (Ultra high pure)	Infra

ANNEXURE B: MISCELLANEOUS SPUTTERING EXPERIMENTS

Some of our experiments, resulted in films with high sheet resistance (values in between 4 and $5x10^6$ Ω/□). List of experiments were given below.

Table B.1. AZO (Al-doped ZnO) growth conditions using RF source (target-substrate distance: 7 cm, Target used: ZnO/Al_2O_3, 98/2 wt%, Kurt J. Lesker)

Target	RF Power(W)	Pressure (mTorr)	Time (min)
ZnO/Al_2O_3	100	11	180
ZnO/Al_2O_3	100	8.7	180
ZnO/Al_2O_3	100	31	180
ZnO/Al_2O_3	100	17	180
ZnO/Al_2O_3	100	7.4	180
ZnO/Al_2O_3	150	1.8	180
ZnO/Al_2O_3	150	11	180
ZnO/Al_2O_3	150	8.7	180
ZnO/Al_2O_3	50	11	180
ZnO/Al_2O_3	50	8.7	180
ZnO/Al_2O_3	50	1.8	180

Table B.2. AZO (Al-doped ZnO) growth conditions using DC source (target-substrate distance: 7 cm, Target used: ZnO/Al_2O_3, 98/2 wt%, Kurt J. Lesker)

Target	DC Power (W)	Pressure (mTorr)	Time (min)
ZnO/Al_2O_3	100	5.2	30
ZnO/Al_2O_3	100	5.2	60
ZnO/Al_2O_3	100	3.4	60
ZnO/Al_2O_3	100	2.4	60
ZnO/Al_2O_3	100	2.4	90
ZnO/Al_2O_3	100	3.7	90
ZnO/Al_2O_3	100	3.7	10
ZnO/Al_2O_3	100	2.4	60

ZnO/Al_2O_3	100	3.7	120
ZnO/Al_2O_3	100	9.6	90
ZnO/Al_2O_3	100	20	90
ZnO/Al_2O_3	100	20	30
ZnO/Al_2O_3	100	9.6	60
ZnO/Al_2O_3	100	4.3	75
ZnO/Al_2O_3	150	8.3	60
ZnO/Al_2O_3	50	2.2	30

Table B.3. IGZO (In and Ga co-doped ZnO) growth conditions using RF & DC source (Target-distance of 7 cm, Targets used: Indium Gallium Zinc Oxide, 99.99% Pure, In/Ga/Zn/O 36.58/22.21/20.83/20.38 wt%, from Kurt J. Lesker)

Target in RF	RF Power (W)	Pressure (mTorr)	Time (min)
IGZO	25	5	30
IGZO	75	5	30
IGZO	50	5	30

Table B.4. IGZO (In and Ga co-doped ZnO) growth conditions using RF & DC source (Target-distance of 7 cm, Targets used: Indium Gallium Zinc Oxide, 99.99% Pure, In/Ga/Zn/O 36.58/22.21/20.83/20.38 wt%, from Kurt J. Lesker)

Target in DC	DC Power (W)	Pressure (mTorr)	Time (min)
IGZO	15	6	60
IGZO	15	6	120
IGZO	50	5.5	60
IGZO	70	5.5	60
IGZO	50	8.6	30
IGZO	50	13	30
IGZO	50	15	60
IGZO	50	20	30
IGZO	50	13	120

IGZO	50	5.5	120
IGZO	75	13	60
IGZO	75	13	120
IGZO	50	8.6	60

ANNEXURE C: CONFERENCES ATTENDED

1) International Workshop on ZnO and Related Materials -2014, Canada.
2) International Materials Research Congress, Cancun, 2014, México.
3) International conference on Electrical engineering, Computing science and Automatic control (CCE) -2014, México.
4) International conference on Electrical engineering, Computing science and Automatic control (CCE) -2015, México
5) MRS Fall Meeting, 2015, Boston, USA.
6) International Materials Research Congress, Cancun, 2016, México.
7) International conference on Electrical engineering, Computing science and Automatic control (CCE) - 2016, México.

ANNEXURE D: LIST OF PUBLICATIONS

1) **V.K. Jayaraman**, A. Maldonado, M. Olvera, "Influence of precursor ball milling in enhancing the structural, morphological, optical and electrical properties of AIZO thin films," ***Mater. Lett. 181(2016)52–55***.

2) **V.K. Jayaraman**, A.M. Álvarez, Y.M. Kuwabara, Y. Koudriavstev, M.D.L.L. Olvera Amador, "Effect of co-doping concentration on structural, morphological, optical and electrical properties of aluminium and indium co-doped ZnO thin films deposited by ultrasonic spray pyrolysis," ***Mater. Sci. Semicond. Process. 47 (2016) 32–36.***

3) **V.K. Jayaraman**, Y.M. Kuwabara, A.M. Álvarez, M.O. Amador, "Importance of substrate rotation speed on the growth of homogeneous ZnO thin films by reactive sputtering," ***Mater. Lett. 169 (2016) 1–4.***

4) **J. V. Kumar**, A. Maldonado, M. Olvera, "A simple and cost-effective zinc oxide thin film sensor for propane gas detection," ***Mater. Lett. 157 (2015) 169–171.***

UNDER REVISION & PREPARATION

1) **V.K. Jayaraman**, A. Maldonado, M. Olvera, "Structural, optical and electrical properties of Al and In co-doped ZnO nanostructures" –Under revision- Journal of Alloys and Compounds.

2) **V.K. Jayaraman**, A. Maldonado, M. Olvera, "Growth of high quality AIZO thin films: Optimization of acetic acid content in the starting solution of ultrasonic spray pyrolysis"–Manuscript under preparation.

3) **V.K. Jayaraman**, A. Maldonado, M. Olvera, "Effect of precursor type in the preparation of AIZO thin films and their physical properties"–Manuscript under preparation.